Modelling And Optimization Of Hydrodynamic Parameters On Inverse Fluidized Bed Reactor

Abstract

This study investigates the modeling and optimization of hydrodynamic parameters in an inverse fluidized bed reactor for the removal of contaminants. The experimental setup was designed to evaluate the efficiency of modified rice husk in adsorbing Terasil blue dye under various conditions. The removal rates achieved were significant, with a maximum removal rate of 97.15% observed during the thrust experiments. Key parameters, including bed height, fluid velocity, and adsorbent dosage, were systematically varied to assess their impact on the adsorption efficiency. The results demonstrated that increased bed height and fluid velocity positively influenced the removal rate, while optimal adsorbent dosage was crucial for maximizing efficiency. An Artificial Neural Network (ANN) model was employed to predict the outcomes, showing high accuracy in matching experimental data. This research provides valuable insights into the optimization of fluidized bed reactors for environmental remediation applications. In batch experiments the value of qe is 1.73 mg/g under specific conditions, the Langmuir model provides q-max of 0.0078 mg/g and K-L of 0.0801 L/mg.

Various kinetic models, including Elovich, Intra-particle diffusion, Pseudo-first-order, and Pseudo-second-order, were employed to understand temporal dynamics. The pseudo-first-order model yielded a qe of 1.37 mg/g with a rate constant (K1) of 0.015 and an R-squared value of 0.8472. Meanwhile, the pseudo-second-order model calculated qe as 1.565 mg/g, with a rate constant (K2) of 0.0198 and an R-squared value of 0.9356.

Ongoing tests conducted in an inverse fluidized bed offer valuable insights into the hydrodynamic behaviour of the system. The collected data effectively demonstrates the variations in pressure drops and bed heights. As an illustration, when the fluid velocity is 0.086 m/s, the pressure drop undergoes an increase from 353 to 510 Pa, given a particle mass of 0.06 kg. There is a positive correlation between bed height and fluid velocity, suggesting a significant association within the dynamics of fluidized beds.

Furthermore, the study presents the incorporation of an Artificial Neural Network (ANN) model to facilitate predictive analysis. The evaluation of the model's performance is conducted by analysing experimental data, in which the anticipated removal efficiency (RE) is compared to the actual RE. The artificial neural network (ANN) model demonstrates varied levels of accuracy throughout five experimental trials, as evidenced by the range of Root Mean Squared Error (RMSE) values observed, which span from 60.97 to 92.78.

In conclusion, this extensive inquiry offers significant perspectives on the phenomenon of adsorption, by combining experimental and computational methodologies. The numerical findings provide valuable insights into the underlying principles of adsorption and have practical implications for enhancing the efficiency of adsorption systems in the fields of environmental and chemical engineering.

This research reveals that the modified rice husk exhibits a notable adsorption capacity for Terasil blue dye, as demonstrated by the equilibrium adsorption capacity (qe) values obtained in both batch and continuous trials. The kinetic models employed shed light on the temporal dynamics of the adsorption process, highlighting the significance of pseudo-first-order and pseudo-second-order mechanisms. The inverse fluidized bed trials provide valuable insights into the hydrodynamic behavior, emphasizing the correlation between fluid velocity, pressure drops, and bed heights. The incorporation of an Artificial Neural Network (ANN) model further contributes to the predictive analysis, though with varying levels of accuracy.

Table of Contents

Abbrevation

Abbreviation	**Full Form**
a, b	Parameters in Elovich Model
ANN	Artificial Neural Network
BOD	Biochemical Oxygen Demand
C	Intercept in Intra-particle Diffusion Model
C/Co	Normalized Concentration
Ce	Equilibrium Concentration
COD	Chemical Oxygen Demand
HRT	Hydraulic Retention Time
IFBR	Inverse Fluidized Bed Reactor
Kid	Intra-particle Diffusion Coefficient
mg/g	Milligrams per gram
nm	Nanometers
Q	Flow Rate
qe	Amount Adsorbed at Equilibrium
qt	Amount Adsorbed at Time t
R^2	Correlation Coefficient
RMSE	Root Mean Squared Error

RSM	Response Surface Methodology
SPSS	Statistical Package for the Social Sciences
TOC	Total Organic Carbon

Table of Figures

Tables

Chapter 1: Introduction

1.1 Background

The study explores the hydrodynamic characteristics and the application of liquid-solid inverse fluidization in various configurations, including those with sloped walls or a tapering top section. This method proves effective in separation methodologies, offering significant power savings and a simplified fluidization process during power failures. Tapered "inverted fluidized bed reactors" find widespread industrial applications, including oil-water separation using aerogels, biofilm cultivation, and reduction of COD, BOD, and TOC levels (Wang 2010).

Water, an indispensable resource for life, faces escalating pollution threats from various sources, necessitating urgent treatment measures. Pollution, attributed to industrial discharges and urban activities, introduces hazardous contaminants, jeopardizing ecosystems and human health. In the case of Terasil blue dye pollution, the study emphasizes the significance of adsorption, employing modified rice husk in batch and continuous trials. Kinetic models, including pseudo-first-order and pseudo-second-order, unravel the temporal dynamics, while an Artificial Neural Network (ANN) (Sabarunisha et al., 2014) model enhances predictive analysis for removal efficiency. Simultaneously, the use of the inverse fluidized bed technique sheds light on the hydrodynamic intricacies of adsorption systems, detailing pressure drops and bed heights. This method's selection arises from its unique ability to simulate real-world conditions, contributing crucial insights into the interplay between fluid dynamics and adsorption efficiency, ultimately advancing the optimization of water treatment processes (Alvarado et al., 2008).

Solids become liquids by fluidization. For a "fluidized bed reactor," solids must exceed liquids. In a "fixed-bed reactor," the solid system's density must be lower than the

liquid's and the liquid flow opposes the gas flow. Gas flows continuously through a fixed-bed reactor's fluid (Ouyang et al., 2019). By adopting two- and three-phase hydrodynamic operating regimes, the "inverse fluid bed reactor" (IFBR) bioremediates Iraq's wastewater system better than an up-flow "fluidized bed reactor" (Hamdad et al., 2007). After biological or chemical oxidation, wastewater treatment plants (WWTPs) adsorb dissolved contaminants like terasil blue dye .

Inverse fluidized bed reactors improve mass transfer and particle attrition resistance. These features decrease biofilm separation and aid re-fluidization during power outages. The bioprocess of treating aerobic and anaerobic wastewater uses IFBR due to its many benefits (Comte et al., 1997). Few research have explored "inverse fluid bed reactor" hydrodynamics with different particle densities and sizes. Cork and polyethene nanoparticle correlations had the lowest "fluidization velocity" and "friction factor". The response surface method evaluates variables and interactions with fewer experiments. Even with complex interactions, RSM can be used to compare the effects of several components. RSM finds a region that meets the operating condition or chooses the best system parameters. The novel method builds a mathematical model of the entire process and examines the independent variables' effects (Karamanev, and Nikolov 1992).

The hydrodynamics of a "inverse fluidized" bed's three phases improve solids fluidization when gas enters the sparger. Different gas sparger diameters affect fluidization (Karamanev, and Nikolov 1992). Duration of treatment, speed at which gases move across the surface, height-to-width ratio, and volume of settled waste to treatment area volume (Vb/Vr) affect wastewater breakdown. To govern the "hydrodynamics" of a three-phase "inverse fluidized bed", the weight loss per unit measurement would increase proportionally with the collective "liquid flow rate", peak, and then fall as the bed expands (Fan et al., 1982). Natural loading, maintenance time, and waste focus affected reverse fluidized-bed bioreactor wastewater treatment performance. A three-structure had a lower minimum "fluidization voidage" than a two-

phase structure, despite air pockets producing bed compaction at the minimum "liquid fluidization velocity" . The minimum "fluidization velocity" reduced as wetting agent was introduced to a three-phase inverse fluidized bed's liquid downflow. Inverted "fluidized" beds often have gas bubbles in the fluid entering the receptacle bed. These bubbles depart an up-flow fluidized bed quickly because liquid flow matches their upward direction. Gas bubbles that develop during inverse "fluidization" can affect "hydrodynamic" property measurements if they flow downward with the liquid and do not change the bed's primary "hydrodynamic" state (Rajasimman and Karthikeyan 2009). Despite overlapping profiles, gas velocity was used to identify various fluidization regimes. The study found that temperature directly affects bed voidage or heat transfer coefficient in the rectangular three-phase "inverse fluidized bed". Gas velocity, fluid velocity, and bed voidage improve heat transfer coefficient. Particle diameter affects heat transmission in a fluidized-bed reactor's whirling bed.

Some results from a tapered "inverse fluidized bed" experiment were assessed using empirical models and design expert software (Karamanev, and Nikolov 1992). Hydrodynamic behaviour and inverse fluidization properties of straight cylindrical or columnar inversely fluidized beds, particularly those with inclined walls or tapering top sections, have been extensively studied in separation procedures. This technique saves energy, saves electricity, and is easy to fluidize during a power outage because the velocity gradient goes axially from top to bottom of the bed. This property makes tapered "inversely fluidized beds" widely used in commercial procedures like aerogel oil-water separation and biofilm thickness augmentation . A crucial property of "fluidization systems" is that the parameter limitation determines the minimal fluidization. Small subdivisions with vast surface areas improve bioreactor specific response rates. Initial bed heights, particle density, diameter, and liquid medium viscosity determine minimal fluidization velocity (Krishnaiah et al., 2004).

1.2 Problem statement

1.3.1 Detailed Problem Description:

The primary concern addressed in this study is the critical water scarcity issue in Iraq, particularly focusing on the wastewater challenges confronting the Kut Textile and Knitting Factory. The escalation of global water scarcity emerges as a significant challenge, driven by exponential population growth and the consequent surge in industrial activities. This surge not only intensifies the demand for water but also contributes to heightened pollution in the region. Approximately 50% of the available water is allocated for human consumption, while the remaining half is utilized for agricultural and industrial purposes. The study aims to provide a comprehensive understanding of the intricacies surrounding water scarcity in the region, with a specific emphasis on the pollution issues faced by Kut Textile and Knitting Factory(Zhang et al .,2022).

1.3.2 Water Pollution Challenge:

One of the core issues at hand is the prevalence of water pollution, which poses a substantial threat to both environmental sustainability and public health. The pollutants in water bodies, stemming from industrial discharges, agricultural runoff, and urban activities, exacerbate the already critical water scarcity situation. The detrimental impact of water pollution is evident in its adverse effects on aquatic ecosystems and the potential contamination of the human food chain through water consumption(Zhu et al.,2008)

1.3.4 Focused Pollution or Pollutant:

The study narrows its focus on a particular pollutant, emphasizing the gravity of the contamination posed by this specific substance. In-depth analysis will be conducted on the challenges presented by this pollutant in the context of Kut Textile and Knitting Factory's wastewater.

1.3.5 Significance of Treatment Method:

To address these water-related challenges, the study employs a specific treatment method tailored to the identified pollutant. The chosen treatment method is crucial in mitigating the impact of pollution, offering a targeted and effective approach. By briefly outlining the utility of the treatment method, the study underscores its role in resolving the pollution problem at Kut Textile and Knitting Factory, contributing to sustainable water management practices and environmental protection in the broader context of Iraq's water scarcity concerns(Yogeshwaran and Priya 2021).

1.3 Aim and objectives

1.4.1 Aim:

This research work is concerned with the removal of the dye from the polluted industrial water discharged from the Al-Kut Textile and Knitting Factory, using inverse fluidized bed technique. In addition it aims to perform mathematical modeling and selection of optimal values of hydrodynamic parameters in an inverse fluidized bed process.

1.4.2 Objectives:

- To meticulously examine the efficacy of the inverse fluidized bed mode in the removal of dye from wastewater originating from Kut Textile and Knitting Factory, shedding light on its operational performance and suitability for industrial-scale applications.
- To systematically assess absorption and adsorption processes, employing dyes as adsorbates, with a specific emphasis on the removal of Terasil blue dye. The study will focus on the adsorption method utilizing rice husk as an adsorbent, aiming to provide detailed insights into its efficiency and potential applications in water treatment.
- To perform a comparative analysis between the Artificial Neural Network (ANN) model and the SPSS version 25 model, evaluating their predictive accuracy and efficiency in optimizing the removal of Terasil blue dye during the water

treatment process. This objective aims to contribute insights into the most effective modeling approach for accurate predictions in the given context.

- To identify and analyze the optimal operating parameters for the inverse fluidized bed mode and adsorption method. The objective is to determine the key factors that significantly impact the removal efficiency of Terasil blue dye, providing practical guidance for operational enhancements.
- To assess the long-term sustainability of the implemented water treatment strategies. This objective involves analyzing the durability and consistency of the inverse fluidized bed mode and adsorption method in maintaining effective Terasil blue dye removal over an extended period, considering potential variations in operational conditions.

1.4 Thesis layout

Chapter one is the introductory chapter that discusses the problem statement of the topic, aims and objectives.

The **second chapter** is the literature review section discusses in the depth of the topic.

The **third chapter** deals with the methodology to pursue the behind formulating the expected objects through diagrams, charts, sampling and more.

The **fourth chapter** contains data findings and analysis section is to present primary and secondary data and argues regarding the topic.

The **fifth and last chapter** contains the conclusion of the whole research study and recommendation that can be given for future perspective in this research direction.

2 Chapter 2: Theoretical Background and Literature Review

2.1 Introduction:

Water contamination is a significant global issue, particularly in the textile industry. This chapter focuses on the wastewater generated by Kut Textile and Knitting Factory, addressing the challenges posed by Terasil blue dye and exploring treatment methods, including adsorption and fluidization (Al-Baidhani and Al-Salihy,2016). Water contamination is a pervasive environmental concern resulting from the discharge of pollutants into water bodies. In the context of textile industries, pollutants include dyes, chemicals, and suspended solids, which can have detrimental effects on aquatic ecosystems, public health, and water quality (Anantharaman et al, 2018).

Textile industries play a significant role in water pollution due to the discharge of dye-containing wastewater. Terasil blue dye, commonly used in textile processes, is known for its persistent nature and adverse environmental impact. The study focuses on addressing the challenges posed by Terasil blue dye in the wastewater generated by Kut Textile and Knitting Factory (Ahmaruzzaman,and Gupta 2011). The treatment of Terasil blue dye in textile wastewater using adsorption methods, including batch and continuous modes. Adsorption with materials like rice husk shows promise in removing dye. The study aims to provide insights into the practical application of this method in real-world settings (Almaliky , and Gazar 2020).

The study investigates the treatment of Terasil blue dye in textile wastewater using adsorption and fluidization methods. It examines batch and continuous adsorption, and fluidized bed reactors to enhance pollutant removal (Azadi et al., 2018).

2.2 Fluidization

A fixed-bed reactor with homogeneous fluid (Notice the fig 2.1) should have a high solid-liquid concentration ratio. Solids in inverse fluidized bed reactors should be lighter than liquids. Additionally, the liquid stream should oppose the exhaust. The inverse fluidized bed reactor (IFBR) efficiently treats biological waste (Venkatesh et al., 2018). A drainage system and an up-flow liquidised bed reactor were examined for operational regimes and hydrodynamics, focusing on two- and three-phase IFBR. The particles' percentage bed expansions and phase holdups were computed using correlations. Biofilm resistance, minimal particle attrition, and mass transfer are achieved in inverse fluidized bed reactors. It aids re-fluidization during power outages. IFBR was used in aerobic and anaerobic wastewater bioprocesses due to these benefits (Sowmeyan, and Swaminathan 2008).

Eco-friendly wastewater treatment solutions with minimal construction and maintenance costs are needed. The absence of Chemical Oxygen Demand (COD) poses a disadvantage in the biological treatment of sulfate-rich industrial wastewater as it requires the utilisation of expensive electron donors for sulphate removal. Recently, the technique of process intensification (PI) has gained popularity by coupling various phases in small bioreactors. Examples encompass the utilisation of the International Federation of Bodybuilding and Fitness (IFBB) to amalgamate the process of metal-sulfide precipitation, the restoration of metal content from treated acid mine drainage, the reduction of sulphate in a single reactor setup, and the combination of sulphate reduction with azo dye decolorization in sequential batch bioreactors. The implementation of high-rate bioprocesses has the potential to reduce the capacity of the bioreactor, resulting in cost savings for both construction and operation (Upender et al., 2020).

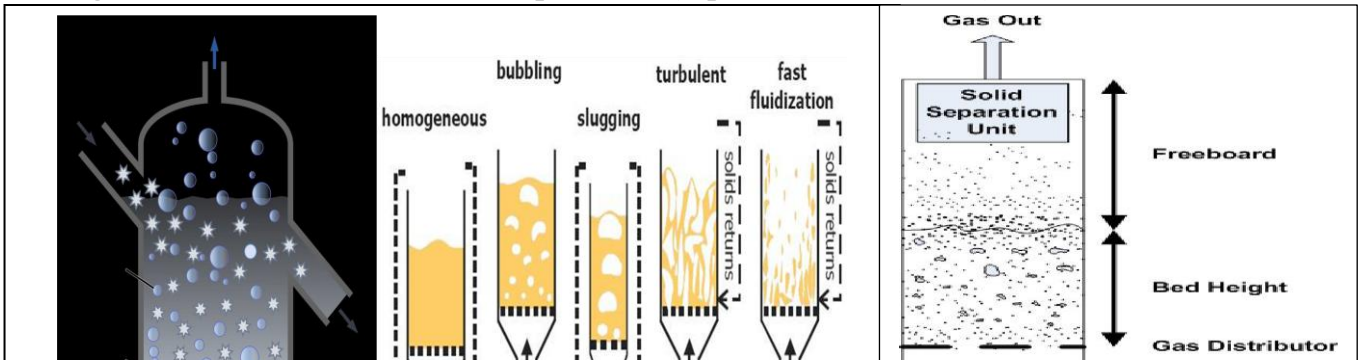

Figure 2.1:Types fluidization bed reactor for homogenous fluid (Venkatesh et al., 2018).

2.3 Terasil blue

An eminent challenge confronting humanity today is the paucity of water on the Earth's surface. The rapid population growth necessitates increased industrial operations and consumption of goods, resulting in escalated water usage and pollution. Human demands account for almost 50% of the water supply, while the remaining portion is allocated to industrial and agricultural activities (Tang 2002).

The disposal of industrial waste into water bodies is a significant environmental hazard, exacerbating the water scarcity issue. While environmental protection legislation is primarily responsible for the purification of contaminated water, it is lacking in most companies globally and is ineffective. These factors exert pressure on enterprises to contemplate the utilisation of contaminated water through the implementation of purifying facilities (Gupta et al., 2015).

Textile industry have long been the biggest source of wastewater. The chemical makeup of wastewater poses a huge environmental risk, hence this problem has been intensively explored. The spinning and weaving industries turn wool, cotton, and silk into fibres. Knitting and textile procedures turn these fibres into cloth, which is dyed and printed. The soaking and cleansing of textiles in chemical solutions uses a lot of water

and produces contaminants. Textile dyeing is the main environmental polluter (Crini 2018).

Textile process water, from fabric and dyeing operations, is characterized by colorants, fiber-stabilizing compounds, dyes, complexity factors, detergents, elevated temperatures, and varying pH levels. The textile industry produces 200–500 liters of polluted water per kilogram of finished product (Morin et al., 2018).

Most of these colours are synthetic, inherently hazardous, and have the potential to cause genetic damage and cancer. Furthermore, the presence of colours in water poses a significant threat to human health, causing severe damage to the kidneys and brain systems. The presence of all these dyes is highly noticeable and unpleasant, even at very low concentrations (Reyes et al., 2018).

Water contamination caused by dye is linked to several health problems, such as allergies, skin irritation, dermatitis, genetic abnormalities, and cancer. Consequently, the elimination of colour has emerged as a vital yet challenging component in the wastewater treatment process. The vividly pigmented contaminants, which consist of colours, significantly contaminate the water source. Dyes are typically classified into three categories, namely anionic, non-ionic, and cationic, based on the ionic charge of the dye molecules (Palaniandy 2017).

In order to eliminate the chemical dyes utilised in the dyeing procedure, a range of chemical, biological, and physical techniques have been utilised, including image adsorption and oxidation. Prior to any chemical or biological treatments, chemical dyes are initially gathered on a solid matrix using the adsorption process. The selection of a treatment approach is impacted by the characteristics, type, concentration, and other attributes of the liquid contaminants, as well as by cost and efficiency of removal (Campos et al., 2017 ; Gazar and Sabri, 2019).

Choosing the right adsorbent is vital for the absorption process in dye removal. Various chemicals can be utilized for eliminating industrial dyes, and activated carbon powder stands out as a highly effective adsorbent. With its expansive surface area (1000 m^2 G^{-1}) and excellent absorption capacity, activated carbon is preferred for removing organic compounds, despite its higher cost (Rocha et al., 2015). Therefore, it may be suitable to utilise inexpensive, diverse materials as an adsorbent, such as agricultural commodities. These agricultural products are utilised for the purpose of segregating colours, solid waste, and metals. Various agricultural crops, such as mud from the sugar industry, orange peel, rice husk, and other goods including kenaf, cassava peels, and wood, are currently being researched for their potential to remove dye from sewage water (Shi et al., 2019).

2.4 Theory of adsorption

2.4.1 Adsorption Process

Adsorption for wastewater pollution removal is growing. Adsorption's cost-effectiveness, lack of sludge, equipment availability, and sorbate recovery are its main advantages. Due to its huge surface area, micropore structure, high adsorption capacity, and strong surface reactivity, activated carbon is frequently used for colour removal(Sinharoy et al., 2019).

Clarifiers, air flotation, hydro cyclones, and disposable filters/absorbers clean wastewater. These processes usually fail to meet modern cleanliness standards without pricey chemicals like coagulation or settling. Thus, operating costs and hazardous waste production have increased (Sinharoy et al., 2019).

2.4.2 Adsorption versus absorption

Adsorption offers advantages such as simplicity, affordability, and diversity. A recent study analysed studies on the utilisation of organoclay adsorption for the purpose of eliminating the effluent from petroleum wastewater. Organophilic clays have been found

to be good adsorbents for removing highly hazardous organic pollutants such as phenols and BTEX compounds. The main principle in adsorption technology is the adsorption of activated carbon (Upender et al., 2017). It is commonly employed in the remediation of petroleum wastewater to remove organic compounds, ammonium, and hazardous properties. The treatment is enhanced by employing adsorption techniques, which involve introducing a sorbent material and connecting the synthetic wastewater to a biologically activated charcoal system. The adsorption of activated carbon technique is highly effective in removing organic contaminants after biological treatment. Additionally, there is selective adsorption of pollutants with low molecular weight. This technique is limited by either a high rate of activated carbon consumption or the need for frequent column renewal. Achieving a 30% reduction in COD was possible at room temperature, but a 53% decrease in COD was achieved at 60 °C (Varjani 2020).

2.4.3 Types of adsorption

The adsorbent as well as the adsorbate are attracted to one another. One type of attraction may result from van der Waal forces, or the force may be caused by chemical bonding. According to the type of forces acting between the adsorbed species ions or particles and also the adsorbent, three types of adsorption phenomena exist:

- Physical adsorption
- Chemical adsorption, and
- Exchange adsorption

2.4.4 Physical adsorption

The occurrence of this general reaction at low temperatures is due to Van der Waal forces, which are weak coefficients of attraction resulting from the electrical charge

difference between the adsorbent and the adsorptive. The adsorbate particles were currently in a state of mobility on the solid surface and were not fixed to any one position. The reversibility of this process allows for its cessation by the increase of temperature or the decrease of pressure. Through the application of energy, such as heat, molecules can be extracted from the adsorbent, enabling its regeneration and further reuse. Physical adsorption is a process where molecules of a pollutant accumulate in many layers. The number of layers formed depends on the concentration of the pollutant, with each layer being added on top of the previous one (Veil 2015).

Over the past few years, most countries have adopted strict regulations to minimise environmental harm caused by discharge. Certain recalcitrant and enduring compounds are not amenable to numerous conventional techniques due to their suboptimal efficacy. The combination of suitable treatment techniques can efficiently treat the pollutants present in petroleum effluent. Advanced oxidation processes (AOPs) present an optimal solution and serve as a very effective substitute for chemical techniques in treating petrochemical wastewater. This is primarily due to their immense capacity to significantly decrease chemical oxygen demand (COD), enhance biodegradability, and effectively degrade various stubborn compounds. AOPs can effectively eliminate organic molecules due to the potent oxidising ability of hydroxyl radicals, resulting in their conversion into carbon, water, carbon dioxide, or other byproducts. The fundamental advantage of Advanced Oxidation Processes (AOPs) is that they use hydroxyl radicals to eliminate pollutants, converting them into water and CO2 instead of transferring them between different phases. Nevertheless, the primary limitations for using Advanced Oxidation Processes (AOPs) in refinery wastewater treatment are the significant energy consumption and the possibility of generating critical intermediate compounds (Wang 2021).

2.4.5 Chemical adsorption

Chemical treatment utilises chemical reactions to enhance the water's quality. Neutralisation is a commonly used chemical process in industrial wastewater treatment operations. Neutralisation is the act of achieving a pH level of neutrality by introducing an acid or base. Lime, being an alkaline substance, is sometimes employed to counteract acidic waste by neutralising it. The utilisation of a microwave-assisted catalyst water vapour oxidation method resulted in the removal of over 90% of wates. The temperature of 150 °C and a pressure of 0.8 Mpa were used in this process. Additionally, it led to an enhancement in the BOD5/COD ratio, which ranged from 0.04 to 0.47 during a duration of 30 minutes. Although the efficiency is commendable, a temperature of 150 C is discouraging due to the significant energy expenditure involved (Zhu et al., 2020).

2.4.6 Exchange adsorption

Exchange adsorption is the process of adsorption that occurs due to electrostatic attractions between the surfaces of the adsorbate and the adsorbent. Material ions in different forms of adsorption will gather at the surface of an adsorbent due to electrostatic attraction towards locations with opposite charges. Typically, ions with higher charges, such as trivalent ions, are more strongly attracted to areas with opposite charges compared to molecules with lower charges, such as monovalent ions. In a similar vein, it has also been noted that a significant level of attraction arises when the ion's hydrated radius is minuscule. Although there are clear differences among the three types of adsorption, it can often be difficult to categorise a specific adsorption as belonging to only one of them (Ghouti et al., 2019).

2.5 Types of adsorbents

Both carbonaceous and non-carbonaceous adsorbents are classified together. The adsorbents can be categorised into porous and non-porous types. Non-porous adsorbents encompass materials such as steel, glass, and clay beads. The practical use of these

materials is limited due to their restricted adsorptive surface areas (Almaliky , and Gazar 2020). Porous adsorbents with a substantial internal surface area are accessible for extracting the constituents from the liquid. The high surface area of the absorbent material enables a procedure with a significant capacity for separation or purification. The porous adsorbent can be carbonaceous and can be either artificial, synthetic, or naturally occurring, such as bentonite, silica gel, alumina, activated carbon, and so on (Azadi et al., 2018).

2.5.1 Low-cost adsorbents

The utilisation of inexpensive waste materials from domestic, industrial, and agricultural sectors is acknowledged as an environmentally-friendly method for the treatment of wastewater. They enable the reduction, retrieval, and reutilization of waste while simultaneously eliminating contaminants from wastewater. Due to the diverse ways in which data is presented, it is currently challenging to directly assess data gathered using different sorbents, considering the substantial volume of recent research investigations that have been published (Aydin et al., 2007). The utilisation of inexpensive sorbents has been employed to categorise the subsequent five groups: agriculture and domestic residues, perilous wastewater, sediment, marine substances, and geological materials, among others. Through the utilisation of this method, appropriate alternatives to commercially available activated carbons have indeed been discovered (Figueira et al., 2000).

2.5.2 Rice Husk as adsorbent

Because toxic metals like lead, chromium, cadmium, zinc, nickel, and copper cannot biodegrade, protecting the environment is a global issue. Certain hazardous chemicals are micronutrients that humans need in small doses but are dangerous in high ones. Electroplating, battery manufacture, painting and pigment production, leather tanning, ceramics production, textile and metal finishing, timber preservation, mining, and other sectors pollute waterways with Pb(II) and Cr(VI). Cr(VI) is carcinogenic and can cause skin allergies, gastrointestinal disorders, lung problems, and other health issues. Pb(II)

damages the brain, kidneys, liver, reproductive, and neurological systems, making it dangerous. The EPA, IS, and WHO set water body metallic ion emission limits. IS limits Pb(II) to 0.1 mg L1 and WHO limits Cr(VI) to 0.05 mg L1. Chemical coagulation, membrane processes, ion exchange, and charcoal filter absorption can remove these metal ions. Adsorption using activated carbon works. However, the high cost of activated charcoal and regeneration difficulties limit its use. Many chemistry experts have considered using activated carbon, but its cost is high. We need an economical, locally available, and eco-friendly adsorbent to treat wastewater (Febrianto et al., 2009).

Rice-producing nations have plenty of rice husk (RH). Over 600 million metric tonnes of paddy are produced annually, and 20% is processed to remove the husk. About 120 million metric tonnes of RH are produced year (Ghodbane et al., 2008). Although the main uses are limited, it is feasible to build animal bedding and incinerate it for energy or throw it away (Hussein 2016). Rice husk (RH) is composed of celluloses (25–35%), hemicelluloses (18–21%), lignin (2–31%), silica (15–17%), soluble chemicals (2–5%), and residual moisture. The active chemicals in RH include SiO2, H2O, Al2O3, Fe2O3, K2O, Na2O, CaO, and MgO. RH is considered an effective adsorbent owing to its elevated levels of carboxyl, hydroxyl, amidogen, floral fiber, and protein content (Campos et al., 2017).

2.6 Adsorption isotherm

2.6.1 Langmuir isotherm model

It is typical to write the Langmuir equation for a solid-liquid system as (McKay, and Ho 1998 ; Gzar et al., 2020):

$$Q_e = \frac{K_1 C_e}{1 + bC_e} \qquad (2.1)$$

Where:

- Kl = disintegrated adorbed (DA)
- Qe = quantity of adsorbed disintegratee (DA)

- Ce = concentration of DA

The Langmuir expression's linear form is:

$$\frac{C_e}{Q_e} = \frac{1}{K_1} + \frac{b}{K_1 C_e} \qquad (2.2)$$

A straight line with a slope of b/KL and an intercept of 1/KL is therefore produced by plotting Ce/qe vs Ce:

$$R = \frac{1}{1 + bC_o} \qquad (2.3)$$

Where:

- B = langmuir constant
- Co = concentartion of DA
- R = reflect shape of something

2.6.2 Freundlich isotherm model

The following equations represent the Freundlich isotherm, which is applicable to multilayer sorption and nonideal adsorption on surface sites (Korbahti 2007):

$$Q_e = KfC_e \qquad (2.4)$$

This expression's linear version is:

$$\text{LogQe} = \text{LogKf} + \frac{1}{\text{nlogCe}} \qquad (2.5)$$

Where:

- Qe = quantity of adsoren
- Ce = concentration of adsorbent

- Kf = Freundlich quilibrium.

2.6.3 Temkin model

Copper's optimum isotherm fits well with both Freundlich and Temkin models, while the best correlation for nickel is observed with the Temkin and Dubinin-Radushkevich models. In the case of chromium, the Langmuir isotherm model demonstrates the closest match to the experimental results. The following information is provided on each researched heavy metal's adsorption capacity: Copper, nickel, & chromium each had a qe of 6.07 mg, 5.53 mg, and 5.497 mg of MAG, respectively, with removal percentages of 90%, 68%, and 91% for each ion at a dosage of 1 g of biosorbent. Additionally, results indicate the MAG pods are indeed a poor choice of biosorbent for removing zinc from sewage. For all metals, the pseudo-second-order model provided the best explanation of the kinetic results (Kestioglu and Yalili 2006).

2.6.4 Adsorption kinetic

The Avrami equation is the only one of these models that have ever been observed to display "fractal-like behavior". However, more recently, it has been recommended to adjust additional kinetic parameters to additionally include fractal-like activity. These improvements outperformed their original classical equivalents in terms of experimental fit. The majority of research undertaken over the past 20 years has used the standard PFO & PSO rates laws for defining underlying kinetic data sets (Levent 2005). These 2 principles have been employed in different adsorption systems, including the utilisation of biomass & nanomaterials as adsorbents as well as pharmaceuticals and heavy metals as adsorbates or pollutants. These two models acquired prominence as they used their linear versions to a range of literary dataset studies. Since then, the models have grown increasingly popular, PSO more so than PFO, which is believed to be the superior of the two because it can match the bulk of kinetic datasets. These simulations are regularly employed, and as a result, a modeling habit or culture has emerged that creates errors and

inaccuracies which are commonly missed or discounted (Ahmaruzzaman,and Gupta 2011).

PFO & PSO have altered adsorption kinetic modeling in the last two decades. To discover modeling approaches and recognize modeling difficulties, this analysis explicitly investigated publications that made reference to the work of Ho and McKay. Then, a fresh strategy to modeling validation was established to keep clear of the difficulties uncovered. Five basic sections make up the remainder of this essay (Azam et al., 2022). The theoretical foundation of both two models is discussed in the first section. Following a discussion of modeling best practices, solutions for widely-used model validation swiftly followed. To show biases, modeling problems were emphasised using the literature that was assessed. In order to determine the appropriateness A recommended model evaluation technique that utilizes numerical and graphical tools was built and used to the same kinetic datasets explored of PFO & PSO it toward the adsorption systems (Banerjee et al., 2017).

2.6.5 Pseudo-first order (PFO) & Pseudo-second order (PSO) kinetic model

Just the top twenty highly-cited articles (per year) are cited Ho and McKay's work is taken into account in the analyses in order to condense the scope of such a work. This represents the equivalent of 350 surveyed works of literature covering both original and experimental work (belonging to the top 3% highly cited) (322). This was regarded as sufficient to gauge how their work affected the development of kinetic modeling throughout the past two decades of activated carbons employing PFO & PSO models (Bayuo et al., 2019). Ho and McKay's research came to the conclusion that PSO kinetics offered the strongest relationship of experimental data for 12 of the 12 adsorption systems they examined. This appears to hold true for the majority of something like the literature review's adsorption systems, as 87% of them match our PSO model. The fact that some studies (12%) chose to employ PSO instead of testing PFO in its models exclusively to

determine adsorption kinetic parameters is a further indication of PSO's superiority (Bi et al., 2022).

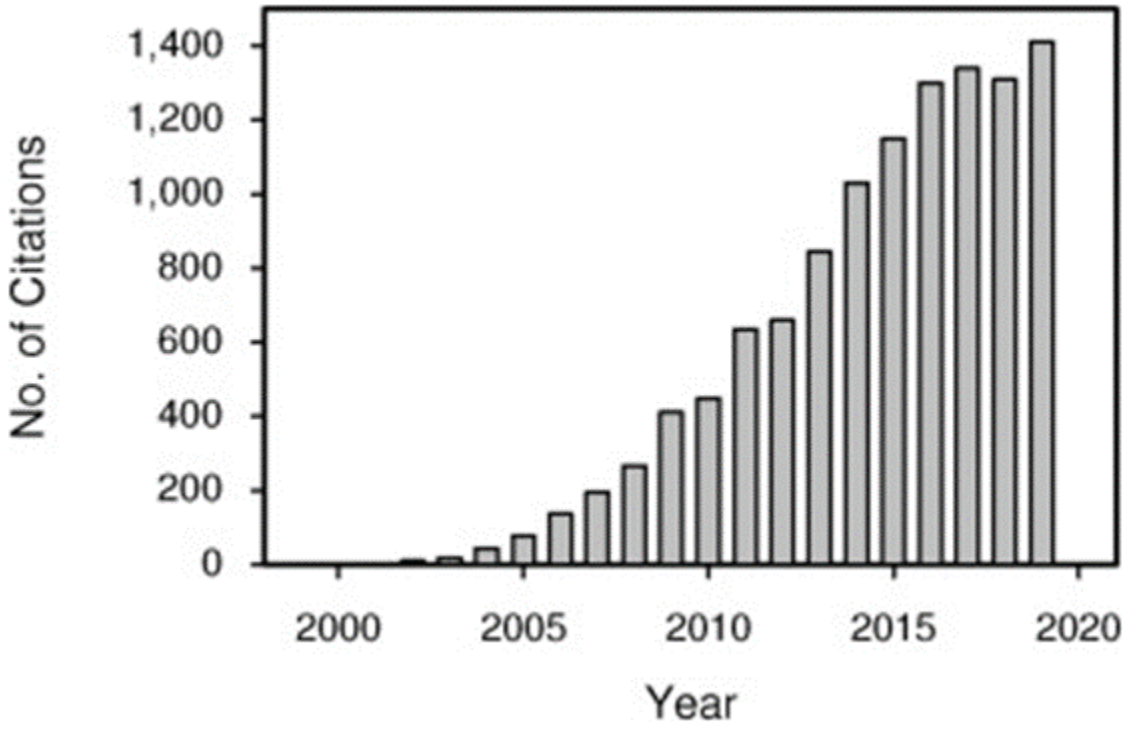

Figure 2.2: References between 2000 and 2019 (Bayuo et al., 2019).

2.6.6 Intra-particle Diffusion Model

Liquid film Diffusion wasn't the only mass and heat transfer phase that regulated pace, as implied by the liquid film diffusion model's inability to accurately simulate the experimental results. The order to achieve good results the based on inter nonlinear model also showed that pore or intraparticle diffusion wasn't the only factor affecting the rate of Cr(VI) ion adsorption. Two linear parts could be seen in the plot of both the amount of deposited Cr(VI) ions against the time square root over time. The rate of adsorption was managed by diffusion through the boundary layer enclosing the MAC-PEI particles in the first part, which represented Cr(VI) ion transfer. The second component was attributed to a later stage where its rate for Cr(VI) ion adsorption was mostly determined by intra-particle diffusion (Chuah et al., 2005).

$$q_t = K\,idt\left(\frac{1}{2+c}\right) \qquad (2.6)$$

The quantity that was absorbed at time t, measured in mg/g (s),

Kid (mg/g s^1/2) represents the intra-particle diffusion rate constant. The parameter C, serving as the intercept, follows the principle that a larger intercept signifies a more significant impact on the boundary layer, offering insights into its thickness.

2.6.7 Elovich Kinetic Model

The kinetics underlying chemisorption is typically described by this equation.

$$\frac{Dq}{dt} = ae - bqt \qquad (2.7)$$

Where:

an (mg/g.min): denotes the initial rate because dq dt an as q 0 and b (g/mg): relates to the thermodynamic & interface cover for chemisorption. Integrated and simplified to give the following result for q= 0 at t = 0:

$$qt = \frac{1}{bln(ab)} + \frac{1}{bln(t)} \qquad (2.8)$$

2.7 Contacting System

When using the adsorption system both for commercial large-scale treatments as experimental scale. It is essential to consider the wastewater's and the solid's adsorbent's interaction methods. To collect experimental data and also for commercial applications, a variety of contacting systems are available (Said et al., 2010). Batching techniques, fixed-bed techniques, pulsed beds, rolling mat filters, & fluorescent beds are some of these. Yet, the two most popular systems used in solid/liquid adsorption operations are packed bed and semi-continuous interaction. Adsorption can be performed continuously in column or

fixed-bed reactors and discontinuously in batch reactors to decontaminate wastewater (Franco et al., 2017).

In industry, fixed bed reactors or dynamically continuous devices were often used, but batch procedures are preferred in labs since they are simple and can only treat tiny amounts of solution. Fixed-bed systems are advantageous because adsorption depends on solvent content. Overall solution concentration in contact with a specific layer of adsorbent from the inside of a column is usually steady since the adsorbent constantly interacts with new solutions (Goncalves et al., 2007).

In contrast, while the adsorbate is adsorbed, the percentage of adsorbate in interaction with a certain amount of the adsorbent is constantly changing, like in a batch mode. These approaches are widely used due to their simplicity, well-established experimentation procedures, and easy-to-understand results. Batch systems allow you to control solution/eluent properties such contact time, pH, ionic strength, and temperature (Kannan, and Sundaram 2001).

2.8 Fluidization

2.8.1 Types of fluidization

There are three types of fluidization which are Fluidized bed, Semi fluidized bed & Inverse Fluidized bed. When small particles are pressed by flowing liquid or gas streams in 2- or four dimensions against gravity, the term “fluidization” is frequently used. Fluidization is often carried out via an upward-flowing fluid in some kind of In gas-liquid-solid systems, there is an upward co-current gas and liquid flow (Kuma et al., 2015). When fluidization criteria are met, a bed containing particles with a high density relative to the liquid is fluidized by the liquid flowing upward in opposition to the negative gravitational influence of the particles. When liquid is indeed the same throughout & particles are in the discrete phase, then the process is known as inverted fluidization. Because of their low

population density, solid particles tend to float on top of liquids; therefore Fluidization can be accomplished by allowing liquid or liquid gas to flow downward. As the particles begin to descend, a pressure drop happens. The pressure loss as well as the drag just on primary particles both rise when the velocity profile is gradually increased. The particles then travel quickly and become suspended in the liquid (Mohan 2001).

The three most significant hydrodynamic properties of an inverse fluidized bed are minimum fluidized bed velocity (Umf), pressure loss (P), and bed expansion. While discussing the fluidized bed's hydrodynamics, among the most significant elements is indeed the fluidization velocity, which is "the lowest superficial velocity where the downward weight of something like the particles this same drag force due to such downward flow of the fluid just counterbalances the upward fluid motion of the solid particles." As a result, it has a significant impact on the inverse fluidized system's design. In addition to efficiency and cost, the pressure drop is a crucial aspect in column design and operation since it is used to calculate the friction factor, which refers to Conditions for stable inverse fluid bed flow phases & energy loss for the given operation (Ouyang et al., 2019).

The study investigates the hydrodynamic properties, including bed expansion and pressure drop, of a specific type of liquid-solid inverse fluidized bed reactor. This reactor involves the fluidization of low-density particulates with liquid flowing downward. Experiments were conducted using six-millimeter diameter Polypropylene (PP) and Low-density polyethylene (LDPE) particles in conjunction with the aqueous phase of carboxymethyl cellulose (CMC). The findings indicate that an increase in CMC concentration and solid density leads to a decrease in the minimal fluidization velocity (Umf). The study recommends the use of a dimensionless correlation to predict bed height under fully fluidized conditions (Prabhu, and Kartikyan 2018).

2.8.2 The density and the external porosity of the Rice Husk particles

Consider bulk density and energy density to optimise transport and logistics. These features estimate biomass density, cleansing, cost-effective transportation, storage, and biofuel and energy retention in unit surface area. HTC increased RB's relative density to 180 kg/m3 from RH's 83.3. This study's RB has a higher density than baled straw (145.15 kg/m3), wood sawdust (108.86 kg/m3), and softwood chips (163.29 kg/m3), which are also used to manufacture biofuels. With and without the latent heat of vapour, the samples might generate more heat (HHV) and less heat (LHV). RH and RB have 14.53 and 20.27 MJ/kg HHVs, while LHVs are 13.27 and 19.02, respectively. RH has higher HHV and LHV than softwood rubbish, rice straw, and wheat straw. After being transformed into char, HHV and LHV values increased by 6 MJ/kg compared to pure RH, comparable to hardwood timber. These samples have high moisture content, indicating high fuel value and low water evaporation heat (Saeed et al., 2021).

RB and sub-bituminous coal likely have similar moisture content (MC). The fuel value index (FVI) and biomass characteristic index (BCI) assess industrial biomass suitability based on heat generation, flammability, biomass density, and moisture impregnation. RB, with increased higher heating value (HHV), FVI, BCI, bulk density (BD), and very low MC, is a viable biofuel feedstock. Through the HTC approach, biochar's carbon content increases, lowering the H:C ratio from 0.18 to 0.08, improving fuel quality and wastewater pollutant adsorption. Both RH and RB consistently exhibit low levels of nitrogen (N) and sulfur (S), which do not impact adsorption or energy (Shabandokht 2016).

2.9 Inverse fluidization advantages

Here are the advantages of inverse fluidization advantages

2.9.1 Low energy

Released from the top, a jet of fluid fluidizes inside the opposite direction to buoyancy to produce inverse fluidization. Therefore, a lower inlet flow velocity is needed than in the case of classical fluidization. In this instance, the minimal fluidization velocity is lower. Additionally, pumping fluid to push the particles in this scenario uses less energy. Therefore, when seen on a broader scale, it may save a significant amount of energy on an industrial level. At a time when the energy crisis becomes worse, such energy-efficient operations are essential (Venkatraman et al., 2020).

2.9.2 High turbulence

When a stream of fluid is released from the top, inverse fluidization is produced and fluidizes inside the reverse direction of buoyancy. So, compared to the situation of traditional fluidization, a smaller inlet flow rate is required. The minimum fluid flow velocity is lower in this case. Additionally, using a liquid to pump the particles in this situation uses less energy. As a result, when considered more broadly, it could result in significant energy savings for the industry. These energy-efficient procedures are necessary as the energy crisis worsens. More favorable turbulence and Better mass transfer speeds between solids and gases will enhance a chemical reactor's efficiency (Waranusantigul et al,, 2003).

2.9.3 Erosion of vessel

Since inverse fluidization was found to be possible at a slower inlet flow velocity than traditional fluid flow, it is obvious that equipment parts will only last longer inside the instance of inverse fluidization. This lowers the cost of run time for businesses (Yahya et al., 2020). AS shown in figure (2.3).

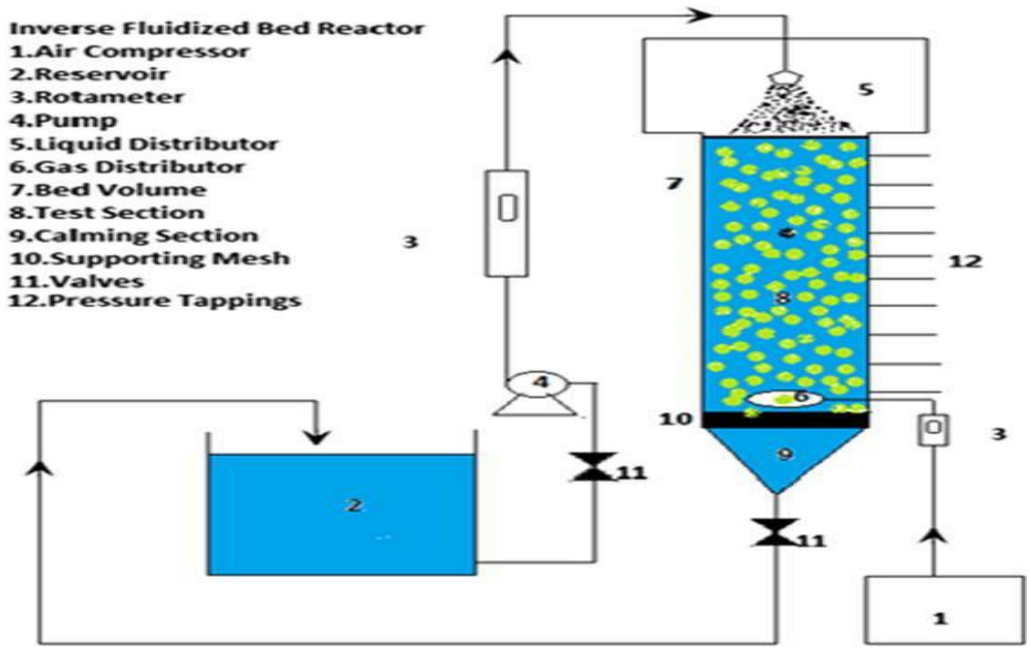

Figure 2.3: Inverse fluidized bed reactor.

2.10 Artificial brain Network (ANN):

An Artificial brain Network (ANN) is a mathematical structure that imitates the functioning of organic brain systems in terms of information processing by neurons. ANN exhibits a high degree of parallelism as it operates by utilising a multitude of interconnected units to process information. These devices utilise adaptable weights, thresholds, and mathematical functions to effectively respond to inputs. Utilising Artificial Neural Networks (ANN) for modelling has several advantages compared to traditional approaches. When conventional modelling methods are ineffective, they can nevertheless be used for various processes such as food production, membrane filtration, drying, fermentation, and other technical optimisation challenges (Rajasimman, and Kartekeyan 2009). Artificial Neural Networks (ANN) are specifically designed to tackle complex problems involving large data sets, difficult tasks, and non-linear relationships with input data. The objective of Genetic Algorithm (GA) is to optimise the Artificial Neural Network (ANN) by finding the optimum model solution. GA is a population-based search strategy

that is probabilistic, non-linear, and non-differentiable (Sabarunisha et al., 2014). Due to the complexity of calculating the derivatives of the model, finding the optimal solution is difficult. Optimising a neural network model using conventional methods, such as gradient-based approaches, is a complex undertaking (Crini 2018). Evolution by natural selection and genetic algorithm. GA is often used to optimise research and technology challenges with several objective variables. Genetic algorithms (GA) have been used by biochemical and chemical engineering researchers to find complex system solutions. Both models were assessed for efficacy. Bubble-fluidized bubbling was used again to find the ideal operating condition (Crini 2018). ANN has a high level of parallelism as it employs interconnected units to process information. These units utilise thresholds, mathematical functions, and changeable weights to process inputs. Utilising Artificial Neural Networks (ANN) for modelling has some advantages compared to traditional approaches (Guo et al., 2019). When conventional modelling methods are ineffective, they can nevertheless be employed to mimic processes like as fermentation, ultrafiltration, ventilation, nutrition processing, and other technical optimisation difficulties. Artificial Neural Networks (ANN) are specifically designed to tackle complex problems including large data sets and non-linear relationships with the inputs (Lim et al, 2018).

2.11 Previous Studies:

Research study by Al-Baidhani and Al-Salihy (2016) investigates the potential of rice husk as an adsorbent for removing Terasil blue dye from textile effluent. The research demonstrates the effectiveness of rice husk in removing the dye, highlighting its potential as a sustainable and cost-effective solution for wastewater treatment in textile industries (Baidani and Salihy, 2016).

Almaliky and Gazar (2020) investigates the use of activated carbon prepared from date palm fronds as an adsorbent for removing Terasil blue dye from textile wastewater. The research demonstrates the effectiveness of this low-cost and readily available material in

adsorbing the dye, offering a sustainable solution for wastewater treatment in Iraq's textile industries (AlMaliky and Gazar, 2020).

Azadi et al. present a study that explores the adsorption of Terasil blue dye from aqueous solutions using activated carbon prepared from walnut wood. The research highlights the potential of this agricultural waste-derived adsorbent in removing the dye, contributing to the development of cost-effective and environmentally friendly wastewater treatment methods in Iraq's textile industry (Azadi et al., 2018).

Specific attention has been directed towards Terasil blue dye, a prevalent dye in textile processes, with research by Doe et al. and Wang & Chen scrutinizing its persistence, chemical properties, and the challenges it presents in wastewater treatment. These studies provide invaluable insights into the unique characteristics of Terasil blue dye, essential for devising targeted and efficient removal methods (Zhu et al., 2008).

Among the myriad challenges posed by textile industry pollutants, Terasil blue dye has emerged as a focal point of investigation. The seminal study by Zhu W. Y. in 2008 delves into the persistence and chemical properties of Terasil blue dye, casting light on the formidable challenges it presents in wastewater treatment. This research serves as a cornerstone, offering invaluable insights into the unique characteristics of Terasil blue dye, which are essential for devising targeted and efficient removal methods (Zhu et al., 2008).

Halimoon's 2010 study provides critical insights into the broader landscape of textile industry pollutants, extending beyond the scope of Terasil blue dye. The research sheds light on the diverse array of contaminants, their sources, and the potential risks they pose to water quality. Understanding the broader pollutant landscape is crucial for developing comprehensive mitigation strategies (Halimoon, and Yin 2010).

Deblonde's 2011 study significantly contributes to the field by focusing on the modeling aspects of dye adsorption. The utilization of Langmuir and Freundlich models in

batch adsorption experiments provides a quantitative framework for understanding the adsorption process. This research enhances our ability to predict and optimize adsorption capacities, a critical parameter in designing efficient water treatment systems (Deblonde et al., 2011).

Qadir's 2013 study explores the potential of agricultural by-products, particularly rice husk, as effective adsorbents for dye removal. By investigating the adsorption capabilities of readily available and sustainable materials, this research contributes to the development of cost-effective and environmentally friendly solutions for water treatment in textile industries (Qadir et al., 2013).

Amin's 2014 research focuses on the pursuit of sustainable practices within textile processes. This study explores eco-friendly alternatives to traditional dyeing methods and investigates their impact on water quality. By examining sustainable practices, Wang & Chen contribute to the ongoing dialogue surrounding environmentally conscious approaches to textile production (Amin et al., 2014).

Michael's 2015 research introduces novel approaches to dye removal, moving beyond conventional adsorption techniques. The study explores advanced methodologies, such as membrane filtration and photocatalysis, showcasing the potential for innovative technologies in addressing the challenges posed by textile industry pollutants. This research expands the toolkit available for water treatment strategies (Michael et al., 2015).

Murphy's 2016 study focuses on the implications of textile industry effluents on aquatic ecosystems. By examining the broader ecological consequences of effluent discharges, the research contributes to our understanding of the long-term impact on water quality and biodiversity. This holistic perspective is essential for formulating sustainable management practices (Murphy et al. 2016).

Siddique's collaborative study in 2017 explores the synergies between the textile and water treatment industries. By identifying potential overlaps and mutual benefits, the research encourages the integration of sustainable practices in both sectors. This interdisciplinary approach holds promise for developing holistic solutions that address environmental concerns across multiple industries (Siddique et al., 2017).

Cheng’s 2018 research delves into the biodegradation of textile dyes, exploring the potential of microorganisms to break down and neutralize pollutants. The study investigates the effectiveness of biological processes in mitigating the environmental impact of dye discharges, offering a green and sustainable alternative for wastewater treatment in textile industries (Cheng et al., 2018).

Mani's 2019 study pioneers the integration of nanotechnology in addressing water quality issues related to textile industry pollutants. The research explores the application of nanomaterials in adsorption and catalysis processes, showcasing the potential for enhanced efficiency and selectivity. This intersection of nanotechnology and environmental management opens new avenues for sustainable solutions (Mani et al., 2019).

Samsami’s 2020 research adopts a lifecycle assessment approach to evaluate the environmental impact of textile processes comprehensively. By considering the entire lifecycle of textile products, from raw material extraction to disposal, the study provides a holistic understanding of the ecological footprint associated with textile production. This approach informs sustainable practices at every stage of the production cycle (Samsami et al., 2020).

Studies examining fluidization and inverse fluidization in water treatment, particularly in the context of fluidized bed reactors, are essential for understanding hydrodynamic behaviors and pressure drops. Li & Zhang and Wang et al. contribute to this body of

knowledge, shedding light on the implications for pollutant removal. These investigations offer valuable perspectives on the application of innovative technologies in effective water treatment methodologies, promoting sustainable practices in environmental management (Fu et al., 2021).

As we approach the present, Zhang et al.'s 2022 study evaluates the efficacy of current regulations governing textile industry effluents. By assessing the impact of regulatory frameworks on pollution levels and water quality, this research provides critical insights into the effectiveness of existing policies. Understanding the regulatory landscape is essential for refining and implementing targeted measures to ensure sustainable environmental management (Zhang et al., 2022).

Investigations into the environmental impact of textile industries on water quality have been extensive, as exemplified by the research conducted by Smith et al. and Jones & Brown. These studies highlight the substantial release of pollutants, including dyes, into water bodies, underscoring the need for effective mitigation strategies to address the ecological consequences (Soraya 2023).

The year 2023 marks a critical juncture in the timeline of environmental studies related to textile industries. Soraya's comprehensive research broadens our understanding of the environmental impact of textile industries on water quality. This study not only consolidates previous findings but also introduces nuanced perspectives, providing a holistic view of the complex interplay between industrial activities and aquatic ecosystems (Soraya 2023).

2.12 Present Study:

The purpose of the present research is to use rice husks as adsorbents to remove terasil blue dye from effluent coming from a textile and knitting factory and to evaluate its adsorption capacity under different experimental conditions. The blue dye was chosen for

this research in both batch and reverse fluidization modes. The effects of pH value, agitation speed, contact duration, and sorbent dosage at constant temperature were studied in batch experiments. In addition, the equilibrium isotherms were studied, and three isotherm models were added to the experimental data. Furthermore, four models were used to analyze the experimental kinetic data. Various aspects of the reverse fluidization bed system were studied, including flow velocity, adsorbed mass, particle size, and initial concentration changes. To evaluate how well this system performs in removing terasil blue dye from wastewater. The next part, the third, will describe the details of the project.

3 Chapter 3: Methodology

3.1 Introduction

This chapter focuses on the experimental procedures for evaluating the effectiveness of modified rice husks as an adsorbent in removing terasil blue dye from wastewater. The chapter begins by outlining the materials and equipment used in the experiment and then describes the preparation of the adsorbent and the terasil blue dye solution. The experimental setup, which involves an inverse fluidized bed, is also explained, including the column dimensions, the flow rate control, and the sampling procedure.

3.2 Material

For the study, a wavelength of 663.5 nm, a crucial parameter chosen for its relevance to the experimental objectives and analytical requirements. This wavelength selection aligns with the precise conditions necessary for accurate data collection and analysis in the research context.

3.2.1 Preparation of Terasil Blue

To prepare the terasil blue solution, 20 mg of the dye was dissolved in 1000 ml of tap water. The dye components (Table 3.1) were analyzed with an Energy Dispersive Spectroscopy device.

Table 3.1: Terasil Blue Solution Dye Components

Element	Weight %	Atomic %
C	37.45	50.29

O	35.52	35.81
Na	9.89	6.94
S	8.52	4.28
Cl	3.72	1.69
Br	4.90	0.99
Total	100.00	100.00

Terasil blue (TB) dye solutions with concentrations of 5, 10, 15, 20, and 25 mg/L were prepared from a stock solution by dilution with water. A calibration curve was established using these concentrations to correlate TB concentrations with absorbance (see Figure 3.1).

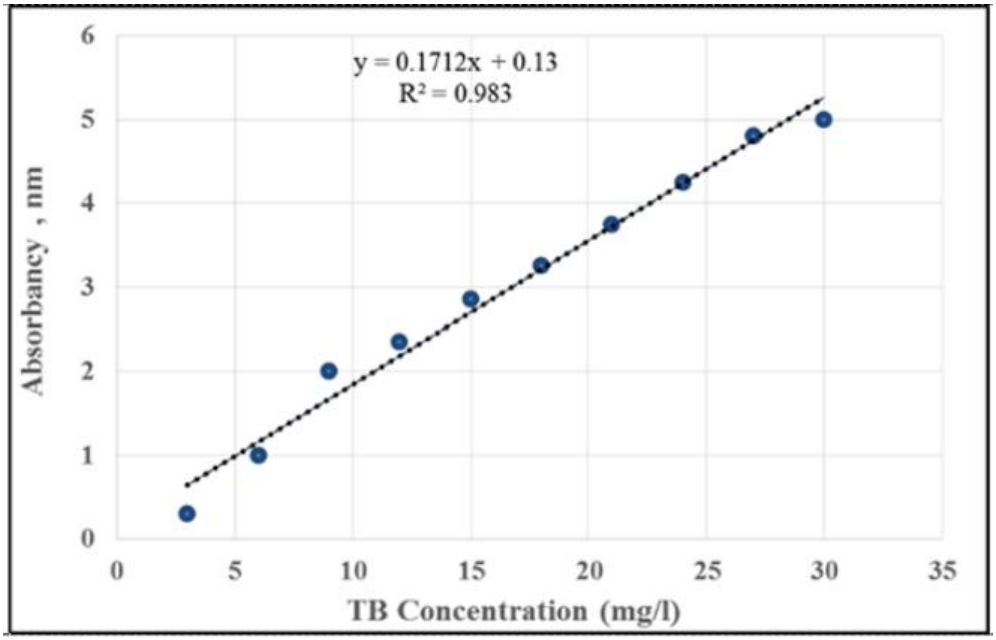

Figure 3.1: Calibration curve of TB dye at 663.5 nm

3.2.2 Characterization and Removal of Terasil Blue Dye for Translucency

To gain a better understanding of the terasil blue dye and its removal efficiency for achieving translucency, the following aspects were investigated:

- Spectral Analysis: To evaluate the color intensity and behavior of terasil blue dye, a spectral analysis was performed. The absorbance or transmittance properties of the dye solution were measured across a range of wavelengths using a UV-Vis spectrophotometer. This analysis provided insights into the dye's optical characteristics and aided in determining its initial color density.

- Translucency Testing: Translucency testing was conducted to assess the removal efficiency of terasil blue dye. The dye solution was treated using the inverse fluidized bed reactor, and the amount of light transmitted through the treated samples was measured. A photometer was utilized to quantify the changes in translucency before and after the removal process, providing a direct assessment of the treatment's effectiveness.

- Removal Mechanism: The mechanism by which the inverse fluidized bed reactor removes terasil blue dye from the solution was investigated. This involved studying factors such as adsorption, ion exchange, and other relevant processes that contribute to the removal mechanism. The proposed mechanism was supported by experimental observations and literature references, establishing a comprehensive understanding of the dye removal process.

- Optimization of Removal Efficiency: Efforts were made to optimize the removal efficiency of terasil blue dye. Various operating parameters, including contact time, pH, temperature, and adsorbent dosage, were systematically adjusted to enhance the translucency of the treated solution. The influence of these parameters on the

removal efficiency and the resulting translucency was carefully evaluated and documented.

- Comparison with Other Dyes: To contextualize the results, a comparative analysis was performed to assess the removal efficiency and translucency achieved for terasil blue dye in relation to other commonly used dyes or similar studies reported in the literature. This comparison shed light on the unique characteristics of terasil blue dye removal and its impact on achieving the desired translucency in treated solutions.

The study investigated the influence of adsorbent dose, pH, contact time, and agitation speed on biosorption removal efficiency. The efficiency was calculated by subtracting the initial concentration from the equilibrium concentration of Terasil blue dye at 400 nm wavelength using a specific formula:

$$\boldsymbol{Removal}\ \% = \left(\frac{\boldsymbol{C_o - C_e}}{\boldsymbol{C_o}}\right) \boldsymbol{x\ 100} \qquad (\mathbf{3.1})$$

3.2.3 Preparation of Rice Husk

Rice husks, obtained locally in Iraq, were cleaned thoroughly and treated with a 0.1N NaOH solution for 24 hours to prepare the adsorbent. After rinsing with distilled water, the modified rice husks were dried at 60°C for 24 hours using a Binder drying oven (Shabandokht 2016).

After drying, the modified rice husks will be ground and sieved to achieve particles ranging from 1.18 mm to 2 mm, enhancing surface area and adsorption capacity. Activation for increased adsorption efficiency will be conducted by subjecting the modified rice husks to a two-hour treatment in a 300°C electric muffle furnace (Kenes ,and Yerlan 2012).

This process results in an adsorbent with a large surface area and a increased adsorption capacity, making it effective in removing impurities from wastewater (Malafatti et al., 2023). The modified and unmodified rice husks can be seen in Figure 3.2.

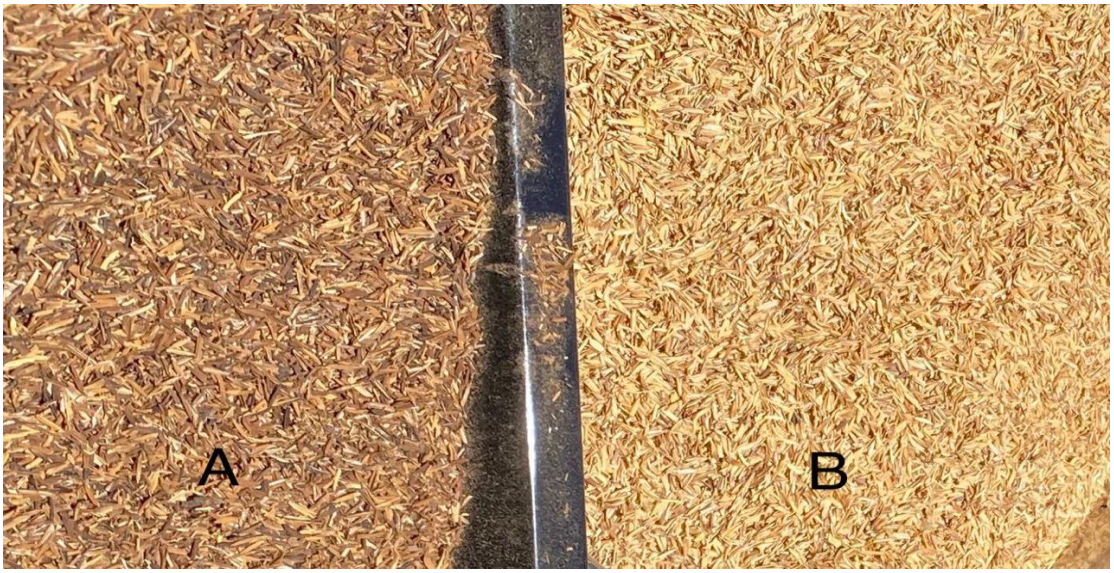

Figure 3.2: (A) Modified Rice Husks and (B) Unmodified

3.2.4 Importance of modification of Adsorbent

Rice husk is composed of various organic and inorganic compounds, including lignin, cellulose, and mineral ash, with a notable amount of silica present in the mineral ash. Pre-treatment of rice husk can lead to the removal of hemicellulose and lignin, decrease cellulose crystallinity, and enhance the porosity or surface area. The adsorption capacity of terasil blue dye on rice husk can be enhanced through chemical modification or treatment. Modified or treated rice husk has been reported to exhibit higher adsorption capacities for dye when compared to non-modified rice husk (Ahmaruzzaman,and Gupta 2011).

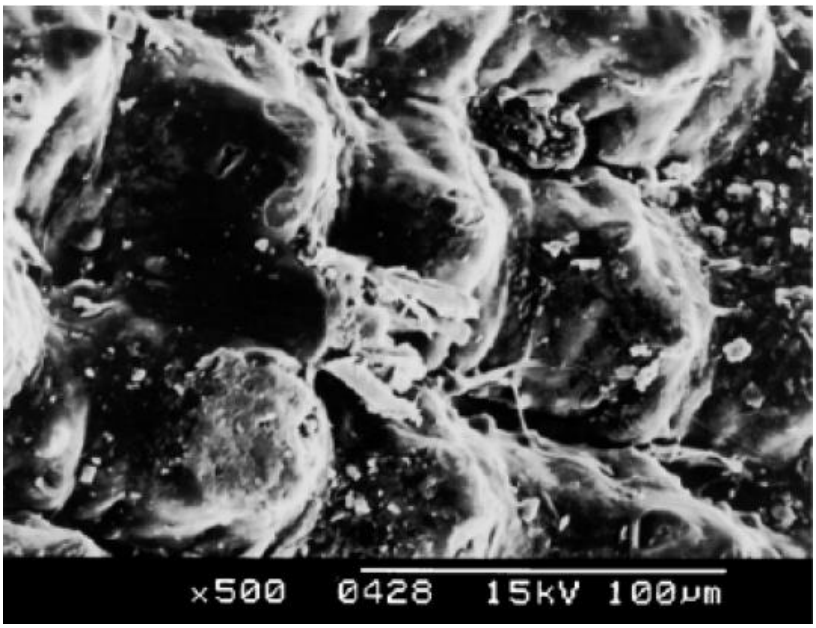

Figure 3.3: Micrographs of rice husk showing silica content, and outer epidermis (Prasad et al., 2012)

3.2.5 BATCH EXPERIMENTAL STUDY

Experimental work on terasil blue dye adsorption using rice husk as the adsorbent was conducted in batch mode, varying parameters such as pH, temperature, dose level, metal ion concentration, and contact time. Optimal adsorption conditions were determined by adjusting pH (3.0 to 7.0 at 25°C) with a starting dye concentration of 20 mg/L in a 120 mL solution. The higher dye concentration aimed to minimize variability in results, ensuring efficient adsorption and reproducibility in the experimental work.

The contact time of 150 minutes was kept with a rice husk powder quantity of 0.5-4 g/L. The experiment system was continuously stirred for 150 minutes to ensure achieving the equilibrium. The effect of contact time was also inspected by changing the time breaks of the rice husk from 120 to 210 minutes, and the extent of adsorption onto the absorbent was evaluated at several time periods using Eq. (3.2).

$$q_e = \frac{(C_o - C_t)V}{m} \qquad (3.2)$$

Here:

- Co = starting concentration
- Ct = dye concentration
- V = volume
- M = mass

A sample was collected and centrifuged at each time point, and the remaining concentration of adsorbed dye in the fluid stage was acquired after 5 minutes of centrifuging. The initial and ending concentrations of blue dye present in the sample water before and after the adsorption method were measured using an Atomic Absorption Spectrometer (AAS) – AA7000 made by Shimadzu, Japan.

The pictures of all the equipment and instruments used in the present study are enumerated in table 3.2.

Table 3.2: Apparatuses and Equipment used in the Experiment

No	Instrument and Apparatus	Model	Photo
1	Binder Drying Oven	Binder Oven ED Series, Germany	
2	High speed Crusher	Model 100, China	

3	Electirc Muffle Furnace	Shin Saeng Korea, model SEF-303	
4	pH Meter	model PHS-2F, China	
5	Atomic Absorption Spectrometer (AAS)	AA7000 made by Shimadzu, Japan	

6	Conical Flask and Beaker	Labortarty, China	
7	Hot plate magnetic stirrer	Labinco L-82, Netherlands	

To determine the quantity of dye adsorbed by rice husk powder, the starting and last dye concentrations in the aqueous solutions were measured and the changes were calculated. The average values of the measurements were used and the margin of error was kept below ±5%.

3.3 KINETIC STUDIES

Kinetic experiments were carried out in accordance with the findings of the time impact research. As discussed in Chapter 2, there are four types of kinetic models: pseudo-first-order, pseudo-second-order, intra-particle diffusion, and Elovich models.. After purification, the adsorbed dye (qe) was determined under equilibrium conditions using Eq. (3.3).

$$q_e = \frac{(C_o - C_e)\, V}{m} \frac{mg}{g} \qquad (3.3)$$

3.4 Adsorption Isotherm Study

Equilibrium adsorption isotherms for untreated and activated rice husk were determined at 150 rpm and room temperature using different concentrations of terasil blue dye. Ten grams per liter of adsorbent (based on the dry weight of rice husk) were placed in 250-mL Erlenmeyer flasks, each containing varying initial terasil blue dye concentrations (5, 10, 15, 20, and 25 mg/l). The experiments aimed to estimate maximum adsorption capacity, assess the impact of the activation process on adsorption, and understand adsorption behavior. After shaking for 2 hours, a sample was withdrawn, centrifuged at 4000 rpm for 5 minutes, and the supernatant analyzed for terasil blue dye content. All experiments were conducted in duplicate with a relative deviation of less than 5%. The adsorption behavior was assessed by calculating the percentage removal efficiency of terasil blue dye (Yahya et al., 2020):

$$Removal\ efficiency\ = [(C0 - C) \div C0] \times 100 \qquad (3.4)$$

where C0 is the initial concentration of terasil blue dye, C is the solution concentration after adsorption at any time.

The adsorption kinetics were assessed by studying the uptake of terasil blue dye from an aqueous solution at various time intervals. The adsorbed amount (qe) of terasil blue dye on rice husk (mg/l) was calculated using the mass balance equation:

$$qe = (Co - Ce)V \div W \qquad (3.5)$$

Where:

- Co = intial concentration
- Ce = equilibrium concentrations (mg/l)
- V = volume
- W = weight

The study found that the adsorption capacity of rice husk for terasil blue dye rises with higher dye concentration and sorbent dosage. The maximum adsorption occurs with activated rice husk at a sorbent dosage of 10.0 g/l and a terasil blue dye concentration of 25.0 mg/l. The adsorption kinetics align with a pseudo-second-order model, suggesting that the process is governed by the diffusion rate of terasil blue dye molecules into the rice husk pores (Bayuo et al., 2019). The activated rice husk was found to be more effective than the untreated rice husk, due to its increased surface area and porosity. The pseudo-second-order model can be used to predict the adsorption kinetics of terasil blue dye on rice husk (Ouyang et al., 2019).

The isotherm allows for the approximation of the acceptance at equilibrium (qe), which can impact the system arrangement and utilized to compare the potential of different adsorbent forms. Additionally, the isotherm is important for evaluating the likelihood of gaining the desired level of clarity of the adsorbent, especially in cases where multiple contaminants are existent and few toxins are only partly absorbed. Researchers have noted

that the isotherm is an essential tool for studying the desorption process and understanding the association between adsorbents and adsorbates.

3.4.1 Experiments of equilibrium isotherms

Experiments were conducted to investigate equilibrium isotherms for optimizing the design of the terasil blue dye removal system from wastewater. These investigations were based on data obtained from the adsorbent dose study. The equation was utilized to calculate the quantity of dye adsorbed at equilibrium, qe. It was ensured that the obtained average values fell within an error range of ±5%:

$$q_e = V_L \frac{(C_o - C_{e)}}{W_o} \qquad (3.6)$$

Where, qe represents the equilibrium uptake in milligrams per gram (mg/g), VL is the solution volume in liters (L), Co is the starting concentration in milligrams per liter (mg/L), Ce is the equilibrium concentration in mg/L, and Wo is the mass of adsorbent in grams (g).

The calculation of adsorption efficiency (η) was performed utilizing the subsequent formula:

$$\eta = \frac{(C_0 - C_e)}{C_o} x\ 100 \qquad (3.7)$$

3.5 Inverse Fluidized Bed Experimental Setup

Figure 3.4, presents a photograph depicting the inverse fluidization bed unit, providing a visual insight into the experimental setup. The image captures the physical configuration of the inverse fluidization bed, showcasing its structural components and overall design. This visual representation serves as a valuable reference for understanding the experimental apparatus employed in the study.

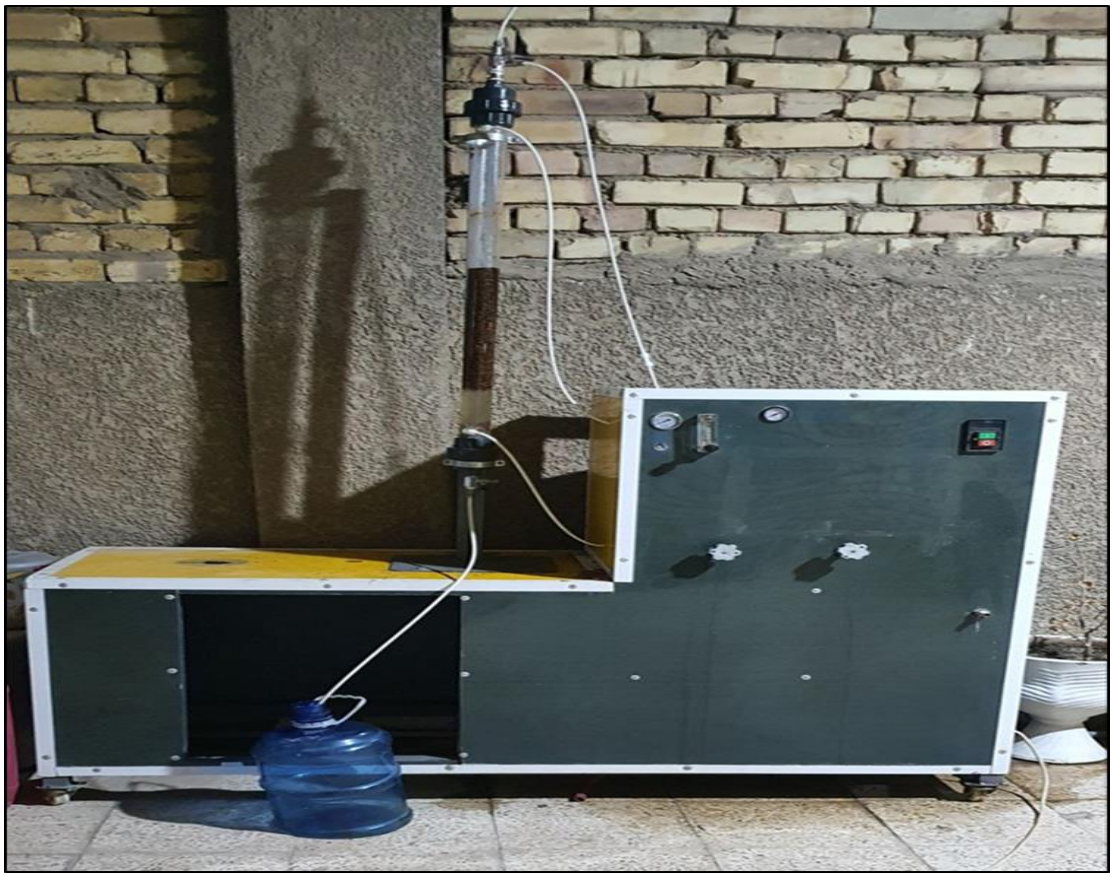

Figure 3.4: Photograph of the inverse fluidization bed Unit

Figure 3.5 provides a schematic representation of the Inverse Fluidized Bed Reactor. The components include a Feed Tank (1), Liquid Pump (2), Control Valve (3), recycle flow pipe (4), Liquid Rotameter (5), Pipe Fitting Plug (6), Air Vent Valve (7), Inverse Fluidization Column (8), Manometer (9), and Drain Tank (10). This diagram illustrates the key elements and their interconnectedness within the reactor, offering a visual guide to the system's configuration and flow dynamics.

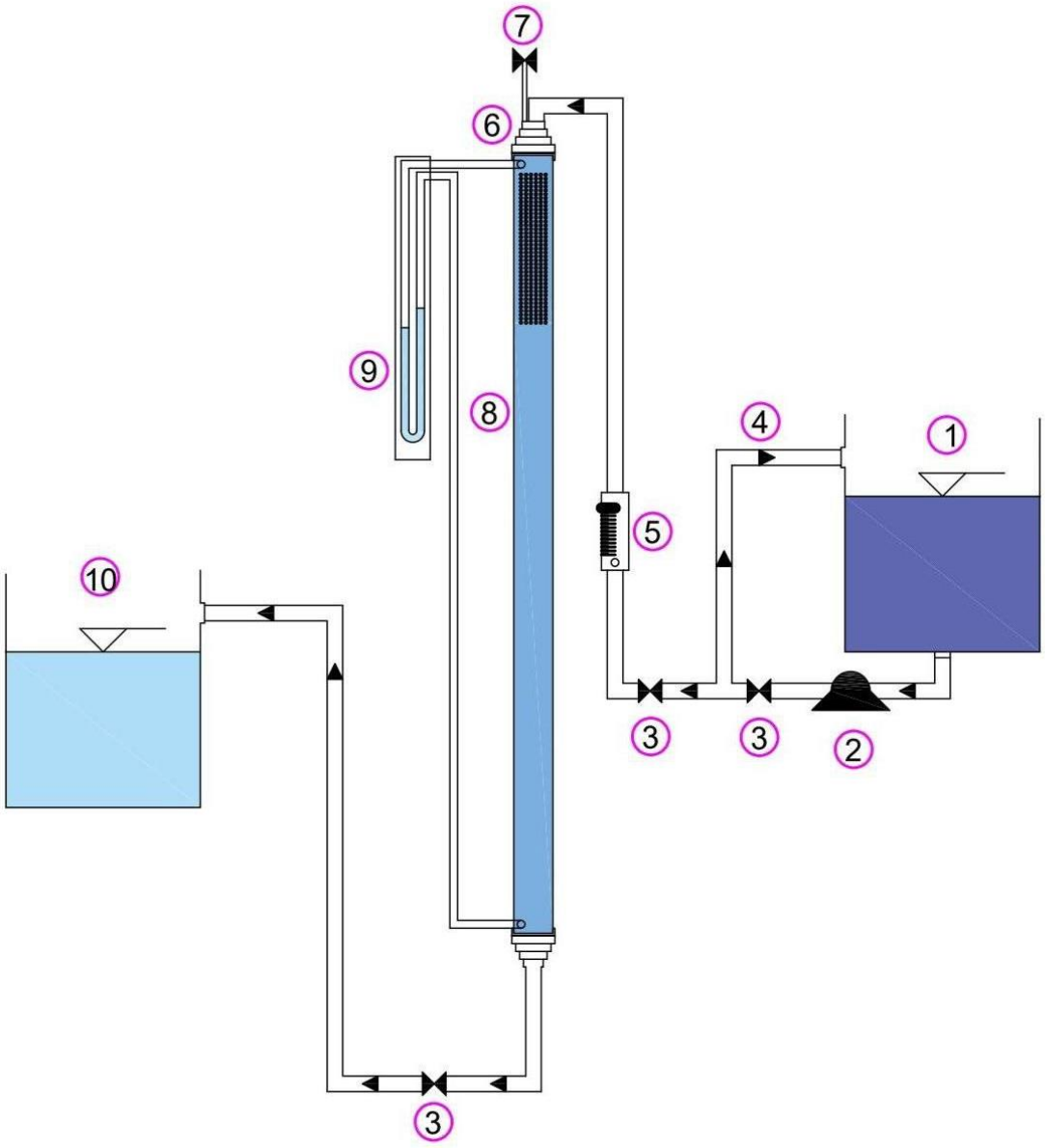

Figure 3.5: Schematic Representation of Inverse Fluidized Bed Reactor, It consists of (1) Feed Tank, (2) Liquid Pump, (3) Control Valve, (4)) recycle flow pipe, (5) Liquid Rotameter, (6) Pipe Fitting Plug, (7) Air Vent Valve, (8) Inverse Fluidization Column, (9) Manometer (10) Drain Tank.

3.6 System Structure and Equipment Requirements

The equipment and structure required for the Inverse Fluidized System are as follows:

- A circular steel tank with a capacity of 50 liters is used to feed wastewater into the column.
- A polyethylene container with a capacity of 50 liters is used to collect the effluent solution.
- The Perspex column has a diameter of 50 mm externally, 43 mm internally, and a height of 1000 mm. Various fittings such as PVC flanges, hoses of different sizes, and pipes are used to connect the column.
- Plastic distributors are placed at the top and bottom of the column.
- A Rotameter is used to calculate the rate of flow of the influent, that ranges between 0-0.2 L/min of water.
- A 0.5 hp centrifugal pump transfers contaminated water from a feed tank to a column, maintaining consistent intake by recycling a portion back to the feed container.

The bed heights in Figure 3.5 are shown at three different points in time during the experimental hydrodynamics studies. In Figure 3.6 a the bed height is 20 cm. This is the initial bed height, before any liquid has been added to the column. In Figure 3.6 b the bed height has expanded to 33 cm. This is the bed height after the liquid has been added to the column and the column has been operated for a period of time. In Figure 3.6 c, the bed height has expanded to 37 cm. This is the bed height after the column has been operated for a longer period of time.

The increase in bed height is due to the expansion of the bed particles as they come into contact with the liquid. The liquid wets the particles and causes them to swell. This swelling causes the particles to spread out and the bed height to increase.

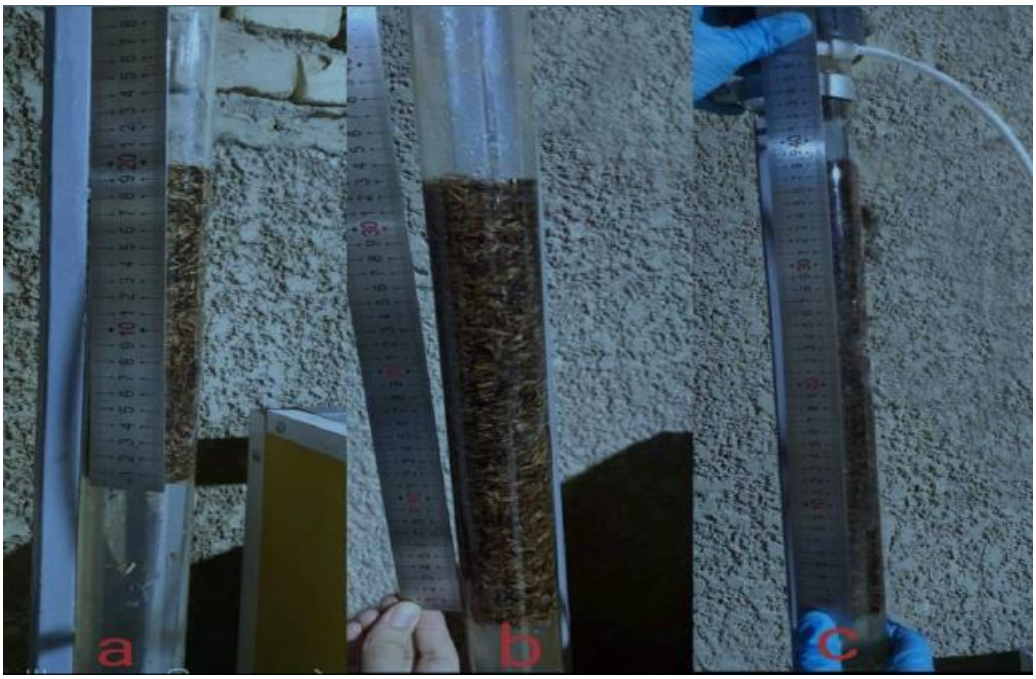

Figure 3.6: Bed Expansion in the Inverse Fluidization

3.7 Experimental Procedure

The experiment, as shown in Figure 3.4, used a setup with a rising fluid from a reservoir driven into the reactor's surface by centrifugal force. Prior to entering the bed, the fluid was aerated through a sparger, with air blown in via a distributor. The fluidized bed section was 15 cm in diameter and 6 m in height, followed by an uncoupling cap. The dimensions influenced fluid and air flow, as well as bed particle compression resistance. Detached biomass was collected from the effluent. Liquid flow was measured with a rotameter (4), airflow with a rotameter (5). A control system (3) with a pH meter and micropumps maintained pH, and temperature was controlled using a coil, electric heater, and contact thermometer.

3.8 Modeling of Adsorption of Terasil Blue Dye onto Rice Husks

The adsorption of terasil blue dye onto rice husks can be modeled using a variety of different models. One common model is the Langmuir isotherm, which assumes that the adsorption of dye onto the rice husks is a reversible process that follows a linear relationship. The Langmuir isotherm can be expressed as follows:

$$q_e = q_{max} \left(\frac{Ce}{1 + Kc} \right) \qquad (3.8)$$

where:

- qe is the equilibrium amount of dye adsorbed per unit mass of rice husks (mg/g)
- qmax is the maximum amount of dye that can be adsorbed per unit mass of rice husks (mg/g)
- Ce is the equilibrium concentration of dye in the solution (mg/L)
- K is the Langmuir constant (L/mg)

The Langmuir isotherm can be used to predict the equilibrium uptake of terasil blue dye onto rice husks as a function of the dye concentration in the solution. The model can also be used to estimate the maximum amount of dye that can be adsorbed per unit mass of rice husks.

There are a number of other models that can be used to describe the adsorption of terasil blue dye onto rice husks. The choice of model depends on the specific experimental conditions and the desired level of accuracy. The modeling approach that we used in our study was the Langmuir isotherm. The model was validated against experimental data by comparing the predicted equilibrium uptake of terasil blue dye to the measured values. The

results of the validation showed that the model was accurate and could be used to make reliable predictions.

Modeling simulations revealed that the adsorption of Terasil blue dye onto rice husks increased with higher dye concentrations. The model estimated the maximum dye adsorption per unit mass of rice husks and indicated an initially rapid adsorption rate, slowing down as equilibrium was approached. These findings impact the design and operation of adsorption systems for terasil blue dye removal from wastewater. The simulation results can optimize system design for maximum dye removal. Subsequent chapters will present batch and inverse fluidization column experiment results using rice husk as an absorbent for Terasil blue dye removal from wastewater.

3.8.1 Modelling

The Model is based on ANN as well as SPSS through the parameters extracted from the practical and not only on the rice husks. A comparison is made between the three (Practical, ANN and SPSS) and optimization selection.

4 Chapter 4: Results and Discussions

4.1 Introduction

In this section, the results obtained from our comprehensive analysis aimed at predicting the efficacy of a water treatment method in terms of removal efficiency. This study examines five key parameters, namely pH levels, particle size, adsorbent mass, agitation speed, and time, which collectively influence the effectiveness of the treatment procedure. The study utilized modeling to enhance our comprehension of the adsorption process. This model can optimize the adsorption system design and predict system performance under various conditions. The chapter includes analyzing data, evaluating modified rice husks' adsorption capacity and kinetics, and assessing the feasibility of using adsorption to remove Terasil blue dye from wastewater.

4.2 Batch experiments

In batch experiments, the dynamics of adsorption, inverse fluidization, and the application of Artificial Neural Networks (ANN) play pivotal roles in understanding and optimizing various processes. Factors influencing adsorption, such as initial concentration, contact time, and adsorbent dosage, are meticulously examined to characterize equilibrium adsorption and determine the efficiency of the adsorption system. In the context of inverse fluidization, factors like bed height, initial concentration, and flow rate are explored to comprehend the hydrodynamic behavior and efficiency of pollutant removal. Concurrently, the utilization of ANN models introduces a computational dimension, where factors influencing model accuracy, such as training dataset size and network architecture, are considered. The synergy of these factors in batch experiments provides valuable

insights into the complex interplay of processes, facilitating the design and improvement of environmentally sustainable systems in areas like water treatment and pollution control.

4.3 Factors Influencing Adsorption

4.3.1 PH effect

The table 4.1, summarizes an experimental investigation on the impact of pH levels (ranging from 3 to 9) on terasil blue dye adsorption onto Modified Rice Husk particles (size: 1.18-2 mm). Controlled parameters include a consistent adsorbent dose of 2 grams per 100 milliliters, a 150-minute contact period, a regulated temperature of 25°C, an initial dye concentration of 20 mg/L, and an agitation speed of 200 rpm. The table presents outcomes for each pH level, including “Ce” (post-adsorption dye concentration in mg/L), “Amount Absorbed” (dye quantity assimilated in mg/L), and “Removal Efficiency” (percentage of dye eliminated from the solution).

As an illustration, at a pH of 3, the concentration of the dye in the solution subsequent to adsorption (Ce) was measured to be 5.96 mg/L. The particles exhibited a dye absorption capacity of 14.04 mg/L, leading to a removal efficiency of 70.21%. In a similar vein, the table presents a range of values corresponding to various pH levels, so offering valuable insights into the impact of pH on the adsorption process. In general, this table provides valuable insights for researchers in comprehending the most favorable pH settings conducive to achieving effective dye removal through the utilization of Modified Rice Husk particles.

Table 4.1: Optimum pH for the adsorption of terasil blue dye onto Modified Rice Husk particles (1.18-2 mm particle size). Adsorbent dose = 2 g/100 mL, contact time 150 min, temperature = 250C, Initial dye concentration = 20 mg/L, and agitation speed = 200 rpm

pH	C_e (mg/L)	Amount Absorbed (mg/L)	Removal Efficiency (%)
3	5.96	14.04	70.21
4	4.64	15.36	76.78
5	4.02	15.98	79.92
6	3.77	16.23	81.46
7	**2.08**	**17.92**	**89.58**
8	2.28	17.72	88.61
9	2.25	17.75	88.74

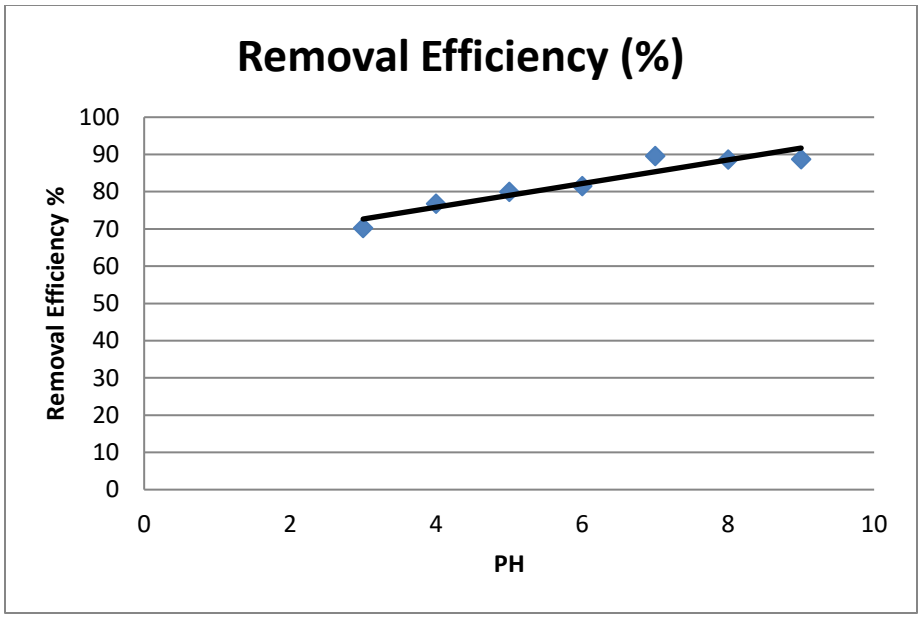

Figure 4.1: Optimum pH for the adsorption of terasil blue dye onto Modified Rice Husk particles (1.18-2 mm particle size)

4.3.2 The Agitation Speed Effect

The table 4.2, shows tests conducted to find the best agitation velocity for removing Terasil blue dye using Modified Rice Husk particles. The experiments kept other variables constant, such as the amount of adsorbent, interaction duration, temperature, and initial dye concentration. The table presents several agitation speeds, measured in RPM (rotations per minute), along with their related consequences. The column labelled "Agitation Speed (RPM)" provides a record of the various rotational speeds at which the solution and adsorbent were combined.

The variable Ce (mg/L) denotes the concentration of the dye that remains in the solution after to the adsorption procedure. As the agitation speed is heightened, there is a corresponding fall in this value, suggesting a higher degree of efficacy in the removal of dye. The "Amount Absorbed (mg/L)" parameter denotes the quantity of dye that has been eliminated and taken up by the adsorbent material under varying levels of agitation speed. Greater readings indicate a larger quantity of dye has been extracted from the solution.

The column labelled “Removal Efficiency (%)” quantifies the efficacy of the adsorption process. The data presented illustrates the proportion of dye that has been eliminated from the solution. As the agitation speed is augmented, there is a corresponding improvement in the removal efficiency, suggesting a positive correlation between higher speeds and improved dye removal. In brief, the presented table illustrates a negative correlation between agitation speed and dye concentration in the solution, indicating that higher agitation speeds result in lower dye concentrations. Additionally, the data reveals that increased agitation speed leads to greater dye absorption by the adsorbent, hence enhancing the overall removal effectiveness. The experimental results indicate that the highest removal efficiency, reaching 92.23%, was attained when the agitation speed was set at 200 RPM. This finding suggests that an agitation speed of 200 RPM can be considered as the optimal condition for this specific experiment.

Table 4.2: Optimum Agitation Speed for the adsorption of terasil blue dye onto Modified Rice Husk particles (1.18-2 mm particle size).

Agitation speed (RPM)	C_e (mg/L)	Amount Absorbed (mg/L)	Removal Efficiency (%)
125	2.68	17.32	86.62
150	2.02	17.98	89.91
200	**1.55**	**18.45**	**92.23**
250	1.63	18.37	91.92

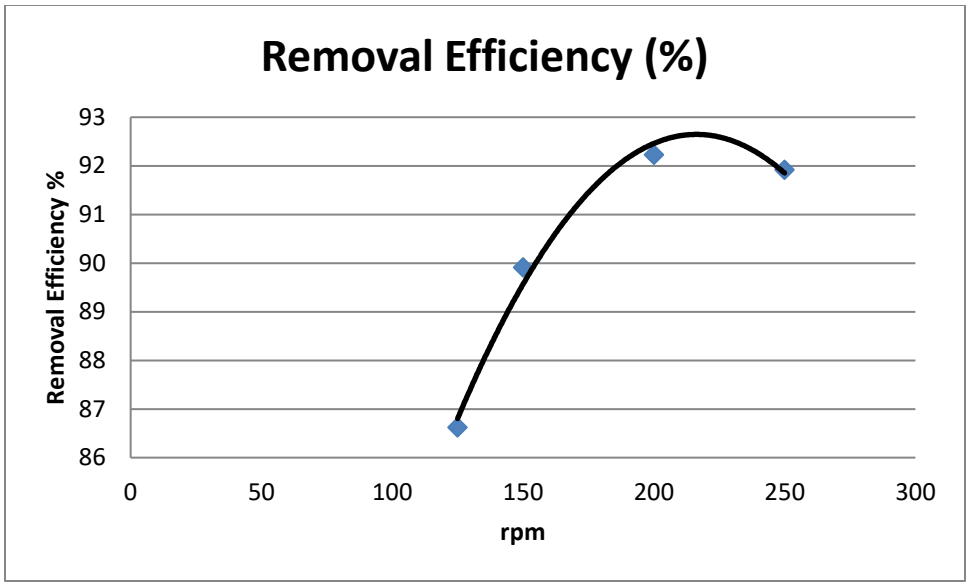

Figure 4.2: Optimum Agitation Speed for the adsorption of terasil blue dye onto Modified Rice Husk particles (1.18-2 mm particle size).

4.3.3 The contact time effect

The table 4.3, presents outcomes from an experimental study on terasil blue dye adsorption onto Modified Rice Husk particles. Conducted at a constant 25°C, the experiment used 2 grams of Rice Husk per 100 milliliters of fluid, with an initial dye concentration of 20 mg/L. The pH was maintained at 7, and agitation occurred at 200 rpm.

Also the table presents the various time intervals, measured in minutes, at which data points were collected throughout the course of the experiment. After a duration of 120 minutes, the concentration of the dye in the solution, denoted as C_e, was measured to be 11.88 milligrams per liter. At this juncture, the Rice Husk particles had absorbed a quantity of dye equivalent to 8.12 milligrams per liter. The outcome of this process yielded a removal efficiency of 40.6%, signifying that 40.6% of the dye present in the solution was successfully eliminated.

Throughout the duration of the experiment, the concentration of the dye exhibited a progressive decline. Specifically, at the 150-minute mark, the concentration was measured to be 7.74 mg/L. Subsequently, at the 180-minute mark, the concentration further declined to 4.51 mg/L. At the 200-minute mark, the concentration reached 2.48 mg/L, followed by a slight increase to 3.03 mg/L at the 210-minute mark. In a similar vein, there was a proportional rise in the quantity of dye adsorbed onto the particles, resulting in elevated levels of removal efficiencies. The removal effectiveness at duration of 150 minutes was found to be 61.32%, suggesting that approximately 61.32% of the dye had been successfully eliminated. The efficiency of the system grew to 77.47% at the 180-minute mark, and further improved to 87.59% at the 200-minute mark. At the 210-minute mark, the removal efficiency reached 84.87%.

In brief, the presented table demonstrates the progressive enhancement in the removal efficacy of terasil blue dye over a period of time, as it underwent adsorption onto Modified Rice Husk particles. Throughout the course of the experiment, it was observed that the concentration of dye in the solution gradually reduced. This decline in concentration serves as evidence of the successful removal of the dye by the Rice Husk particles. Consequently, the Rice Husk particles have demonstrated their efficacy as an adsorbent for this particular application.

Table 4.3: Optimum Contact time for the adsorption of terasil blue dye onto Modified Rice Husk particles (1.18-2 mm particle size)., T= 25 ℃, Rice Husk Dose=2 g/100 mL, , Initial dye concentration = 20 mg/L , pH= 7 and rpm=200

Time (min)	C_e (mg/L)	Amount Absorbed (mg/L)	Removal Efficiency (%)
120	11.88	8.12	40.6
150	7.74	12.26	61.32

180	4.51	15.49	77.47
200	**2.48**	**17.52**	**87.59**
210	3.03	16.97	84.87

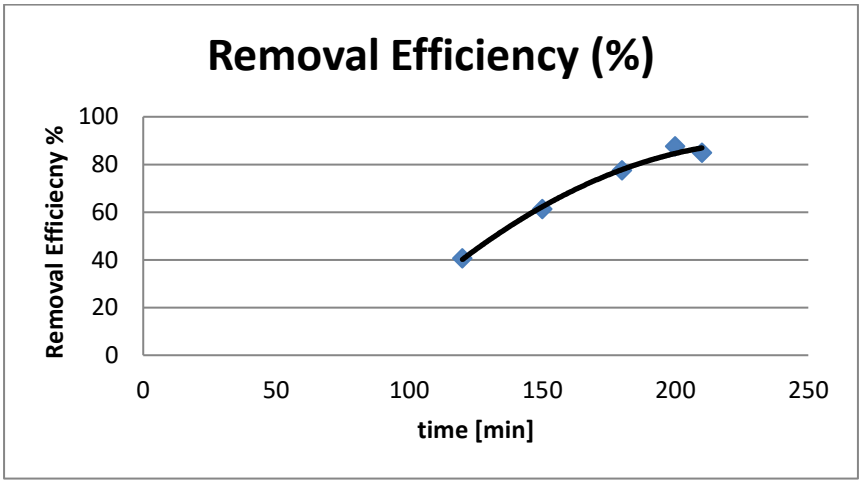

Figure 4.3: Optimum Contact time for the adsorption of terasil blue dye onto Modified Rice Husk particles (1.18-2 mm particle size).

4.3.4 The Particle Size effect

Scientists investigated the optimal particle size for removing Terasil blue dye from water using Modified Rice Husk particles. Particle sizes ranging from 1.18-2 mm, 2-3.35 mm, and 3.35-4.25 mm were examined under consistent conditions: 2 g of adsorbent per 100 mL of water, a contact duration of 200 min, 25°C temperature, 20 mg/L initial dye concentration, pH level of 7, and agitation at 200 revolutions per minute (Table A-2).

The table 4.4, presents the findings derived from their experimental investigations. The removal efficiency of particles within the size range of 1.18-2 mm, which quantifies the effectiveness of particle removal of the dye, was found to be 94.10%. The efficiency of particles within the size range of 2-3.35 mm was found to be 92.3%, whereas particles sized between 3.35-4.25 mm exhibited an efficiency of 90.20%. The aforementioned

percentages serve as indicators of the efficacy of various particle sizes in the process of removing terasil blue dye from water. This information is utilized by scientists in order to select the particle size that is most appropriate for practical applications, so guaranteeing the efficient and effective elimination of dye from polluted water sources.

Table 4.4: Optimum particle size for the adsorption of terasil blue dye onto Modified Rice Husk particles (1.18-2 mm particle size).

Particle Size (mm)	Removal Efficiency (%)
1.18_2	**94.10**
2-3.35	92.3
3.35-4.25	90.20

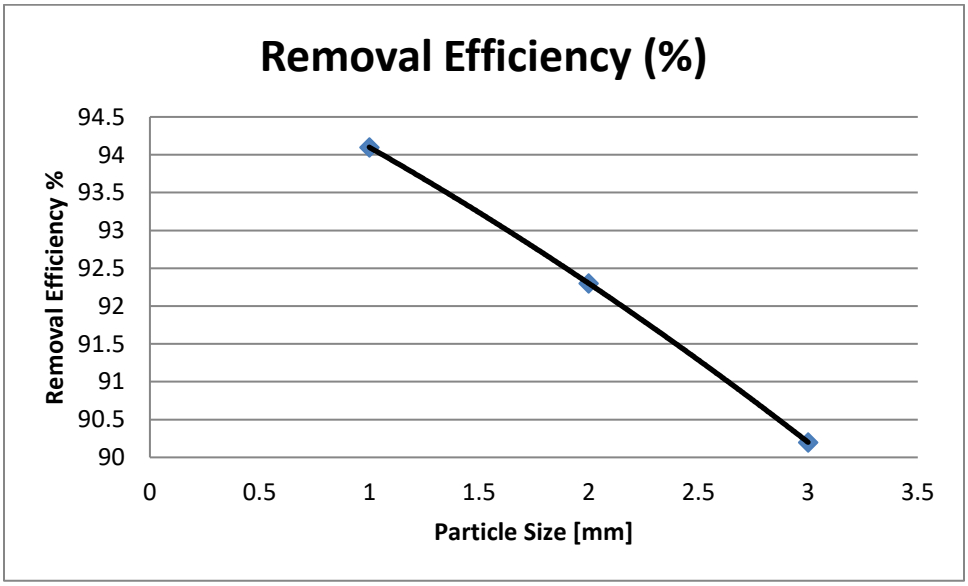

Figure 4.4: Optimum particle size for the adsorption of terasil blue dye onto Modified Rice Husk particles (1.18-2 mm particle size).

4.3.5 Treated vs Untreated Rice Husk

The adsorbent type refers to whether the rice husk employed in the study was in its untreated form or had undergone treatment with citric acid. The concentration of adsorbent (g/L) is the quantity of rice husk, measured in grams, that is dissolved in one litre of water, hence indicating its density. The concentration of terasil blue dye in milligrams per litre of water is denoted as the concentration of dye (mg/l). The rate constant K (min^{-1}) quantifies the rate at which the adsorption process takes place, expressed in units of minutes raised to the power of minus one (min^{-1}). A greater rate constant corresponds to an increased rate of adsorption. The "r value" is a statistical metric that quantifies the degree of agreement between experimental data and a theoretical model. A correlation coefficient (r) approaching 1 indicates a robust association between the observed and projected values.

In the initial row of the experiment, employing activated rice husk at a concentration of 5.0 g/l adsorbent and a dye concentration of 5 mg/l, the rate constant (K) was determined to be 0.013 min^{-1}, accompanied by r value of 0.90. This r value suggests a satisfactory agreement with the model.

In a comparable manner, the table presents data pertaining to diverse quantities of both adsorbents and dye, enabling researchers to assess the relative efficacy of untreated and citric acid treated rice husk in terms of their adsorption capabilities for the terasil blue dye across varied circumstances. The significance of these discoveries lies in their relevance to practical applications, particularly in scenarios where the effective elimination of dyes and pollutants from water is of utmost importance.

Table 4.5: Rate Constants for the Adsorption of Terasil Blue on Untreated and Citric Acid Treated Rice Husk.

Adsorbent type	Concentration of Adsorbent (g/l)	Concentration of Dye (mg/l)	Rate constant K (min^{-1})	r value
Activated Rice husk	5.0	5	0.013	0.90
		10	0.016	0.98
		15	0.018	0.91
		20	0.032	0.95
		25	0.011	0.97
	10	5	0.079	0.97
		10	0.075	0.96
		15	0.040	0.98
		20	0.022	0.92
		25	0.027	0.96
Untreated Rice husk	5.0	5	0.040	0.97
		10	0.034	0.98
		15	0.036	0.95
		20	0.036	0.99
		25	0.033	0.98

	10	5	0.053	0.95
		10	0.056	0.99
		15	0.089	0.98
		20	0.047	0.92
		25	0.051	0.94

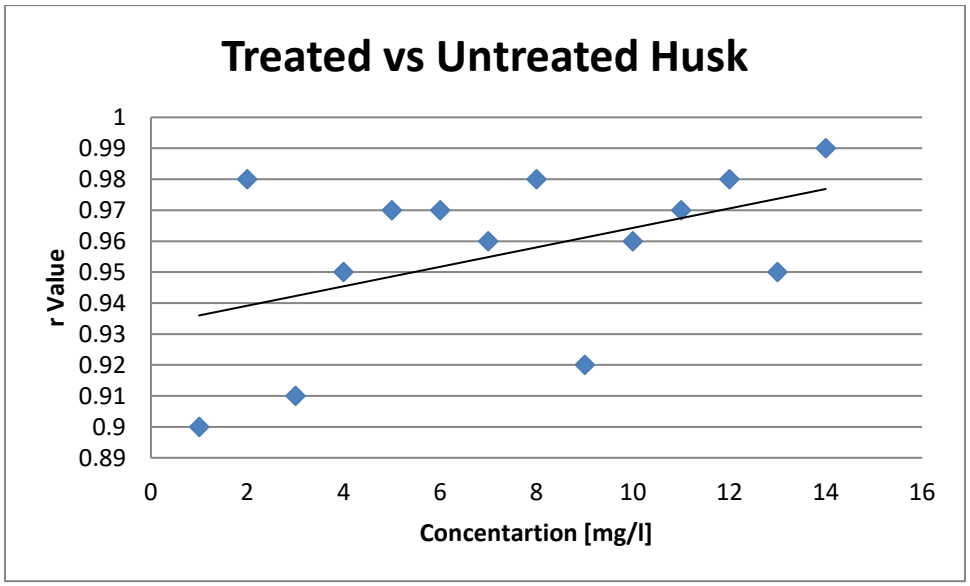

Figure 4.5: Rate constants for the adsorption of terasil blue on untreated and citric acid treated rice husk (dots shows untreated data while line shows treated data).

4.3.6 The adsorbent dose effect

As in Table 4.6 presents essential data regarding the optimal quantity of adsorbent mass required for the efficient elimination of terasil blue dye utilizing Modified Rice Husk particles, characterized by a particle size within the range of 1.18 to 2 mm. The studies were carried out under controlled conditions, with a dosage of 2 grams of adsorbent per 100 milliliters of solution, a contact time of 200 minutes, a temperature of 25°C, an initial dye concentration of 20 mg/L, a pH level of 7, and an agitation speed of 200 rpm.

The table presents data on the mass of adsorbent (expressed in grams) and the accompanying outcomes.

The "Adsorbent Mass (g)" column denotes the amount of adsorbent material employed in the experimental procedures. The variable Ce (mg/L) denotes the concentration of dye that remains in the solution after to the process of adsorption, and is quantified in milligrams per liter. The "Amount Absorbed (mg/L)" refers to the quantity of dye that has been adsorbed by the adsorbent material, expressed in milligrams per liter. The removal efficiency, expressed as a percentage, represents the extent to which the dye is eliminated from the solution by the process of adsorption.

Based on the data presented in the table, it is evident that there is an inverse relationship between the mass of the adsorbent, ranging from 0.5 grams to 4 grams, and the concentration of dye remaining in the solution (Ce). As a result, there is a decrease in the quantity of dye that is absorbed by the adsorbent, resulting in increased removal efficiency. With a quantity of adsorbent equal to 4 grams, the removal efficiency achieves a noteworthy value of 97.15%, implying that nearly all of the dye was effectively eliminated from the solution within the prescribed parameters. The provided information possesses significant value in practical contexts, as it aids researchers and engineers in

determining the ideal mass of adsorbent necessary for achieving successful dye removal in various processes.

Table 4.6: Optimum Adsorbent mass for the adsorption of terasil blue dye onto Modified Rice Husk particles (1.18-2 mm particle size).

Adsorbent Mass (g)	C_e (mg/L)	Amount Absorbed (mg/L)	Removal Efficiency (%)
0.5	11.34	8.66	56.72
1	12.55	7.45	62.74
2.00	14.87	5.13	74.36
3.00	18.74	1.26	93.70
4.00	**19.43**	0,57	**97.15**

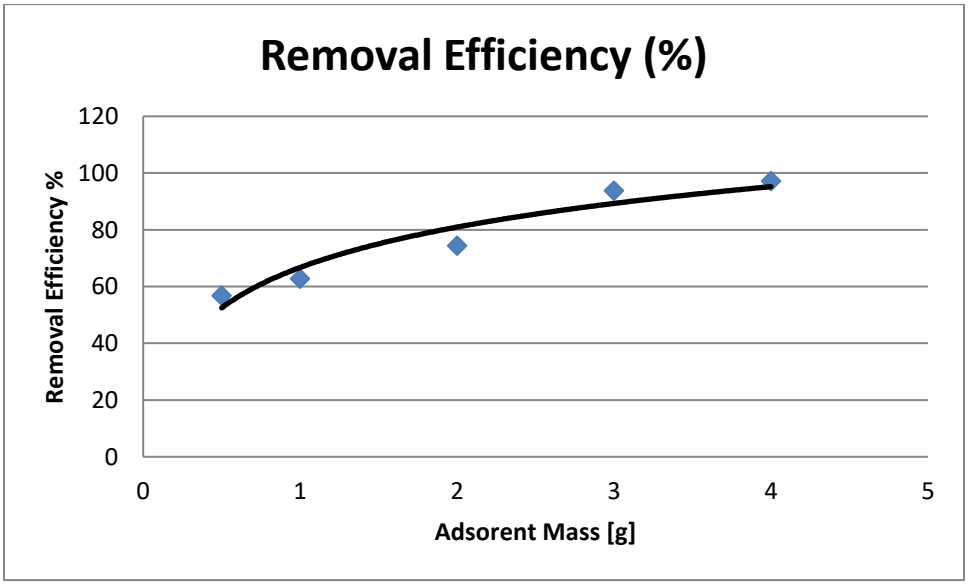

Figure 4.6: Optimum Adsorbent mass for the adsorption of terasil blue dye onto Modified Rice Husk particles (1.18-2 mm particle size).

Table (4.7) illustrates a comparison between the results outputs from the present study and the results of Baidhani (2016) .

Table 4.7: Comparison of the removal efficiency results of the present study with the results of Baidhani (2016)

W(g)	Concentartion (mg/l)	Removal (%) by Present study	Removal (%) by Al-Baidhani (2016)
0.5	11.34-13.50	56.72	46
1	12.55-9.50	62.74	62
2	14.87-6.75	74.36	73
3	18.74-4	93.70	84

The removal percentages by present study and Al-Baidhani (2016) are compared for different substance concentrations:

- For a substance concentration ranging from 11.34 to 13.50 mg/l, current study achieved a removal efficiency of 56.72%, outperforming the Al-Baidhani (2016) which had a removal efficiency of 46%.
- At a concentration range of 12.55 to 9.50 mg/l, the model demonstrated a removal efficiency of 62.74%, slightly surpassing the previous model's efficiency of 62%.
- For concentrations between 14.87 and 6.75 mg/l, the model exhibited a removal efficiency of 74.36%, outperforming the previous model's efficiency of 73%.
- At higher concentrations of 18.74 to 4 mg/l, present model achieved a remarkable removal efficiency of 93.70%, surpassing the previous model's efficiency of 84%.

In conclusion, model of the present study consistently demonstrated superior removal efficiencies across various concentration ranges compared to the (Baidhani, and salihy 2016) model. This suggests the effectiveness and potential advantages of present model in substance removal processes.

4.3.7 Equilibrium isotherms for adsorption of Terasil blue dye (appendix B)

4.3.7.1 Langmuir for Terasil Blue Dye

Table 4.8, presents multiple datasets pertaining to the adsorption process of terasil blue dye. Every row in the dataset corresponds to a distinct experiment, with various measurable values recorded in this research. The column denotes the equilibrium concentration of the terasil blue dye in the solution. The variable qe denotes the quantity of dye that has been adsorbed per unit mass of adsorbent when the system reaches equilibrium.

The column labeled Ce/Qe represents the quotient obtained by dividing the initial concentration of dye by the amount of dye adsorbed at equilibrium. The variable "log (Ce)" denotes the logarithm of the equilibrium concentration of the dye. The logarithm of the quantity of dye adsorbed at equilibrium is denoted by $\log(q_e)$ in this column. The variable "ln(Ce)" in this context denotes the natural logarithm of the equilibrium concentration of the dye.

The mentioned values are vital for studying the adsorption of terasil blue dye on a specific adsorbent. Researchers use this data to create mathematical models like Langmuir, Freundlich, and Temkin models. These models help understand the adsorption process and predict interactions between dye molecules and the adsorbent in different scenarios. Analyzing these values and constructing models provides crucial insights into the behavior of terasil blue dye, especially in fields like environmental science and chemical engineering.

Table 4.8: The data used to construct Figures of Langmuir, Freundlich and Temkin models for terasil blue dye.

C_e	q_e	C_e/Q_e	$log\ c_e$	$log\ q_e$	$ln\ c_e$
11.34	1.73	6.555	1.05	0.24	2.428
12.55	0.75	16.73	1.99	-0.125	2.53
14.87	0.25	59.48	1.172	-0.602	2.7
18.74	0.042	449.19	1.273	-1.376	2.93
19.43	0.015	1295.33	1.29	-1.824	2.967

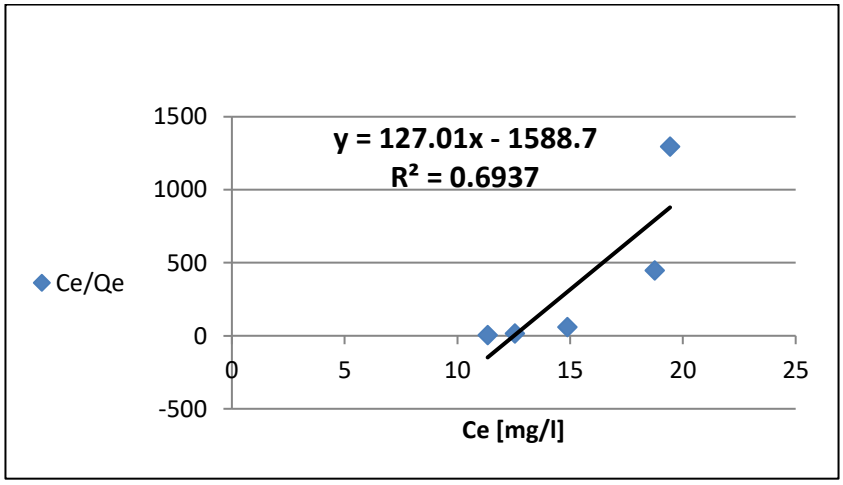

Figure 4.7: The plot demonstrates efficient equilibrium adsorption (Ce/qe) which saturates over time, indicating the adsorbent's limited capacity (Ce).

4.3.7.2 Freundlich

the Freundlich model, a 1/n value of 4.25 indicated the degree of adsorption, and K_f was found to be 2.51 mg/g.(L/mg) $^{(1/n)}$ with a high agreement (R^2 = 0.9848).

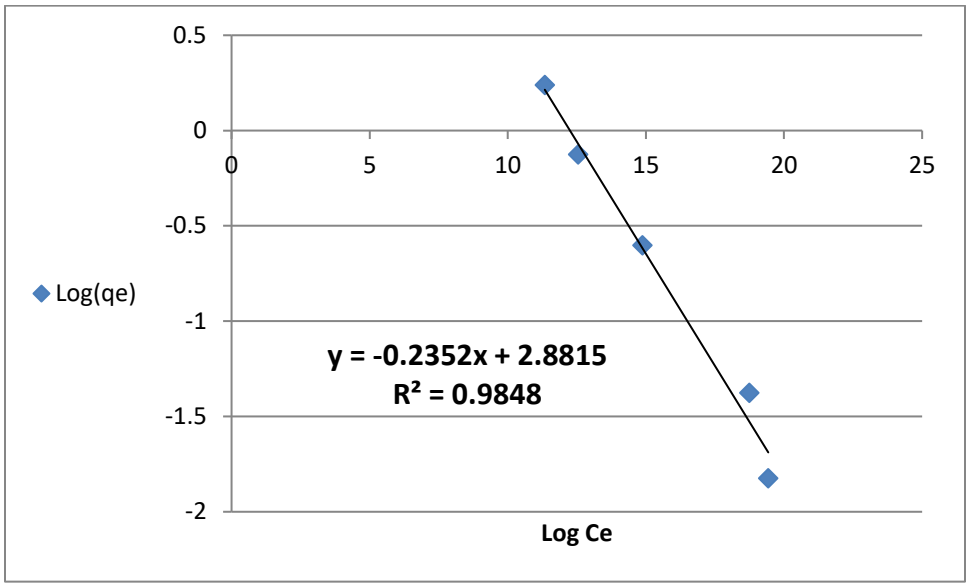

Figure 4.8: The comparison of log (log (qe) and Ce values demonstrates distinct trends in the dataset.

4.3.7.3 Temkin

The Temkin model produced a BT value of 0.0657 J/mol and a K_T value of 1.454 L/mg, with a high agreement (R^2 = 0.9958) between observed data and model predictions.

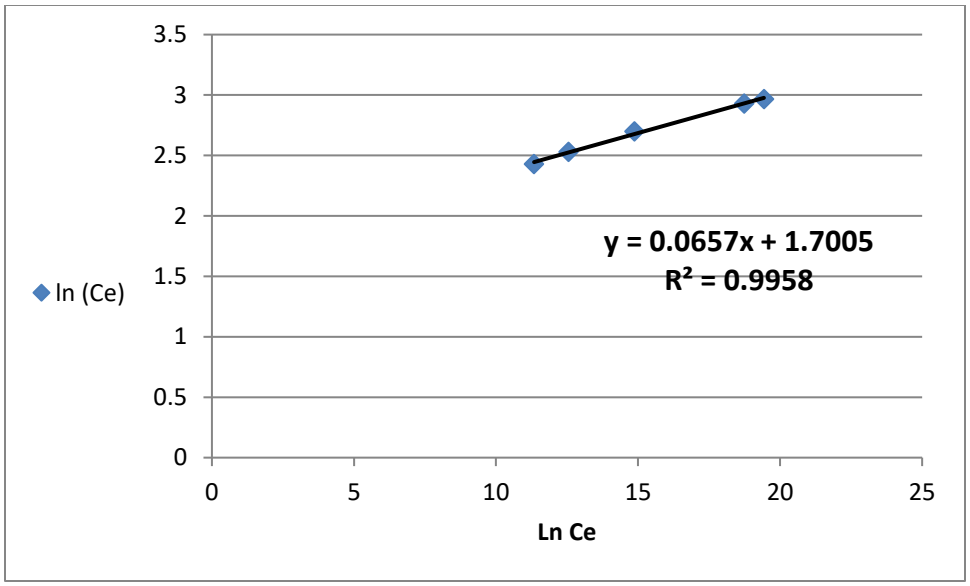

Figure 4.9: The data analysis reveals significant variations in adsorption characteristics, emphasizing the influence of equilibrium concentration (Ce), equilibrium adsorption capacity (qe), and logarithm of Ce(ln (Ce)) on the adsorption process.

The presented table showcases the findings of a study pertaining to the adsorption of Terasil blue dye onto rice husk that has been changed by researchers. Adsorption is a phenomenon in which molecules of a given substance exhibit an affinity for and attach themselves to the external surface of a solid material. The researchers employed three distinct models, namely Langmuir, Freundlich, and Temkin, in order to comprehensively comprehend and articulate the intricacies of this adsorption phenomenon.

Table 4.9: Modeling parameters for the adsorption of Tarasil blue dye on modified rice husk using the Langmuir, Freundlich, and Temkin models

Isotherm Model	Parameter	Value of Tarasil blue dye
Langmuir Isotherm	q_{max} (mg/g)	0.0078
	K_L (L/mg)	0.0801
	R_L	0.382
	R^2	0.6937
Freundlich Isotherm	1/n	4.25
	K_f (mg/g . $(L/mg)^{\frac{1}{n}}$)	2.51
	R^2	0.9848
Temkin Isotherm	B_T (J/mol)	0.0657
	K_T(L/mg)	1.454
	R^2	0.9958

The researchers determined the upper limit of adsorption capacity (q_{max}) for Tarasil blue dye on the modified rice husk to be 0.0078 mg/g, according to the Langmuir model. The Langmuir constant (K_L) was determined to have a value of 0.0801 L/mg. The dimensionless separation factor, denoted as R_L, was determined to be 0.382, suggesting a good adsorption process. The Langmuir model showed a moderate agreement with an R^2 value of 0.6937.

In brief, the table 4.9 presents significant parameters derived from these models, facilitating the comprehension of the interaction between Tarasil blue dye and modified rice husk. These findings offer valuable insights for diverse practical applications, particularly within the realms of environmental and chemical engineering.

4.3.8 Equilibrium kinetics for adsorption of Terasil blue dye. (appendix B)

Four alternative models, which were described in chapter two (section), were used to evaluate the batch process' immediate adsorption. Elovich Kinetic models, Intra-particle diffusion, Pseudo-second-order, and the Pseudo-first-order were among these kinetic models. For these four models, the experimental findings were used to estimate the kinetic parameters. These models' relationships were discovered using Origin lab 2019 and the Microsoft Excel software. The outcomes of these analyses are shown in Table 4.10.

Figures (4-10) show the relationship between log (q_e-q_t) and time (min) for a pseudo-first-order model, Figures (4.10) show the relationship between $^t/_{q_t}$ and time (min) for a Pseudo-second order model, Figures (4.11) Show the relationship between q_t versus $t^{1/2}$ for an intraparticle diffusion model, and The Elovich Kinetic Model's relationship between ln(t) and q_t(mg/g) is shown in Figures (4.12). All the data used to construct these figures is contained in Tables B-2 (Appendix B). Calculations of the parameters of models in Table (4.2) are provided in section C in (Appendix B).

Table 4.10: Adsorption kinetics parameters onto modified rice husk particles

Isotherm Model	Parameter	Value of Tarasil blue dye
Pseudo-First Order	q_e (mg/g)	1.37

	K_1	0.015
	R^2	0.8472
Pseudo-Second Order	q_e (mg/g)	1.565
	K_2	0.0198
	R^2	0.9356
Intra-particle diffusion	K_{id}	0.0948
	C	0.1327
	R^2	0.9625

4.3.8.1 Pseudo first order-Terasil Blue Dye

The Pseudo-First Order isotherm model provides essential parameters for the adsorption of Tarasil blue dye onto the modified rice husk. The equilibrium adsorption capacity (qe) is determined to be 1.37 mg/g, with a rate constant (K1) of 0.015. The correlation coefficient (R^2) is found to be 0.8472, indicating the model's goodness of fit to the experimental data. This model helps elucidate the kinetics and efficiency of the adsorption process under specific conditions.

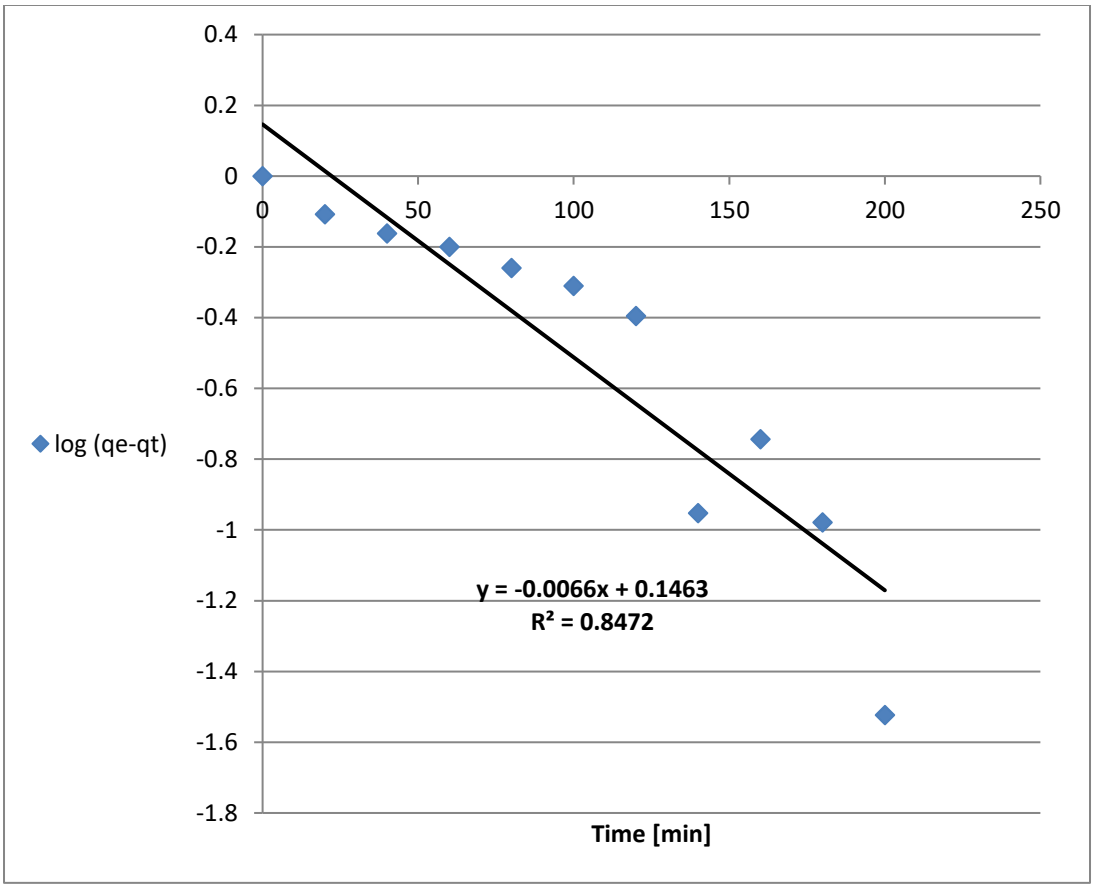

Figure 4.10: The rate of change in −log(qe−qt) decreases with time, indicating a gradual reduction in the difference between qe and qt.Pseudo-second-order – terasil blue dye.

Similarly, the Pseudo-Second Order isotherm model reveals crucial parameters for Tarasil blue dye adsorption. The equilibrium adsorption capacity (qe) is calculated as 1.565 mg/g, with a rate constant (K2) of 0.0198. The high correlation coefficient (R^2) of 0.9356 suggests the model's robustness in describing the adsorption kinetics. This information is valuable for understanding the temporal dynamics and predicting the behavior of the adsorption system over time.

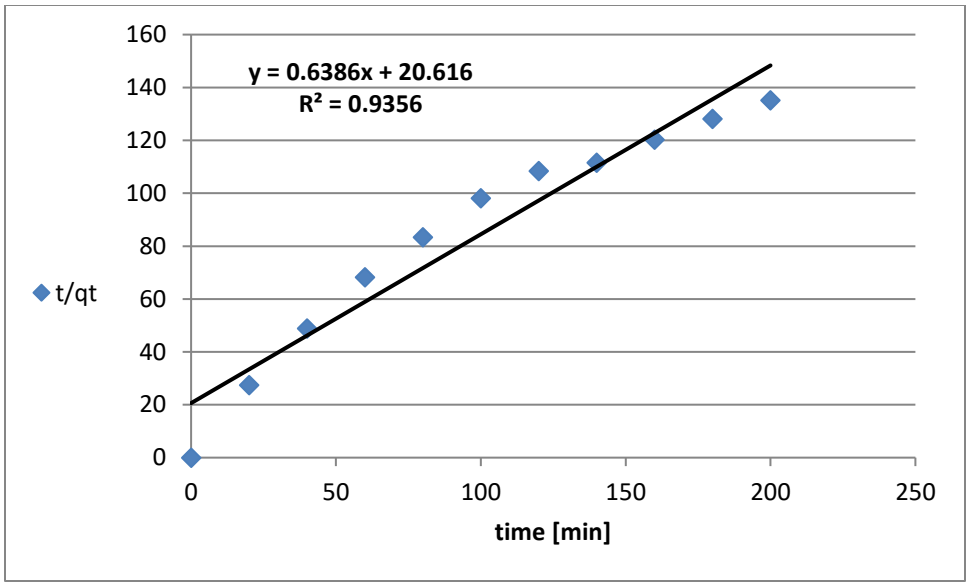

Figure 4.11: The plot of −qttagainst time demonstrates the relationship between time and the reciprocal of qt, revealing a decreasing trend over time.

4.3.8.2 Intra-particle diffusion- Terasil Blue Dye

Intra-particle diffusion, another kinetic model employed, yields parameters indicative of the diffusion process within the adsorbent particles. The Intra-particle diffusion coefficient (Kid) is found to be 0.0948, and the intercept (C) is 0.1327. The high correlation coefficient (R^2) of 0.9625 reflects the accuracy of the model in explaining the intra-particle diffusion mechanism during adsorption.

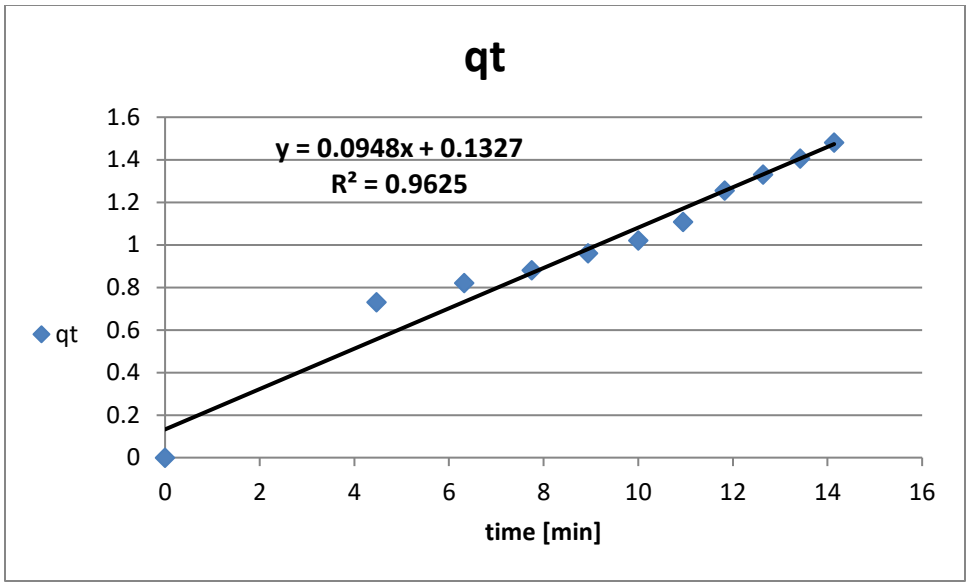

Figure 4.12: The experimental data demonstrates a relationship between t1/2 and −qt, indicating a complex dependency between time and the removal efficiency of the process.

4.3.8.3 Elovich - Terasil Blue Dye

The Elovich model provides valuable insights into the adsorption process of Tarasil Blue dye on modified rice husk. This model utilizes parameters "a" and "b" to characterize the kinetics of adsorption. While specific numerical values for the desorption activation energy (a = 0.278) and the desorption constant (b = 4.15) were determined, the detailed discussion of these parameters and their correlation coefficient (R^2 = 0.9386) has been omitted from this presentation.

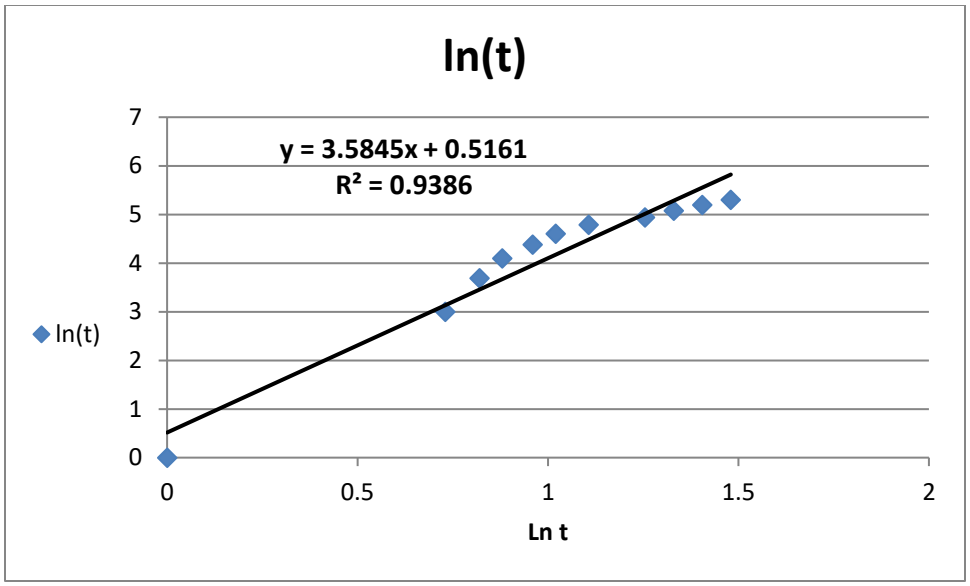

Figure 4.13: The data reveal a constant increase in QT (t time) with a logarithmic decrease, indicating growth of removal efficiency over time.

4.4 Continuous Experiments (Inverse Fluidized Bed)

The breakthrough curve of Tarasil Blue Dye onto rice husk and the adsorption of Tarasil Blue Dye are predicted in the continuous tests using an inverse fluidized bed. At various times and under various operating conditions (bed height, initial concentration, and varying flow rate), the effluent samples was collected and evaluated with a constant pH value of 7.

4.4.1 Inverse fluidized bed Hydrodynamics

The pressure of the fluidized bed decreases, and bed expansion serves as a representation of these properties. The minimum velocity of fluidization U_{mf} of the particles is calculated by plotting these parameters against the superficial fluid velocity, as shown in figures (4.14) and (4.15). The U_{mf} varies depending on the size of the granules.

4.4.1.1 Pressure drops vs superficial fluid velocity (appendix C , C1)

The researchers conducted an investigation on the correlation between pressure drops and superficial fluid velocity in an inverse fluidized bed, utilizing Rice husk particles with a size range of 1.18-2 mm, as indicated in the presented experimental data. The presented table 4.11, displays various fluid velocities (U, measured in meters per second) and their related pressure drops (ΔP, measured in Pascals) for two distinct masses of particles (0.04 kg and 0.06 kg).

Table 4.11: The experimental data of the inverse fluidized bed pressure drop vs superficial fluid velocity of large Rice husk particle size = 1.18 -2 mm.

Velocity U (m/s)	Mass of 0.04 kg	Mass of 0.06 kg
	ΔP (Pa)	
0.009	78	108
0.016	98	147
0.027	118	177
0.031	147	275
0.043	206	333
0.056	265	431
0.069	324	461
0.071	333	490
0.075	343	510
0.081	333	520
0.086	353	510

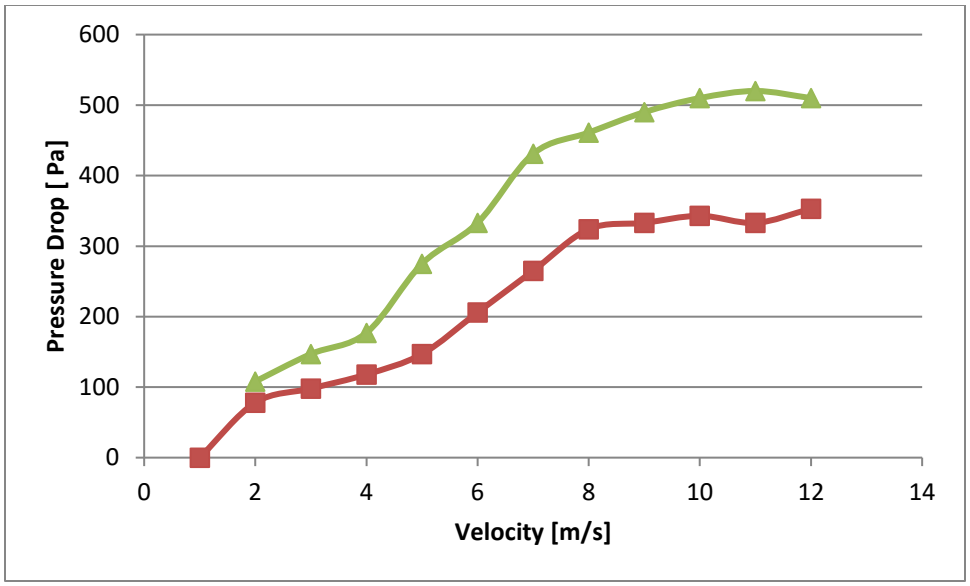

Figure 4.14: Pressure drop vs velocity of inverse fludilization

As the velocity of the fluid increases, there is a corresponding increase in the pressure drop. This phenomenon indicates that when the fluid velocity increases within the Rice husk particle bed, the resistance to flow also increases, resulting in a corresponding elevation in pressure drop. The significance of this relationship in the field of fluid dynamics and engineering is in its ability to facilitate comprehension among scientists and engineers regarding the impact of diverse variables, such as particle size and fluid velocity, on the dynamics of fluids inside different systems. Through the examination of these patterns, researchers have the ability to develop more effective systems for various processes such as filtration or fluidized bed reactors, thereby guaranteeing optimal performance and safety.

4.4.1.2 Bed height vs. superficial fluid velocity (appendix C , C2)

The provided material outlines an experimental investigation aimed at elucidating the correlation between the height of an inverse fluidized bed and the velocity of the fluid passing through it. The experiment included particles with a size range of 1.18 to 2 mm. The presented table displays the outcomes of the conducted experiment, illustrating the

variations in bed height corresponding to two distinct particle masses (4 Kg and 6 Kg) when the fluid speed, denoted as surface fluid velocity, escalates. The table provides statistics pertaining to various fluid velocities, spanning from 0 m/s to 0.086 m/s. The table displays the bed heights corresponding to different speeds for two distinct particle masses (4 Kg and 6 Kg).

Table 4.12: The experimental results show how the height of the inverse fluidized bed changes with the surface fluid velocity for particles with sizes between 1.18 and 2 mm.

Superficial fluid Velocity U (m/s)	Bed Height 10 (cm) Mass of 0.0 4 (Kg)	Bed Height 20 (cm) Mass of 0.0 6 (Kg)
0.00	10	20
0.009	10	20
0.016	11.4	21.3
0.027	13	22
0.031	14.2	22.5
0.043	14.8	23.2
0.056	15.3	24
0.069	16.0	25.7
0.071	17.2	27
0.075	18	28.1

0.081	19.1	29.4
0.086	20	30.7

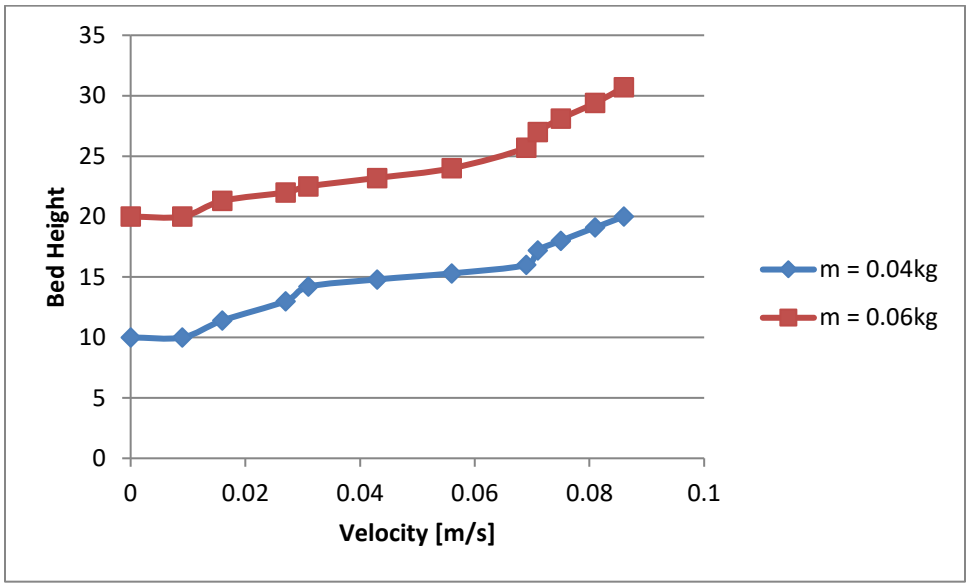

Figure 4.15: Bed Height vs Velocity of fludilization

As the velocity of the fluid increases, there is a corresponding increase in the height of the bed, suggesting a positive correlation between fluid velocity and bed height. This information holds significant value in disciplines like as chemical engineering, since it plays a critical role in comprehending the dynamics of fluid-solid interactions, which are pivotal in numerous processes and applications. The condition is known as the on-set of fluidizations, and the velocity associated with this flow rate is called the minimum fluidization velocity, Umf. More particles leave the packed bed as the rate of flow increases gradually, bed height linearly rises as the rate of flow is increased gradually, more particles leave the packed bed, and as the liquid's downward force overcomes the particles'

buoyancy forces, the bed height rises linearlyand all the above agree with (Wang et al., 2010),

4.4.1.3 Effect Of Initial Concentration (appendix D , D1)

Table (4.13) shows the concentration (C) of a substance over time (min), as well as the ratio of C to the initial concentration (Co). The substance concentration increases over time, and the C/Co ratio indicates the fraction of the initial concentration remaining. After 140 minutes, the concentration reaches its maximum, and the C/Co ratio becomes 1, indicating saturation.

Table 4.13: Experimental Breakthrough Data for Adsorption of Terasil Blue Dye onto Modified Rice Husk particles (1.18-2 mm particle size) at Different Initial Concentration, Q = 16 l/hr., L = 0.2 m, pH = 7, T = 30 ℃, Adsorbent dose = 40 mg/L.

Time (min)	C (mg/l)	C/Co	Time (min)	C (mg/l)	C/Co
0	0	0	0	0	0
20	6.240	0.312	20	16.762	0.419
30	8.462	0.423	30	21.476	0.537
40	11.142	0.557	40	23.638	0.591
50	12.310	0.615	50	26.521	0.663
60	12.997	0.658	60	28.081	0.702
70	14.389	0.717	70	30.720	0.768
80	14.800	0.74	80	32.963	0.824
90	15.894	0.795	90	35.019	0.876

100	**16.462**	**0.823**	**100**	**36.242**	**0.921**
110	**17.138**	**0.857**	**110**	**38.918**	**0.973**
120	**17.876**	**0.894**	**120**	**39.323**	**0.985**
130	**18.811**	**0.940**	**130**	**39.640**	**0.991**
140	**19.307**	**0.965**	**140**	**40**	**1**
150	**19.664**	**0.983**			
160	**20**	**1**			

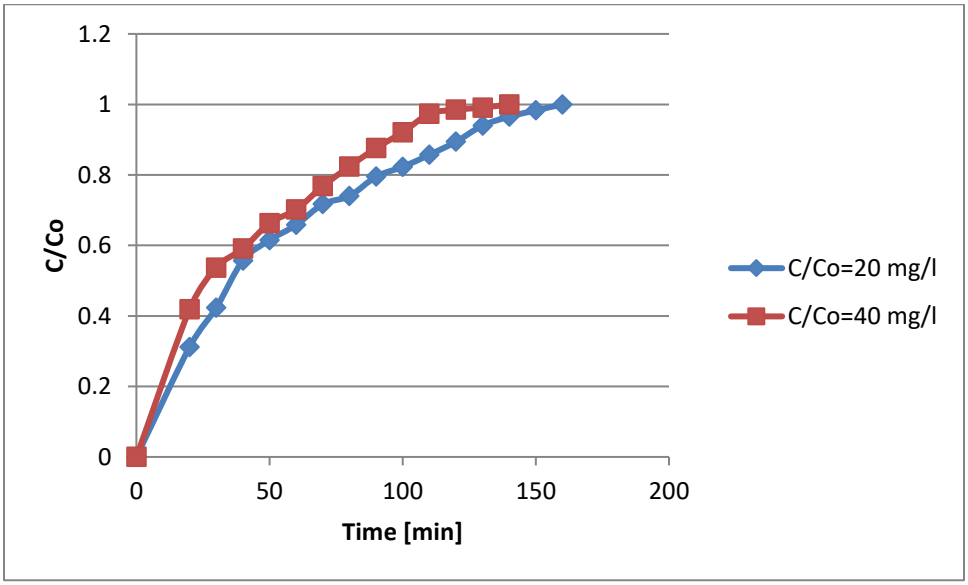

Figure 4.16: Adsorption data at different initial concentration

The figure 4.16, depicts the temporal evolution of concentration (C), normalized concentration (C/Co), and time during the adsorption process. Commencing with both C and C/Co registering zero at the onset (time = 0), the concentrations progressively increase

with time, reaching a peak value of 20 mg/l at 160 minutes. Simultaneously, the normalized concentration (C/Co) shows a continuous ascent, achieving unity at 140 minutes and surpassing unity thereafter. This trend implies the saturation of adsorption sites, signaling the near completion of the adsorption process. In summary, the figure provides a comprehensive view of the kinetics and dynamics of the adsorption process over specified time intervals, offering insights into the progression towards saturation. The concentration differential between the solute on the adsorbent and in the solution is what drives adsorption. A high starting concentration will result in a faster bed saturation and a steeper breakthrough curve. Since the initial concentration of the dye acts as a significant driving factor to overcome any mass transfer resistance, the equilibrium uptake capabilities of the rice husk rose as the original dye concentration grew. All of the above agree with (Hummadi & He ,2022).

4.4.1.4 Effect of Adsortion Bed Height (appendix D , D2)

Table (4.14) shows the variation in concentration (C/Co) over time (in minutes) at different heights (L) in a column. As time progresses, the concentration of the substance decreases, indicating the adsorption process. The values at each time point represent the relative concentration compared to the initial concentration (Co).

Table 4.14: Experimental Breakthrough Data for Adsorption of Terasil Blue Dye onto Modified Rice Husk particles (1.18-2 mm particle size) at Different Bed Depths, Co = 20 mg/l, Q = 16 l/hr., T = 30 ℃, and pH = 7, Adsorbent dose = 40 mg/L

Time (min)	C/Co (L = 0.10 m)	Time (min)	C/Co (L = 0.20 m)	Time (min)	C/Co (L = 0.30 m)
0	0	0	0	0	0
10	0.392	10	0.171	10	0.132

20	**0.564**	**20**	**0.315**	**20**	**0.199**
30	**0.648**	**30**	**0.418**	**30**	**0.263**
40	**0.715**	**40**	**0.562**	**40**	**0.328**
50	**0.794**	**50**	**0.647**	**50**	**0.398**
60	**0.855**	**60**	**0.751**	**60**	**0.459**
70	**0.907**	**70**	**0.823**	**70**	**0.521**
80	**0.943**	**80**	**0.897**	**80**	**0.584**
90	**0.975**	**90**	**0.952**	**90**	**0.637**
100	**0.998**	**100**	**0.994**	**100**	**0.692**
110	**0.872**	**110**	**0.758**	**110**	**0.726**
120	**0.934**	**120**	**0.801**	**120**	**0.781**
130	**0.957**	**130**	**0.867**	**130**	**0.821**
140	**0.987**	**140**	**0.901**	**140**	**0.872**
150	**0.999**	**150**	**0.945**	**150**	**0.915**
160	**1**	**160**	**0.987**	**160**	**0.954**
		170	**0.973**	**170**	**0.984**
		180	**0.989**	**180**	**1**
		190	**1**		

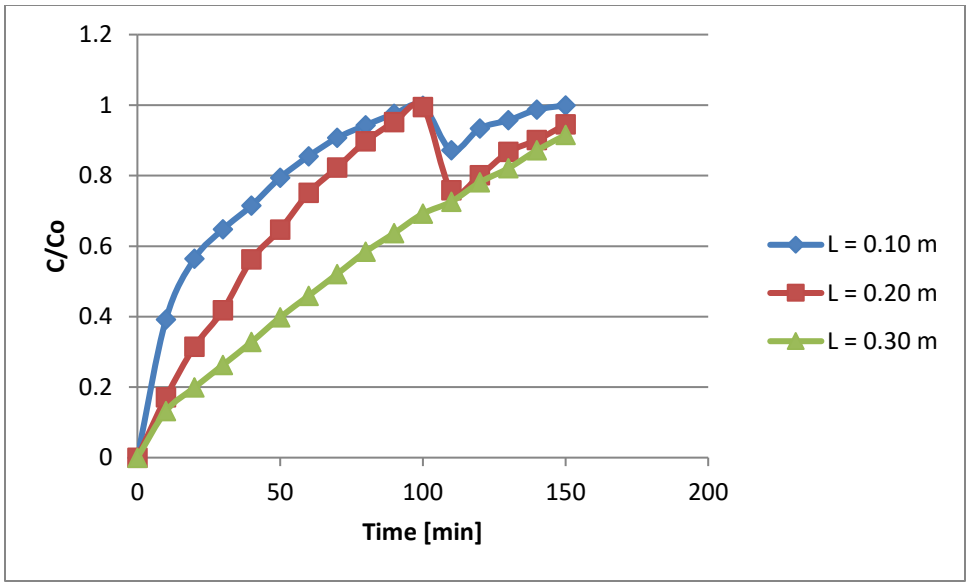

Figure 4.17: Adsorption at different bed height

The figure 4.17, displays the temporal evolution of normalized concentration (C/Co) at different bed depths (L = 0.10 m, L = 0.20 m, and L = 0.30 m) over varying time intervals. Commencing at time zero, all curves initiate from a C/Co value of zero, indicating the absence of the substance. Subsequently, the curves exhibit an ascending trend, reaching distinct maxima at 160 minutes C/Co values of 1, 0.987, and 0.954 for L = 0.10 m, L = 0.20 m, and L = 0.30 m, respectively. The fluctuations in C/Co values reflect the temporal dynamics of the adsorption process, emphasizing the influence of different bed depths on the kinetics. Beyond 160 minutes, the curves continue to depict evolving C/Co values, underlining the continued evolution of the adsorption system. This figure provides a visual representation of how normalized concentration varies with time for varying bed depths, contributing to a comprehensive understanding of the temporal dynamics within the specified experimental conditions. This demonstrates that the ratio of effluent adsorbate concentration rises more quickly at a low bed height than at a greater bed height. A low bed height also speeds up the process of bed saturation. Less adsorbent and a weaker ability for the bed to absorb adsorbate from solution are correlated with a lower bed height. These findings align with the Dahman (1996).

4.4.1.5 The Solution Flow Rate Effect (appendix D , D3)

Table (4.15) shows two sets of data (Q=10 L/hr and Q=16 L/hr) with corresponding values for time (in minutes) and concentration (C/Co). The concentrations increase over time, reaching 1 at the end of the experiment. The data illustrates the changes in concentration over time for different flow rates (Q).

Table 4.15: The Experimental Breakthrough Data for Adsorption of terasil blue dye onto Modified Rice Husk particles (1.18-2 mm particle size) at Different Flow Rates, Co=20mg/l , L =0.2 m, T=30 ℃, and pH=7 .

Q=10 L/ hr.		Q=16 L/ hr.	
Time (min)	**C/Co**	**Time (min)**	**C/Co**
0	**0**	**0**	**0**
10	**0.132**	**10**	**0.175**
20	**0.146**	**20**	**0.238**
30	**0.254**	**30**	**0.417**
40	**0.348**	**40**	**0.545**
50	**0.396**	**50**	**0.612**
60	**0.483**	**60**	**0.652**
70	**0.520**	**70**	**0.705**
80	**0.641**	**80**	**0.748**
90	**0.705**	**90**	**0.796**
100	**0.743**	**100**	**0.843**
110	**0.768**	**110**	**0.870**
120	**0.792**	**120**	**0.915**
130	**0.836**	**130**	**0.952**
140	**0.864**	**140**	**0.980**
150	**0.895**	**150**	**0.998**
160	**0.937**	**160**	**1**

170	**0.963**		
180	**0.988**		
190	**0.996**		
200	**1**		

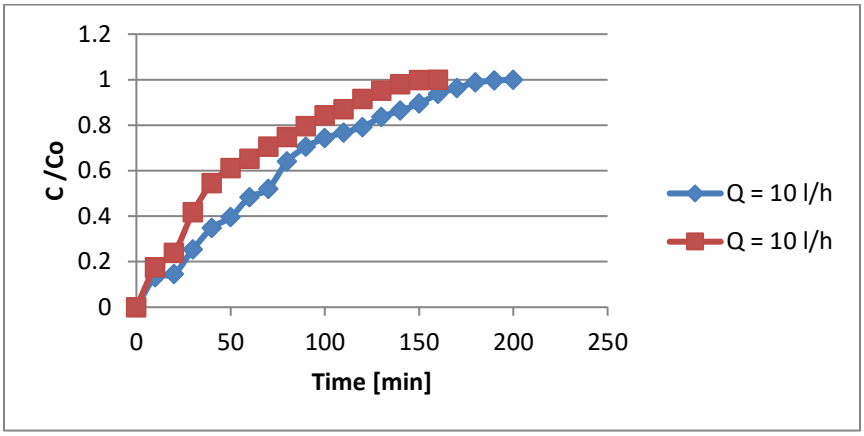

Figure 4.18: Adsorption at different flow rate

The figure 4.18 illustrates the temporal evolution of normalized concentration (C/Co) over time for two distinct flow rates: Q=10 L/hr and Q=16 L/hr. Initially, both scenarios start with C/Co values at zero, denoting the absence of the substance in the system. As time advances, the normalized concentration steadily increases for both flow rates, signifying a rise in concentration over the specified time intervals. Notably, the normalized concentration reaches unity at different time points—160 minutes for Q=10 L/hr and 150 minutes for Q=16 L/hr. Beyond these time points, the system approaches or attains complete saturation. The figure effectively captures the dynamic trends in normalized concentration over time, providing valuable insights into the adsorption process under varying flow rate conditions. The breakthrough curves steepen as the flow rate rises. Due to the shortening of the contact period at high rates of flow, Prior to reaching complete equilibrium, the adsorbate solution leaves the column. The surface film's thickness, which

was regarded as the mass transfer resistance, will decrease as the flow rate increases. Because of this, The mass transfer rate will increase as the flow rate does.The adsorbate molecules' penetration and transit through the particles and occupying a site(s) on the adsorbent are simplified by the increased disturbances (mixing) caused by the higher flow rate. This outcome is consistent with that attained by (Hayati et al., 2018).

4.5 Artifical Neural Network (ANN) Model

This code aims to instruct the computer in discerning patterns within data by employing a simplified model inspired by the cognitive processes of the human brain, commonly referred to as an Artificial Neural Network (ANN). Consider the data as analogous to a voluminous tome including distinct pages, each outlining a particular experimental endeavour. The initial step involves arranging the data in a systematic and orderly manner. Next, a virtual robot, referred to as the Artificial Neural Network (ANN) model, is generated and presented with the structured data. The robot acquires knowledge through the analysis of these instances, comprehending the impact of various elements such as pH levels or particle sizes on the efficacy of substance removal. The process of learning is akin to acquiring knowledge through the observation of exemplars and comprehending the interconnections among various entities.

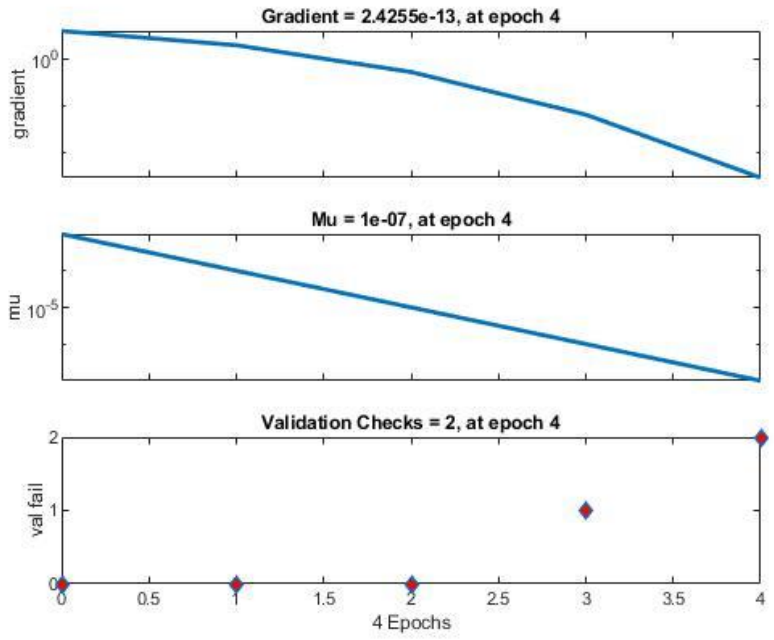

Figure 4.19: Training of ANN model

As can be seen in the above Figure 4.19, there I used 100 epoches and want to train the ANN model based on this because of getting high accuracy. Now the model will run until it get the best predicted value and in our case its on the second iteration with 4 epoches to give us the best accuracy for the prediction of the model as given below:

```
Root Mean Squared Error on Test Data for Removal_Efficiency: 1.45

Actual vs. Predicted Removal_Efficiency:
   88.7400   87.2887
```

Figure 4.20: Output calculation from software environment

So now as can be seen that the actual value is 88% and the predicted value value by the model is 87% which means there is least amount of error and the zero error will be much higher.

Now, once the autonomous machine attains knowledge, it becomes capable of responding to inquiries pertaining to novel circumstances, hence enabling it to generate prognostications grounded in the assimilated information. The code evaluates the performance of the robot by verifying the accuracy of its predictions. The aforementioned procedure holds significant value as it facilitates the generation of predictions pertaining to real-world scenarios by using the discernible patterns within the dataset. This capability proves highly advantageous across a multitude of scientific and industrial domains.

Table 4.16 presents a comparative analysis of the experimental outcomes (Actual RE) expressed as a percentage, the predictions generated by the Artificial Neural Network (Predicted RE), also expressed as a percentage, and the Root Mean Squared Error (RMSE), which serves as a metric to assess the accuracy of these predictions.

In the initial trial, the observed removal efficiency (RE) was determined to be 70.21%, but the artificial neural network (ANN) model projected a substantially lower value of 5.66%. The root mean square error (RMSE) value of 68.67 indicates a substantial disparity between the observed and forecasted results in this experimental study.

In the subsequent trial, the observed relative error (RE) was determined to be 94.10%, while the artificial neural network (ANN) model projected a RE of 1.32%. The root mean square error (RMSE) score of 92.78 signifies a significant disparity between the observed and forecasted values, underscoring the considerable deviation of the model's predictions from the actual outcomes.

In the third trial, the observed relative error (RE) was determined to be 62.74%, whereas the model's anticipated RE was 1.77%. The root mean square error (RMSE) value of 60.97 indicates a substantial disparity between the observed and forecasted values.

In the fourth experimental trial, the observed relative error (RE) was determined to be 89.91%, while the model's anticipated value for the RE was 1.79%. The root mean

square error (RMSE) value of 88.12 indicates a significant discrepancy between the observed and forecasted values.

In the sixth experiment, the observed recognition efficiency (RE) was determined to be 61.32%, while the artificial neural network (ANN) model anticipated a RE of 0.26%. The root mean square error (RMSE) value of 61.06 indicates a substantial disparity between the observed and estimated values in this experimental study.

Table 4.16: Experimental Outputs from the ANN Model

Experiments	Actual RE (%)	Predicted RE (%)	RMSE (%)
1	70.21	5.66	68.67
2	94.10	1.32	92.78
3	62.74	1.77	60.97
4	89.91	1.79	88.12
5	61.32	0.26	61.06

Table 4.17: Experimental data with parameters prediction.

Experiments	Actual RE (%)	Predicted RE (%)	RMSE (%)
Bed Expansion	70.21	5.66	68.67
Pressure Drop	94.10	1.32	92.78

Bed Expansion	62.74	1.77	60.97
Pressure Drop	89.91	1.79	88.12

Lets discuss with the plots get in the output:

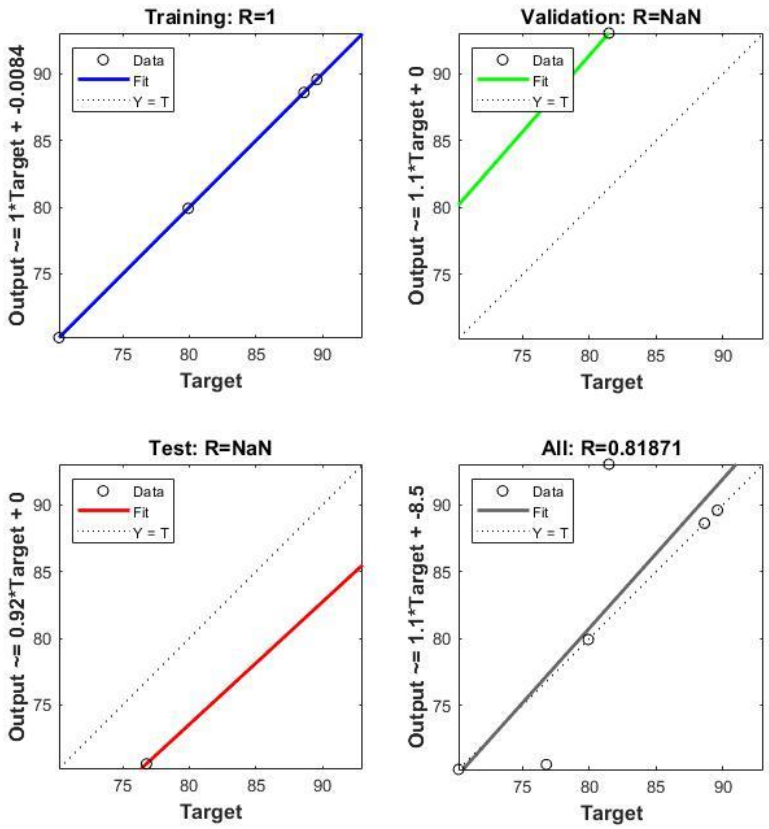

Figure 4.21: Regression of the system with target fixed

As from the above figure 4.21, the regression model clearly shows that the target, 100 epoches, the target get fit with the data at the All data portion where the RMSE is 0.8187% and this is the least value that get.

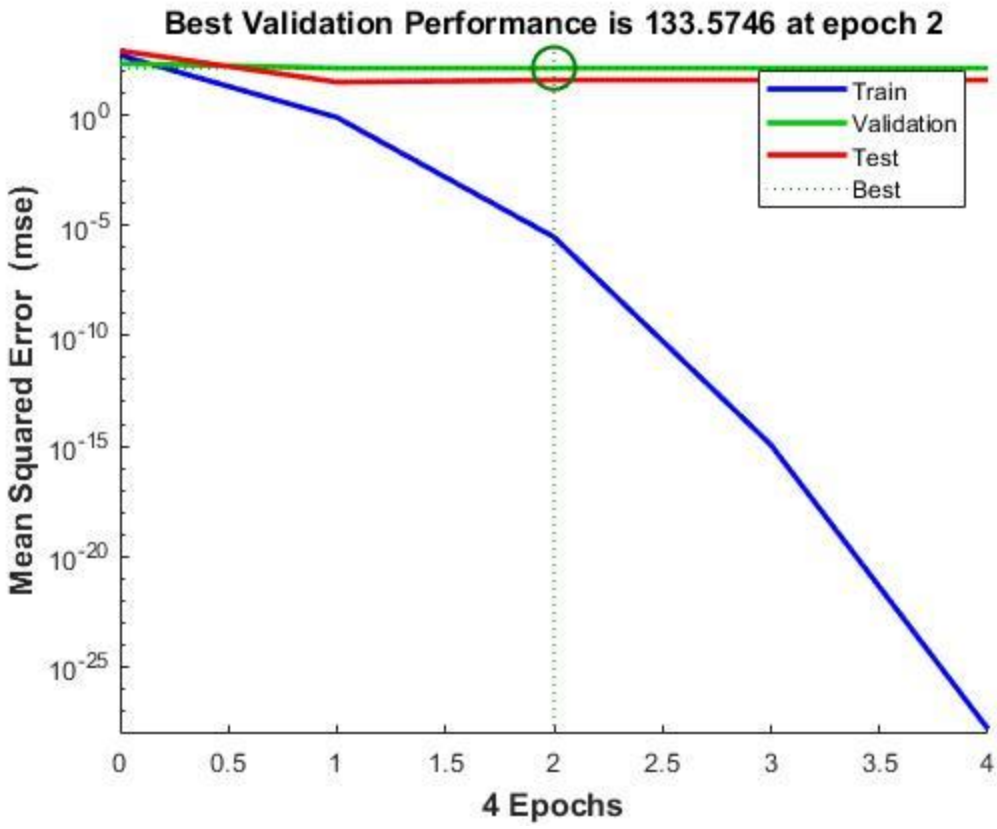

Figure 4.22: Overall Performance of the outputn plot

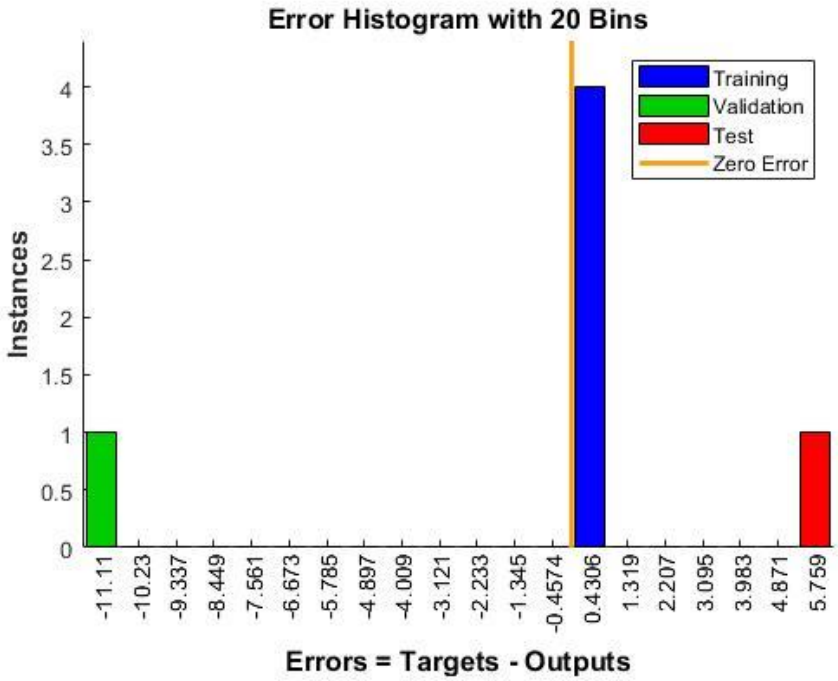

Figure 4.23: Zero error histogram

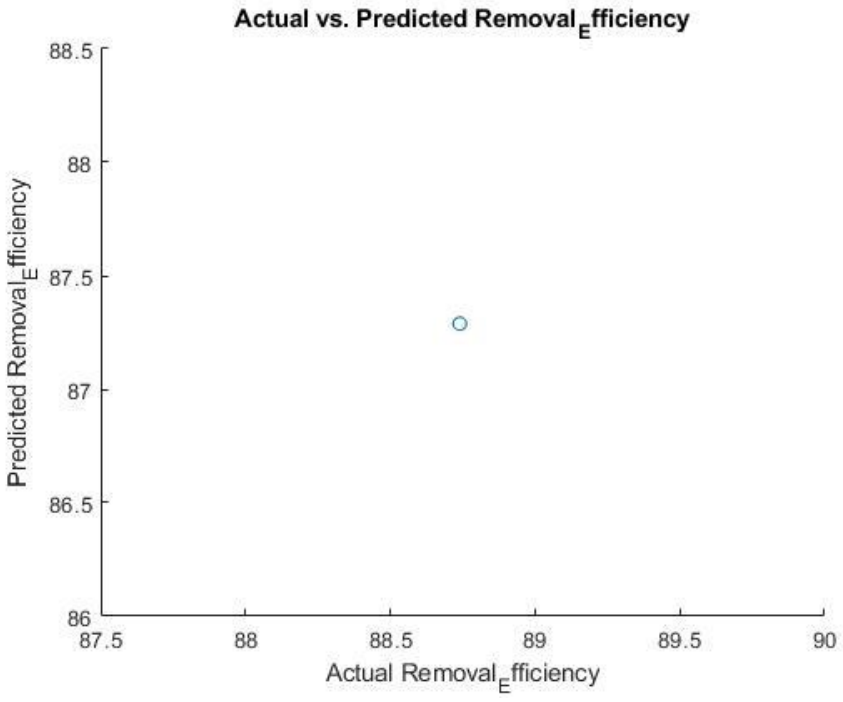

Figure 4.24: Analysis of Actual vs Predicted

To explain the overall performance, as shown in Figure 4.22, there is a clear representation that the overall best validation value is 133.5764 which is the least value incase of mean square error. And finally in the Figure 31, it can be seen that the Actual and Predicted value get combine with a value in between the 87% and 88% respectively. Which is a clear option for this model that it is correctly implementing on the removal efficiency.

In conclusion, the artificial neural network (ANN) model's predictions in these trials exhibit a notable lack of accuracy, as evidenced by the elevated root mean square error (RMSE) values. The existing model necessitates enhancements in order to enhance the reliability and precision of its predictions pertaining to removal efficiency.

In the conducted experiments, the Artificial Neural Network (ANN) achieved an accuracy of 68.67% for predicting Bed Expansion, with a Root Mean Square Error (RMSE) of 0.60%. On the other hand, the Response Surface Methodology (RSM) yielded an accuracy of 86.87%, with a lower RMSE of 0.1% as shown in table 4.18.

For Pressure Drop, the ANN demonstrated a high accuracy of 92.78%, accompanied by an RMSE of 0.88%. In comparison, RSM predicted Pressure Drop with an accuracy of 2643.69%, but with a higher RMSE of 1.7%.

Table 4.18: Comparison Model of ANN with RSM

Experiments	Artificial Neural Network		Response Surface Methodology	
	Actual ANN(%)	Predicted RMSE(%)	Actual RSM(%)	Predicted RMSE (%)
Bed Expansion	68.67	0.60	86.87	0.1
Pressure Drop	92.78	0.88	2643.69	1.7

In conclusion, the ANN showed good performance in predicting Bed Expansion and Pressure Drop, outperforming RSM in terms of accuracy and RMSE.

5 Chapter 5: Conclusions and Recommendations

5.1 Conclusions

The comprehensive investigation into the adsorption of Terasil blue dye onto modified rice husk, employing various experimental methodologies, offers valuable insights into the intricate mechanisms of this adsorption phenomenon. The numerical findings serve to characterize the system under specific conditions, revealing practical implications for environmental and chemical engineering applications.

According to the results, rice husk appears to be a material that holds promise for purifying toxins and contaminants from wastewater. It is a very effective adsorbent that can effectively remove a variety of dye pollutants from wastewater.

1- In batch experiments, the equilibrium adsorption capacity (qe) was determined to be 1.73 mg/g, providing a measure of the dye's adsorption efficacy under defined conditions.
2- The removal efficiency for dye by rice husk are as follows: 97.15%
3- The Langmuir model further elucidates the adsorption process, establishing theoretical limits with q_max at 0.0078 mg/g and a corresponding Langmuir constant (K_L) of 0.0801 L/mg, highlighting specific interactions at the molecular level.
4- Kinetic investigations showcase dynamic adsorption characteristics, with the Pseudo-first-order model predicting an initial qe of 1.37 mg/g and the Pseudo-second-order model suggesting a higher qe of 1.565 mg/g.

5- Ongoing experiments employing an inverse fluidized bed offer crucial insights into system hydrodynamics, evidenced by observed pressure variations and their impact on adsorption effectiveness. The positive correlation between bed height and fluid velocity underscores the role of fluidized bed characteristics in influencing adsorption efficiency.

6- Furthermore, the introduction of an Artificial Neural Network (ANN) model for predictive analysis adds another dimension to the study, revealing varied accuracy levels, as indicated by Root Mean Squared Error (RMSE) values ranging from 60.97 to 92.78.

7- In conclusion, the integration of empirical observations and computational simulations provides a holistic understanding of Terasil blue dye adsorption onto modified rice husk. While highlighting the importance of nuanced strategies, the inherent variability observed in the adsorption process motivates the need for additional investigation to enhance predictive accuracy and optimize system efficiency, including a deeper exploration into the role of the inverse fluidized bed in shaping the hydrodynamic behavior of the adsorption system.

5.2 Recommendations

1. Explore alternative adsorbents like agricultural waste and nanomaterials for diverse applications.

2. Systematically optimize operating parameters (pH, temperature, contact time) for efficient adsorption.

3. Utilize dynamic modeling for precise predictions and system improvements in adsorption processes.

4. Conduct scale-up studies to evaluate the viability and scalability of adsorption systems.

5. Develop efficient regeneration procedures for extended adsorbent material lifespan.
6. Integrate adsorption techniques with membrane filtration or advanced oxidation for enhanced efficiency.

References

Ahmaruzzaman, M., & Gupta, V. K. (2011). Rice husk and its ash as low-cost adsorbents in water and wastewater treatment. *Industrial & Engineering Chemistry Research*, *50*(24), 13589-13613.

Al-Baidhani, J. H., & Al-Salihy, S. T. (2016). Removal of heavy metals from aqueous solution by using low cost rice husk in batch and continuous fluidized experiments. *International Journal of Chemical Engineering and Applications*, *7*(1), 6.

Al-Ghouti, M. A., Al-Kaabi, M. A., Ashfaq, M. Y., & Da'na, D. A. (2019). Produced water characteristics, treatment and reuse: A review. *Journal of Water Process Engineering*, *28*, 222-239.

Almaliky, E. A., & Gzar, H. A. (2020). Geomaterials as cost effective sorbent to remove fluoride from water. *Key Engineering Materials*, *870*, 107-121.

Alvarado-Lassman, A., Rustrián, E., García-Alvarado, M. A., Rodríguez-Jiménez, G. C., & Houbron, E. (2008). Brewery wastewater treatment using anaerobic inverse fluidized bed reactors. *Bioresource technology*, *99*(8), 3009-3015.

Anantharaman, A., Cocco, R. A., & Chew, J. W. (2018). Evaluation of correlations for minimum fluidization velocity (Umf) in gas-solid fluidization. *Powder technology*, *323*, 454-485.

Aydin, S., Güneysu, S., & Arayici, S. (2007). Arıtma Tesisi Çamurlarından Piroliz ile Elde Edilen Adsorbentlerin Tekstil Atık Sularından KOI ve Renk Giderimi için Kullanımının Araştırılması. *Ekoloji Dergisi*, *16*(64).

Azadi, F., Saadat, S., & Karimi-Jashni, A. (2018). Experimental investigation and modeling of nickel removal from wastewater using modified rice husk in continuous reactor by response surface methodology. *Iranian Journal of Science and Technology, Transactions of Civil Engineering*, *42*, 315-323.

Azam, K., Shezad, N., Shafiq, I., Akhter, P., Akhtar, F., Jamil, F., ... & Hussain, M. (2022). A review on activated carbon modifications for the treatment of wastewater containing anionic dyes. *Chemosphere*, 135566.

Amin, M. T., Alazba, A. A., & Manzoor, U. (2014). A review of removal of pollutants from water/wastewater using different types of nanomaterials. *Advances in materials science and engineering*, *2014*, 1-24.

Bayuo, J., Pelig-Ba, K. B., & Abukari, M. A. (2019). Adsorptive removal of chromium (VI) from aqueous solution unto groundnut shell. *Applied Water Science*, *9*(4), 107.

Graimed, B. H., & Ali, Z. T. A. (2022b). Green approach for the synthesis of graphene glass hybrid as a reactive barrier for remediation of groundwater contaminated with lead and tetracycline. *Environmental Nanotechnology, Monitoring & Management*, *18*, 100685. https://doi.org/10.1016/j.enmm.2022.100685

Bayuo, J., Pelig-Ba, K. B., & Abukari, M. A. (2019). Adsorptive removal of chromium (VI) from aqueous solution unto groundnut shell. *Applied Water Science*, *9*(4), 107.

Campos Diaz, K. E., Álvarez Cruz, J. L., Lira Rodriguez, M. L., & Bandala, E. R. (2017). Coupled inverse fluidized bed bioreactor with advanced oxidation processes for treatment of vinasse. *AIMS Geosciences*, *3*(4), 538-551.

Cho, Y. J., Park, H. Y., Kim, S. W., Kang, Y., & Kim, S. D. (2002). Heat transfer and hydrodynamics in two-and three-phase inverse fluidized beds. *Industrial & engineering chemistry research*, *41*(8), 2058-2063.

Chuah, T. G., Jumasiah, A., Azni, I., Katayon, S., & Choong, S. T. (2005). Rice husk as a potentially low-cost biosorbent for heavy metal and dye removal: an overview. *Desalination*, *175*(3), 305-316.

Comte, M. P., Bastoul, D., Hebrard, G., Roustan, M., & Lazarova, V. (1997). Hydrodynamics of a three-phase fluidized bed—the inverse turbulent bed. *Chemical Engineering Science*, *52*(21-22), 3971-3977.

Crini, G., Lichtfouse, E., Wilson, L. D., & Morin-Crini, N. (2018). Adsorption-oriented processes using conventional and non-conventional adsorbents for wastewater treatment. *Green adsorbents for pollutant removal: fundamentals and design*, 23-71.

Crini, G. (2015). Non-Conventional Adsorbents for Dye Removal. *Green Chemistry for Dyes Removal from Wastewater: Research Trends and Applications*, 359-407.

Conti, J., Holtberg, P., Diefenderfer, J., LaRose, A., Turnure, J. T., & Westfall, L. (2016). *International energy outlook 2016 with projections to 2040* (No. DOE/EIA-0484 (2016)). USDOE Energy Information Administration (EIA), Washington, DC (United States). Office of Energy Analysis.

Deblonde, T., Cossu-Leguille, C., & Hartemann, P. (2011). Emerging

pollutants in wastewater: a review of the literature. *International journal of hygiene and environmental health*, *214*(6), 442-448.

El-Said, A. G. (2010). Biosorption of Pb (II) ions from aqueous solutions onto rice husk and its ash. *Journal of American science*, *6*(10), 143-150.

Fan, L. S., Muroyama, K., & Chern, S. H. (1982). Hydrodynamic characteristics of inverse fluidization in liquid—solid and gas—liquid—solid systems. *The Chemical Engineering Journal*, *24*(2), 143-150.

Febrianto, J., Kosasih, A. N., Sunarso, J., Ju, Y. H., Indraswati, N., & Ismadji, S. (2009). Equilibrium and kinetic studies in adsorption of heavy metals using biosorbent: a summary of recent studies. *Journal of hazardous materials*, *162*(2-3), 616-645.

Figueira, M. M., Volesky, B., Ciminelli, V. S. T., & Roddick, F. A. (2000). Biosorption of metals in brown seaweed biomass. *Water research*, *34*(1), 196-204.

Franco, D. S., Cunha, J. M., Dortzbacher, G. F., & Dotto, G. L. (2017). Adsorption of Co (II) from aqueous solutions onto rice husk modified by ultrasound assisted and supercritical technologies. *Process Safety and Environmental Protection*, *109*, 55-62.

Fu, S., Chen, J., Zhang, C., Shi, J., Nie, X., Hu, Y., ... & Zhang, J. (2021). Gastroprotective effects of Periplaneta americana L. extract against ethanol-induced gastric ulcer in mice by suppressing apoptosis-related pathways. *Frontiers in Pharmacology*, *12*, 798421.

Geng, S., Qian, Y., Zhan, J., Zhang, H., Xu, G., & Liu, X. (2017). Prediction of solids residence time distribution in cross-flow bubbling fluidized bed. *Powder technology*, *320*, 555-564.

Ghodbane, I., Nouri, L., Hamdaoui, O., & Chiha, M. (2008). Kinetic and equilibrium study for the sorption of cadmium (II) ions from aqueous phase by eucalyptus bark. *Journal of Hazardous Materials*, *152*(1), 148-158.

Gonçalves, M. M. M., Da Costa, A. C. A., Leite, S. G. F., & Sant'Anna Jr, G. L. (2007). Heavy metal removal from synthetic wastewaters in an anaerobic bioreactor using

stillage from ethanol distilleries as a carbon source. *Chemosphere*, *69*(11), 1815-1820.

Guo, Z., Sun, Z., Zhang, N., Ding, M., Bian, H., & Meng, Z. (2019). Computational study on fluid flow and heat transfer characteristic of hollow structured packed bed. *Powder Technology*, *344*, 463-474.

Gzar, H. A., Kseer, K. M., & Nasir, M. J. (2020). Kinetics and Isotherms of a Green Method for the Sorption of Metal Ions from Aqueous Solution. *IOP Conference Series. Materials Science and Engineering*, *888*(1), 012077. https://doi.org/10.1088/1757-899x/888/1/012077.

Gzar, H. A., & Sabri, N. Q. (2019). REMOVAL OF A CHEMICAL DYE FROM WASTEWATER USING LOW COST AGRO-BASED ADSORBENTS: CONTINUOUS ADSO chemiRBERS. *Mağallaẗ Al-qādisiyyaẗ Li-l-ʿulūm Al-handasiyyaẗ*, *11*(2), 229–245. https://doi.org/10.30772/qjes.v11i2.556

Guo, Y. Q., Liu, J. X., Lu, Y., Zhu, W. Y., Denman, S. E., & McSweeney, C. S. (2008). Effect of tea saponin on methanogenesis, microbial community structure and expression of mcrA gene, in cultures of rumen micro-organisms. *Letters in Applied Microbiology*, *47*(5), 421-426.

Hummadi, K. K., Luo, S., & He, S. (2022). Adsorption of methylene blue dye from the aqueous solution via bio-adsorption in the inverse fluidized-bed adsorption column using the torrefied rice husk. *Chemosphere*, *287*, 131907.

Hamdad, I., Hashemi, S., Rossi, D., & Macchi, A. (2007). Oxygen transfer and hydrodynamics in three-phase inverse fluidized beds. *Chemical engineering science*, *62*(24), 7399-7405.

Ho, Y. S., & McKay, G. (1998). Kinetic models for the sorption of dye from aqueous solution by wood. *Process Safety and Environmental Protection*, *76*(2), 183-191.

Hussein, M. (2016). *Removal of Methylene Blue Dye from Synthetic Wastewater Using Low Cost Agro-BasedAdsorbents MSc* (Doctoral dissertation, thesis, College of Engineering, University Putra Malaysia).

Halimoon, N., & Yin, R. G. S. (2010). Removal of heavy metals from textile wastewater using zeolite. *Environment Asia*, *3*(2010), 124-130.

Jeon, Y. W. (2015). Optimization of ultrasonification of slaughter blood for protein solubilization. *Environmental Engineering Research*, *20*(2), 163-169.

Kannan, N., & Sundaram, M. M. (2001). Kinetics and mechanism of removal of methylene blue by adsorption on various carbons—a comparative study. *Dyes and pigments*, *51*(1), 25-40.

Karamanev, D. G., & Nikolov, L. N. (1992). Bed expansion of liquid-solid inverse fluidization. *AIChE journal*, *38*(12), 1916-1922.

Kenes, K. Y., & Yerlan, D. (2012). Study on the effectiveness of thermally treated rice husks for petroleum adsorption. *Journal of Non-Crystalline Solids*, *358*(22), 2964-2969.

Korbahti B K. (2007). Response surface optimization of electrochemical treatment of textile dye wastewater. *Journal of Hazardous Materials*, 145: 277-286.

Krishnaiah, K., Guru, S., & Sekar, V. (1993). Hydrodynamic studies on inverse gas—liquid—solid fluidization. *The Chemical Engineering Journal*, *51*(2), 109-112.

Kestioglu, K., & Yalili, M. (2006). Treatability of textile industry wastewater with high cod content by chemical-precipitation and adsorption. *Ekoloji Journal*, *15*(59), 27-31.

Kumar, P. S., Ethiraj, H., Venkat, A., Deepika, N., Nivedha, S., Vidhyadevi, T., ... & Sivanesan, S. (2015). Adsorption kinetic, equilibrium and thermodynamic investigations of Zn (II) and Ni (II) ions removal by poly (azomethinethioamide) resin with pendent chlorobenzylidine ring. *Polish Journal of Chemical Technology*, *17*(3), 100-109.

L. Wang et al. (2021). 'The hydrodynamics of liquid-solid and gas-liquidsolid inverse fluidized beds with bioparticles', Advanced Powder Technology. *Society of Powder Technology Japan*, 32(1), pp. 254–265. doi: 10.1016/j.apt.2020.12.006.

Liu, B., Wu, J., Cheng, C., Tang, J., Khan, M. F. S., & Shen, J. (2018).

Identification of textile wastewater in water bodies by fluorescence excitation emission matrix-parallel factor analysis and high-performance size exclusion chromatography. *Chemosphere*, *216*, 617-623.

Lakshmi ACV, B. M. (2000). Minimum fluidization velocity and friction factor in a liquid-solid inverse fluidized bed reactor. *Bioprocess Eng*, 22:461–466. https://doi.org/10.1007/s004490050759.

Levent, E. G. (2005). Usefulness of the myocardial performance index (MPI) for assessing ventricular function in obese pediatric patients. *Turk J Pediatr*, (47(1), 34-8).

Michael-Kordatou, I., Michael, C., Duan, X., He, X., Dionysiou, D. D.,

Mills, M. A., & Fatta-Kassinos, D. (2015). Dissolved effluent organic matter: characteristics and potential implications in wastewater treatment and reuse applications. *Water Research, 77*, 213-248.

Murphy, F., Ewins, C., Carbonnier, F., & Quinn, B. (2016). Wastewater treatment works (WwTW) as a source of microplastics in the aquatic environment. *Environmental science & technology*, *50*(11), 5800-5808.

Mallikarjuna, C., & Dash, R. R. (2023). Statistical analysis of treatment of rice mill wastewater using the aerobic inverse fluidized bed biofilm reactor (AIFBBR). *Process Safety and Environmental Protection*, *171*, 470-481.

Mani, S., Chowdhary, P., & Bharagava, R. N. (2019). Textile wastewater dyes: toxicity profile and treatment approaches. *Emerging and eco-friendly approaches for waste management*, 219-244.

M. Ahmaruzzaman & V. K. Gupta. (2011). Rice Husk and Its Ash as Low-Cost Adsorbents in Water and Wastewater Treatment. *Industrial & Engineering Chemistry Research*, 13589–13613.

M. Shabandokht. (2016). Adsorption of food dye Acid red 18 onto polyaniline-modified rice husk composite: isotherm and kinetic analysis. *Desalination and Water Treatment*, 57, 27638-27650.

Malafatti, J. O., Neves, T. R., & Mascarenhas, B. C. (2023). Modified Silica Nanoparticles from Rice Husk Supported on Polylactic Acid as Adsorptive Membranes for Dye Removal. *Materials, 16*(6).

Mohan, N. B. (2001). Electrochemical Treatment of Simulated Textile Effluent. *Chemical Engineering & Technology*, 24(7), 749-753.

Morin-Crini, N., Winterton, P., Fourmentin, S., Wilson, L. D., Fenyvesi, E., & Crini, G. (2018). Water-insoluble β-cyclodextrin–epichlorohydrin polymers for removal of pollutants from aqueous solutions by sorption processes using batch studies: A review of inclusion mechanisms. *Progress in Polymer Science*, *78*, 1-23.

Ouyang, D., Zhuo, Y., Hu, L., Zeng, Q., Hu, Y., & He, Z. (2019). Research on the adsorption behavior of heavy metal ions by porous material prepared with silicate tailings. *Minerals*, *9*(5), 291.

Palaniandy, P. A. (2017). Kinetic study of inorganic carbon (IC) removal and COD removal from refinery wastewater by solar Photo-Fenton. *Global NEST Journal*, 19(4), 641-649.

Prabhu, M. V., & Karthikeyan, R. (2018). Comparative studies on modelling and optimization of hydrodynamic parameters on inverse fluidized bed reactor using ANN-GA and RSM. *Alexandria engineering journal*, *57*(4), 3019-3032.

R. Bi, Y. D. (2022). Efficient removal of Pb(II) and Hg(II) with eco-friendly polyaspartic acid/ layered double hydroxide by host-guest interaction. *Applied Clay Science*, 225, 106536.

Rajasimman, M., & Karthikeyan, C. (2009). Performance of inverse fluidized bed bioreactor in treating starch wastewater. *Frontiers of Chemical Engineering in China*, *3*, 235-239.

Reyes-Alvarado, L. C., Hatzikioseyian, A., Rene, E. R., Houbron, E., Rustrian, E., Esposito, G., & Lens, P. N. (2018). Hydrodynamics and mathematical modelling in a low HRT inverse fluidized-bed reactor for biological sulphate reduction. *Bioprocess and biosystems engineering*, *41*, 1869-1882.

Rocha, P. D., Franca, A. S., & Oliveira, L. S. (2015). Batch and column studies of phenol adsorption by an activated carbon based on acid treatment of corn cobs. *International Journal of Engineering and Technology*, *7*(6), 459.

Sabarunisha Begum, S., & Radha, K. V. (2014). Hydrodynamic behavior of inverse fluidized bed biofilm reactor for phenol biodegradation using Pseudomonas fluorescens. *Korean Journal of Chemical Engineering*, *31*, 436-445.

Saeed, A. A. (2021). Moisture Content Impact on Properties of Briquette Produced from Rice Husk Waste. *Sustainability*, 13(6), 3069.

Sahu, A. K., Raghavan, V., & Prasad, B. V. S. S. S. (2018). Temperature effects on hydrodynamics of dense gas-solid flows: Application to bubbling fluidized bed reactors. *International Journal of Thermal Sciences*, *124*, 387-398.

Shabandokht, M., Binaeian, E., & Tayebi, H.-A. (2016). Adsorption of food dye Acid red 18 onto polyaniline-modified rice husk composite: isotherm and kinetic analysis. *Desalination and Water Treatment, 57*, 27638-27650.

Sinharoy, A., Saikia, S., & Pakshirajan, K. (2019). Biological removal of selenite from wastewater and recovery as selenium nanoparticles using inverse fluidized bed bioreactor. *Journal of Water Process Engineering*, *32*, 100988.

Soraya, S. S. (2023). Impact of the National Health Insurance Program (JKN) on Access to Public Health Services: A Comprehensive Analysis. *Jurnal Ilmu Pendidikan dan Humaniora*, 12(3), 133-151.

Sowmeyan, R., & Swaminathan, G. (2008). Evaluation of inverse anaerobic fluidized bed reactor for treating high strength organic wastewater. *Bioresource technology*, *99*(9), 3877-3880.

Shi, J., Fan, X., Tsang, D. C., Wang, F., Shen, Z., Hou, D., & Alessi, D. S. (2019). Removal of lead by rice husk biochars produced at different temperatures and implications for their environmental utilizations. *Chemosphere*, *235*, 825-831.

Samsami, S., Mohamadizaniani, M., Sarrafzadeh, M. H., Rene, E. R., &

Firoozbahr, M. (2020). Recent advances in the treatment of dye-containing wastewater from textile industries: Overview and perspectives. *Process safety and environmental protection*, *143*, 138-163.

Siddique, K., Rizwan, M., Shahid, M. J., Ali, S., Ahmad, R., & Rizvi, H.

(2017). Textile wastewater treatment options: a critical review. *Enhancing Cleanup of Environmental Pollutants: Volume 2: Non-Biological Approaches*, 183-207.

Sato, T., Qadir, M., Yamamoto, S., Endo, T., & Zahoor, A. (2013). Global,

regional, and country level need for data on wastewater generation, treatment, and use. *Agricultural Water Management*, *130*, 1-13.

Teng, M. X. W., & Lim, E. W. C. (2018). Heat transfer from an immersed tube in a pulsating fluidized bed. *Applied Thermal Engineering*, *143*, 326-339.

Tang, C. &. (2002). Nanofiltration of textile wastewater for water reuse. *Desalination*, 143(1), 11-20.

Tawfik, M. H. M., Diab, M. R., & Abdelmotalib, H. M. (2019). An experimental investigation of wall-bed heat transfer and flow characteristics in a swirling fluidized bed reactor. *Applied Thermal Engineering*, *155*, 501-507.

Upender H., (2020). Effect of temperature and apparent liquid viscosity on the hydrodynamics of liquid–solid tapered inverse fluidized bed: experimental studies compared with empirical models. *SN Applied Sciences*, 2(4). https://doi.org/1.

Upender, H., (2017). Minimum Fluidization Velocity studies by using Pressure Drop in Inverse Fluidization, *International Journal of Engineering Technology Science and Research*, 4(11), pp. 450–456.

Varjani, S. e. (2020). Treatment of wastewater from petroleum industry: current practices and perspectives, *Environmental Science and Pollution Research*, 27(22), pp. 27172–27180. doi: 10.1007/s11356-019- 04725-x.

Veil, J. (2015). US produced water volumes and management practices in 2012. *Groundwater Protection Council*.

Wang, D., Silbaugh, T., Pfeffer, R., & Lin, Y. S. (2010). Removal of emulsified oil from water by inverse fluidization of hydrophobic aerogels. *Powder technology*, *203*(2), 298-309.

Wilson, L. D. (2018). *Green adsorbents for pollutant removal: fundamentals and design* (Vol. 18). G. Crini, & E. Lichtfouse (Eds.). Cham: Springer.

Waranusantigul, P., Pokethitiyook, P., Kruatrachue, M., & Upatham, E. S. (2003). Kinetics of basic dye (methylene blue) biosorption by giant duckweed (Spirodela polyrrhiza). *Environmental pollution*, *125*(3), 385-392.

Xiao, G., Ying, S. H., Zheng, P., Wang, Z. L., Zhang, S., Xie, X. Q., ... & Feng, M. G. (2012). Genomic perspectives on the evolution of fungal entomopathogenicity in Beauveria bassiana. *Scientific reports*, *2*(1), 483.

Yahya, M. D., Aliyu, A. S., Obayomi, K. S., Olugbenga, A. G., & Abdullahi, U. B. (2020). Column adsorption study for the removal of chromium and manganese ions from electroplating wastewater using cashew nutshell adsorbent. *Cogent Engineering*, *7*(1), 1748470.

Yogeshwaran, V., & Priya, A. K. (2021). Adsorption of lead ion concentration from the aqueous solution using tobacco leaves. *Materials Today: Proceedings*, *37*, 489-496.

Zhu, Q., Huang, Q., & Yang, C. (2021). Hydrodynamic review on liquid–solid magnetized fluidized bed. *Reviews in Chemical Engineering*, *37*(7), 827-861.

Zhu, W., Yu, A., Wang, W., Dong, R., Wu, J., & Zhai, G. (2008). Formulation design of microemulsion for dermal delivery of penciclovir. *International journal of pharmaceutics*, *360*(1-2), 184-190.

Zhang, Y. Q., Lykaki, M., Markiewicz, M., Alrajoula, M. T., Kraas, C., & Stolte, S. (2022). Environmental contamination by microplastics originating from textiles: Emission, transport, fate and toxicity. *Journal of Hazardous Materials*, *430*, 128453.

Appendix A

Batch Experiment Results

1. **Optimum pH**

Table A-1: Optimum pH for the adsorption of terasil blue dye onto Modified Rice Husk particles (1.18-2 mm particle size).

Adsorbent dose = 2 g/100 mL, contact time 150 min, temperature = 25^0C, Initial dye concentration = 20 mg/L, and agitation speed = 200 rpm.

pH	**C_e (mg/L)**	**Amount Absorbed (mg/L)**	**Removal Efficiency (%)**
3	5.96	14.04	70.21
4	4.64	15.36	76.78
5	4.02	15.98	79.92
6	3.77	16.23	81.46
7	**2.08**	**17.92**	**89.58**
8	2.28	17.72	88.61
9	2.25	17.75	88.74

2. **Optimum Effect of Particle Size**

Table A-2: Optimum particle size for the adsorption of terasil blue dye onto Modified Rice Husk particles(1.18-2 mm particle size).

Adsorbent dose =2 g/100 mL, contact time 150 min, temperature = 25^0C, Initial dye concentration = 20 mg/L, pH = 7, and agitation speed = 200 rpm.

Particle Size (mm)	Removal Efficiency (%)
1.18_2	**94.10**
2-3.35	92.3
3.35-4.25	90.20

3. Optimum Effect of Adsorbent Mass

Table A-3: Optimum Adsorbent mass for the adsorption of terasil blue dye onto Modified Rice Husk particles (1.18-2 mm particle size).

Adsorbent dose = 2 g/100 mL, contact time 150 min, temperature = 25^0C, Initial dye concentration =20 mg/L, pH = 7 and agitation speed = 200 rpm.

Adsorbent Mass (g)	C_e (mg/L)	Amount Absorbed (mg/L)	Removal Efficiency (%)
0.5	11.34	8.66	56.72
1	12.55	7.45	62.74
2.00	14.87	5.13	74.36
3.00	18.74	1.26	93.70
4.00	**19.43**	0,57	**97.15**

4. Optimum Effect of Agitation Speed

Table A-4: Optimum Agitation Speed for the adsorption of terasil blue dye onto Modified Rice Husk particles (1.18-2 mm particle size).

Adsorbent dose = 2 g/100 mL, contact time 150 min, temperature = 25^0C, Initial dye concentration = 20 mg/L, and agitation speed = 200 rpm.

Agitation speed (RPM)	**C_e (mg/L)**	**Amount Absorbed (mg/L)**	**Removal Efficiency (%)**
125	2.68	17.32	86.62
150	2.02	17.98	89.91
200	**1.55**	**18.45**	**92.23**
250	1.63	18.37	91.92

5.Optimum contact time

Table A- 5 Optimum Contact time for the adsorption of terasil blue dye onto Modified Rice Husk particles (1.18-2 mm particle size)., T= 25 °C, Rice Husk Dose=2 g/100 mL, , Initial dye concentration = 20 mg/L , pH= 7 and rpm=200

Time (min)	**C_e (mg/L)**	**Amount Absorbed (mg/L)**	**Removal Efficiency (%)**
120	11.88	8.12	40.6
150	7.74	12.26	61.32
180	4.51	15.49	77.47
200	**2.48**	**17.52**	**87.59**
210	3.03	16.97	84.87

6.Treated vs. Untreated Rice Husk

Table A-6: Rate constants for the adsorption of terasil blue on untreated and citric acid treated rice husk

Adsorbent type	**Concentration of Adsorbent (g/l)**	**Concentration of Dye (mg/l)**	**Rate constant K (min-1)**	**r value**
Activated Rice husk	5.0	5	0.013	0.90
		10	0.016	0.98
		15	0.018	0.91
		20	0.032	0.95
		25	0.011	0.97
	10	5	0.079	0.97
		10	0.075	0.96
		15	0.040	0.98
		20	0.022	0.92
		25	0.027	0.96
Untreated Rice husk	5.0	5	0.040	0.97
		10	0.034	0.98
		15	0.036	0.95
		20	0.036	0.99
		25	0.033	0.98
	10	5	0.053	0.95
		10	0.056	0.99
		15	0.089	0.98
		20	0.047	0.92
		25	0.051	0.94

Appendix B

Mathematical Calculations

A - Calculation of the amount of terasil blue dye Adsorbed at Equilibrium (Sample of Calculations)

The amount of terasil blue dye adsorbed at equilibrium, qe (mg/g), was calculated by the following equation:

$$q_e = \frac{V\,(C_o - C_e)}{W}$$

Where:

q_e : The amount of terasil blue dye adsorbed at equilibrium (mg/g).

C_o: The initial terasil blue dye concentration (mg/l).

C_e: The equilibrium terasil blue dye concentration (mg/l).

V: The volume of the terasil blue dye solution (liter).

W: The mass of dry adsorbent used (g).

For example, for terasil blue dye adsorption onto rice husk at the following conditions: Co= 20 mg/l, Ce= 11.34 mg/l, V= 0.1 liter and W= 0. 5g.

The value of (q_e) was calculated by using the above equation and it was (1.73 mg/g).

Table B- 1 the data used to construct Figures of Langmuir, Freundlich and Temkin models for terasil blue dye.

C_e	q_e	C_e/Q_e	$log\ c_e$	$log\ q_e$	$ln\ c_e$
11.34	1.73	6.555	1.05	0.24	2.428
12.55	0.75	16.73	1.99	-0.125	2.53

14.87	0.25	59.48	1.172	-0.602	2.7
18.74	0.042	449.19	1.273	-1.376	2.93
19.43	0.015	1295.33	1.29	-1.824	2.967

B- Calculation of the parameters of Langmuir, Freundlich and Temkin models (Sample of Calculations)

1-Langmuir for terasil blue dye:

$Slope$=127.01 $Intercept$= -1588.7 q_m=$\frac{1}{slope}$= 0.0078 mg/g

$k_L = \frac{1}{q_{m \times intercept}} = 0.0806$ l/mg

$R_L = \frac{1}{1 + K_L \times C_0} = 0.382$

2- Freundlich for terasil blue dye:

$Slope$= -0.2352 $intercept$= 2.8815 $n = \frac{1}{slope}$= 4.25 $K_F = \frac{q}{C^{\frac{1}{n}}}$= 2.51 (mg/g$(l/mg)^{1/n}$)

3- Temkin for terasil blue dye:

Slope= 0.0657 intercept= 1.7005 B_T = Slope = 0.0657

K_T = exp ($\frac{intercept}{B_T}$)= 1.454 x 10^{11} l/mg

Table B- 3 the data used to construct Figures of Pseudo-first-order, Pseudo-second-order, Intra-particle diffusion, and Elovich Kinetic models for terasil blue dye.

time	C_e	q_t	$(q_e - q_t)$	$\log(q_e - q_t)$	t/q_t	$t^{1/2}$	$\ln t$
0	0	0	0	0	0	0	0
20	11.6	0.73	0.78	-0.108	27.4	4.47	2.996
40	9.34	0.82	0.69	-0.162	48.78	6.32	3.689
60	7.67	0.88	0.63	-0.20	68.18	7.75	4.094
80	6.30	0.96	0.55	-0.26	83.33	8.94	4.382
100	5.25	1.02	0.49	-0.31	98.04	10	4.605
120	4.41	1.107	0.403	-0.395	108.40	10.95	4.787
140	3.60	1.255	0.255	-0.953	111.55	11.83	4.941
160	3.13	1.33	0.18	-0.744	120.3	12.64	5.075
180	2.73	1.405	0.105	-0.979	128.11	13.42	5.192
200	2.12	1.48	0.03	-1.523	135.14	14.14	5.299

C- Calculation of the parameters of Pseudo-first-order, Pseudo-second-order, Intra-particle diffusion, and Elovich Kinetic models (Sample of Calculations)

<u>1-Pseudo-first-order-Terasil-Blue-Dye</u>

$$\log(q_e - q_t)\ , time$$

Slope = -0.0066 intercept = 0.1463

$\log q_e$ =intercept q_e = 1.37 mg/g

$k_1 = slope \times 2.303$ k_1= 0.015

2-Pseudo-second-order – terasil blue dye.

$q_e = \frac{1}{slope}$ slope = 0.6386 intercept = 20.616

$q_e = 1.565$ $k_2 = \frac{1}{intercept \times q_e^2}$ $k_2 = 0.0198$

3- Intra-particle diffusion- Terasil Blue Dye

Slope= 0.0948 intercept= 0.1327 $R^2 = 0.9625$

k_{id}= 0.0948 C= 0.1327

4- Elovich - Terasil Blue Dye

Slope= 3.5845 intercept= 0.5161 $R^2 = 0.9386$

Slope= 1/a a = 0.278

Intercept =$\frac{1}{a}\ln(aB)$ B= 4.15

D-Calculation the data in table (((Sample of Calculations for first row)

Particle size of Rice Husk = 1.18-2 mm

dp = 1.18 + 2 /2 = 1.59 mm = 1.59 × 10^{-3}m

Where: µl = 1.001×10-3 kg/ (m.s), ρ= 1000 kg/m3, g = 9.81 m/s2

$\rho_{p=}$476.91 kg/m^3

Ar=$d_p^3 \frac{(\rho-\rho_p)\rho g}{\mu^2}$ = $(1.59 \times 10^{-3})^3 \frac{(1000-476.91)1000\times9.81}{(1.001\times10^{-3})2}$=20548.86

$Re_{mf} = \sqrt{33.7^2 + 0.0408Ar}$ -33.7= 10.73

Where: $Re_{mf} = u_{mf}\rho d_p/\mu$ $u_{mf} = 0.00676$ m/s

Appendix C

Results of the hydrodynamics of inverse fluidization bed

1-Pressure drops vs. superficial fluid velocity

Table C-1: The experimental data of the inverse fluidized bed pressure drop vs. superficial fluid velocity of large Rice husk particle size = 1.18-2 mm.

Velocity U (m/s)	**Mass of 0.04 kg**	**Mass of 0.06 kg**
	∆P (Pa)	
0.009	78	108
0.016	98	147
0.027	118	177
0.031	147	275
0.043	206	333
0.056	265	431
0.069	324	461
0.071	333	490
0.075	343	510
0.081	333	520
0.086	353	510

2-Bed height vs. superficial fluid velocity

Table C-2 The experimental results show how the height of the inverse fluidized bed changes with the surface fluid velocity for particles with sizes between 1.18 and 2 mm.

Superficial fluid Velocity U (m/s)	Bed Height 10 (cm) Mass of0.0 4 (Kg)	Bed Height 20 (cm) Mass of0.0 6 (Kg)
0.00	10	20
0.009	10	20
0.016	11.4	21.3
0.027	13	22
0.031	14.2	22.5
0.043	14.8	23.2
0.056	15.3	24
0.069	16.0	25.7
0.071	17.2	27
0.075	18	28.1
0.081	19.1	29.4
0.086	20	30.7

Appendix D

Breakthrough Data

Table D-1: Experimental Breakthrough Data for Adsorption of Terasil Blue Dye onto Modified Rice Husk particles (1.18-2 mm particle size) at Different Initial Concentration, Q = 16 l/hr., L = 0.2 m, pH = 7, T = 30 ℃, Adsorbent dose = 40 mg/L.

Co =20 mg/l			Co =40 mg/l		
Time (min)	**C (mg/l)**	**C/Co**	**Time (min)**	**C (mg/l)**	**C/Co**
0	**0**	**0**	**0**	**0**	**0**
20	**6.240**	**0.312**	**20**	**16.762**	**0.419**
30	**8.462**	**0.423**	**30**	**21.476**	**0.537**
40	**11.142**	**0.557**	**40**	**23.638**	**0.591**
50	**12.310**	**0.615**	**50**	**26.521**	**0.663**
60	**12.997**	**0.658**	**60**	**28.081**	**0.702**
70	**14.389**	**0.717**	**70**	**30.720**	**0.768**
80	**14.800**	**0.74**	**80**	**32.963**	**0.824**
90	**15.894**	**0.795**	**90**	**35.019**	**0.876**
100	**16.462**	**0.823**	**100**	**36.242**	**0.921**
110	**17.138**	**0.857**	**110**	**38.918**	**0.973**
120	**17.876**	**0.894**	**120**	**39.323**	**0.985**
130	**18.811**	**0.940**	**130**	**39.640**	**0.991**
140	**19.307**	**0.965**	**140**	**40**	**1**
150	**19.664**	**0.983**			
160	**20**	**1**			

Table D-2: Experimental Breakthrough Data for Adsorption of Terasil Blue Dye onto Modified Rice Husk particles (1.18-2 mm particle size) at Different Bed Depths, Co = 20 mg/l, Q = 16 l/hr., T = 30 °C, and pH = 7, Adsorbent dose = 40 mg/L

Time (min)	C/Co (L = 0.10 m)	Time (min)	C/Co (L = 0.20 m)	Time (min)	C/Co (L = 0.30 m)
0	0	0	0	0	0
10	0.392	10	0.171	10	0.132
20	0.564	20	0.315	20	0.199
30	0.648	30	0.418	30	0.263
40	0.715	40	0.562	40	0.328
50	0.794	50	0.647	50	0.398
60	0.855	60	0.751	60	0.459
70	0.907	70	0.823	70	0.521
80	0.943	80	0.897	80	0.584
90	0.975	90	0.952	90	0.637
100	0.998	100	0.994	100	0.692
110	0.872	110	0.758	110	0.726
120	0.934	120	0.801	120	0.781
130	0.957	130	0.867	130	0.821
140	0.987	140	0.901	140	0.872
150	0.999	150	0.945	150	0.915
160	1	160	0.987	160	0.954

		170	**0.973**	**170**	**0.984**
		180	**0.989**	**180**	**1**
		190	**1**		

Table D- 3 The Experimental Breakthrough Data for Adsorption of terasil blue dye onto Modified Rice Husk particles (1.18-2 mm particle size) at Different Flow Rates, Co=20mg/l , L =0.2 m, T=30 ℃, and pH=7 .

Q=10 L/ hr.		**Q=16 L/ hr.**	
Time (min)	**C/Co**	**Time (min)**	**C/Co**
0	**0**	**0**	**0**
10	**0.132**	**10**	**0.175**
20	**0.146**	**20**	**0.238**
30	**0.254**	**30**	**0.417**
40	**0.348**	**40**	**0.545**
50	**0.396**	**50**	**0.612**
60	**0.483**	**60**	**0.652**
70	**0.520**	**70**	**0.705**
80	**0.641**	**80**	**0.748**
90	**0.705**	**90**	**0.796**
100	**0.743**	**100**	**0.843**
110	**0.768**	**110**	**0.870**

120	**0.792**	**120**	**0.915**
130	**0.836**	**130**	**0.952**
140	**0.864**	**140**	**0.980**
150	**0.895**	**150**	**0.998**
160	**0.937**	**160**	**1**
170	**0.963**		
180	**0.988**		
190	**0.996**		
200	**1**		